STUDY OF STRUCTURAL STABILITY

AND

MAGNETIC PROPERTIES OF $Ni_{1-x}Fe_2O_4$ MATERIALS.

MD. MOSTAK HOSSAIN
B.Sc. (Hons.), M.Sc.

A THESIS SUBMITTED TO THE DEPARTMENT OF PHYSICS, BUET, DHAKA

IN PARTIAL FULFILMENT FOR THE DEGREE OF

MASTER OF PHILOSOPHY.

BANGLADESH UNIVERSITY OF ENGINEERING & TECHNOLOGY, DHAKA

FEBRUARY, 1995

BANGLADESH UNIVERSITY OF ENGINEERING AND TECHNOLOGY, DHAKA.

DEPARTMENT OF PHYSICS

Certification of Thesis work

A THESIS ON

"STUDY OF STRUCTURAL STABILITY
AND
MAGNETIC PROPERTIES OF $Ni_{1-x}Fe_2O_4$ MATERIALS"

BY

Md. Mostak Hossain

has been accepted as satisfactory in partial fulfillment for the degree of Master of Philosophy in Physics and certify that the student demonstrated a satisfactory knowledge of the field covered by this thesis in an oral examination held on 27th March, 1995.

BOARD OF EXAMINERS

1. Dr. Mominul Huq
   Associate Professor of Physics
   BUET, Dhaka.
   — Supervisor & Chairman

2. Dr. Tafazzal Hossain
   Professor & Head
   Dept. of Physics,
   BUET, Dhaka
   — Member

3. Dr. Gias uddin Ahmad
   Professor of Physics
   BUET, Dhaka.
   — Member

4. Dr. M. Ali Asgar
   Professor of Physics
   BUET, Dhaka.
   — Member

5. Dr. A. K. Roy
   Professor of Physics
   Dhaka University,
   Dhaka.
   — Member (External)

CERTIFICATE

This is to certify that this work was done by me and it has not been submitted elsewhere for the award of any degree or for the publication.

Countersigned

Dr. Mominul Huq

Supervisor

Signature of the candidate

Md.Mostak Hossain

ACKNOWLEDGEMENT

First and foremost I offer my grateful thanks and indebtedness to my supervisor Dr. Mominul Huq, Associate Professor, Department of Physics, Bangladesh University of Engineering and Technology, Dhaka, for his keen interest, sincere help, indispensable guidance, constant encouragement throughout the progress of this research work.

I would also like to express my gratitude to Professor Tafazzal Hossain, Head, Department of Physics , BUET, Professor Gias uddin Ahmad and Professor M. Ali Asgar of the same department for their encouragement and keen interest in my work.

I express my indebtedness to M. A. Mazid, C.S.O, and Mr. A. Hakim, Principal Engineer of Magnetic materials Division, Atomic Energy Center, Dhaka, for their generous help in course of taking measurements of magnetization and frequency Characteristics.

ABSTRACT

This thesis reports the

i. preparation and determination of lattice parameters of the nickel deficient $Ni_{1-x}Fe_2O_4$ ($x = 0.00, 0.01, \ldots, 0.10$) samples.

ii. measurements of magnetization of $Ni_{1-x}Fe_2O_4$ samples performed at room temperature of 300°K

iii. measurements of initial permeability in the frequency range of 100 KHz to 13 MHz.

The ferrite samples were prepared using conventional ceramic technique. The homogeneity, and crystal structure of the samples were checked taking the x-ray diffraction pattern. The indexing of diffraction planes show that the withdrawal of nickel content upto $x = 0.10$ does not effect the cubic structure of the parent $NiFe_2O_4$. However the cell dimension is found to increase slightly with the increasing deficiency in nickel.

Magnetization measurements performed at room temperature show that the with the decrease in nickel content the value of the magnetic moment decreases. The measurement is found to be

inconformity with the ferrimagnetic coupling in $Ni_{1-x}Fe_2O_4$ having the spin arrangement as $\uparrow Fe^{III}\ [\downarrow Ni_{1-x}\ \downarrow Fe^{II}]\ O_4$.

The measurements of the real and imaginary part of the initial permeability μ' and μ'' and the loss tangent $\tan\delta$ $(=\mu''/\mu')$, of the $Ni_{1-x}Fe_2O_4$ samples performed in the frequency range of 100 KHz to 13 MHz have been compared with that of the $NiFe_2O_4$ sample. Measurements show that the domain wall movement is the main contributing factor in determing the permeability of the samples as was the case with the $NiFe_2O_4$ sample.

CONTENTS

CHAPTER 5

CHAPTER-1

INTRODUCTION

1.1 Introduction to ferrites :

The term ferrite is used to mean magnetic oxides containing iron oxides as their main components regardless of their crystal structure [1]. Ferrites are derived crystallographically from three natural compounds the spinel, the garnet, and the magnetoplumbite. The crystallographic structure of the cubic ferrites of the spinel type and of the hexagonal ferrites of the magnetoplumbite type is determined by a closely packed structure of oxygen ions. The oxygen ions are assumed to be rigid spheres (ionic radius of oxygen ions r_{O2} = 1.32 A°). Some of the remaining hollow spaces are occupied by the smaller metal ions (radius of the metal ions $r_{Me} \approx$ 0.6A° to 1A°) The close packing of the oxygen ions consists of a layer of spheres B arranged on top of a close packed layer of spheres A (Fig.1.1). As there are twice as many interstices as B spheres, every second interstice remains unfilled. The third layer can have two positions. If it is identical with layer A, the layer stacking has a hexagonal symmetry and the resulting structure is h.c.p. with the sequence ABABAB..(Fig.1.2). If the oxygen in the third layer occupy a third position, C; the stacking has a trigonal symmetry and the structure formed is f.c.c with the sequence ABCABCABC.. (Fig.1.3). The mineral spinel crystallizes in the cubic system and contains eight formula units $MgAl_2O_4$ per unit cell. The spinel ferrites are derived from Mg Al_2O_4 by substituting Fe^{III} for Al . Any divalent cation with an ionic

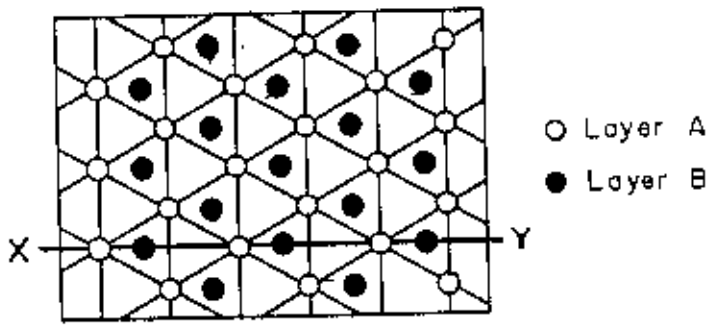

Fig.1.1 Horizontal projection of close-packed layers ABABAB....

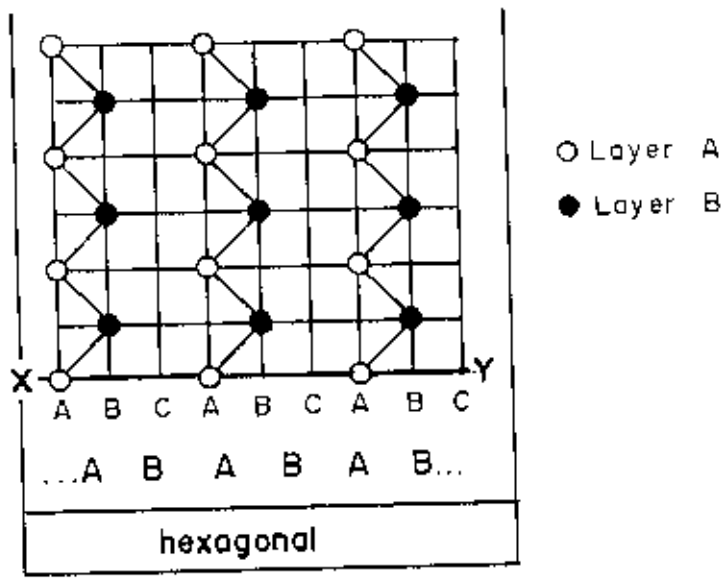

Fig.1.2 Vertical layer stracking of hexagonal close-packed structures.

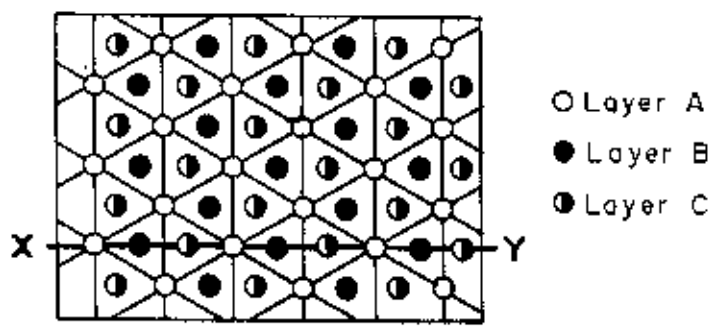

Fig.1.3 Horizontal projection of closely packed layers of ABCABCABC....

radius between about 0.6A° and 1.0 A° can be substituted for Mg, according to the general formula,

$$Me^{II}\ Fe_2^{III}O_4$$

where Me^{II} is Mg, Ni, Co, Cu, Fe Zn, Mn or Cd., for the cubic spinel lattice there are two kinds of lattice sites available for cations Fig.1.4,tetrahedral sites(A-sites) surrounded by four oxygen ions which are situated in the corners of a tetrahedrons, with only 8 of the 64 sites available in each unit cell occupied and octahedral sites (B sites), surrounded by eight oxygen ions, which are situated at the corners of an octahedron, with 16 of the 32 sites in each unit cell occupied. The hollow spaces available in an ideal closed packed structure of rigid oxygen anions would be able to incorporate on tetrahedral sites only ions with a maximum radius $r_{tetra} \leq 0.30A°$ and on octahedral sites only ions with a maximum radius $r_{oct} \leq 0.55A°$. This would result in a cell edge a = 7.47A°. To incorporate the cations mentioned above $r_{Me} \approx 0.6$ to 1A° the lattice has to be expanded somewhat. The difference in expansion of the tetrahedral and octahedral interstices is characterized by an oxygen parameter u. For an ideal lattice tetrahedral and octahedral interstices are enlarged in the same ratio. The distance between the tetrahedral sites (0,0,0) and oxygen sites (3/8,3/8,3/8) is $u_{ideal} = 3/8$. In incorporating the divalent cations, u_{obs} is always larger than u_{ideal} owing to the stronger

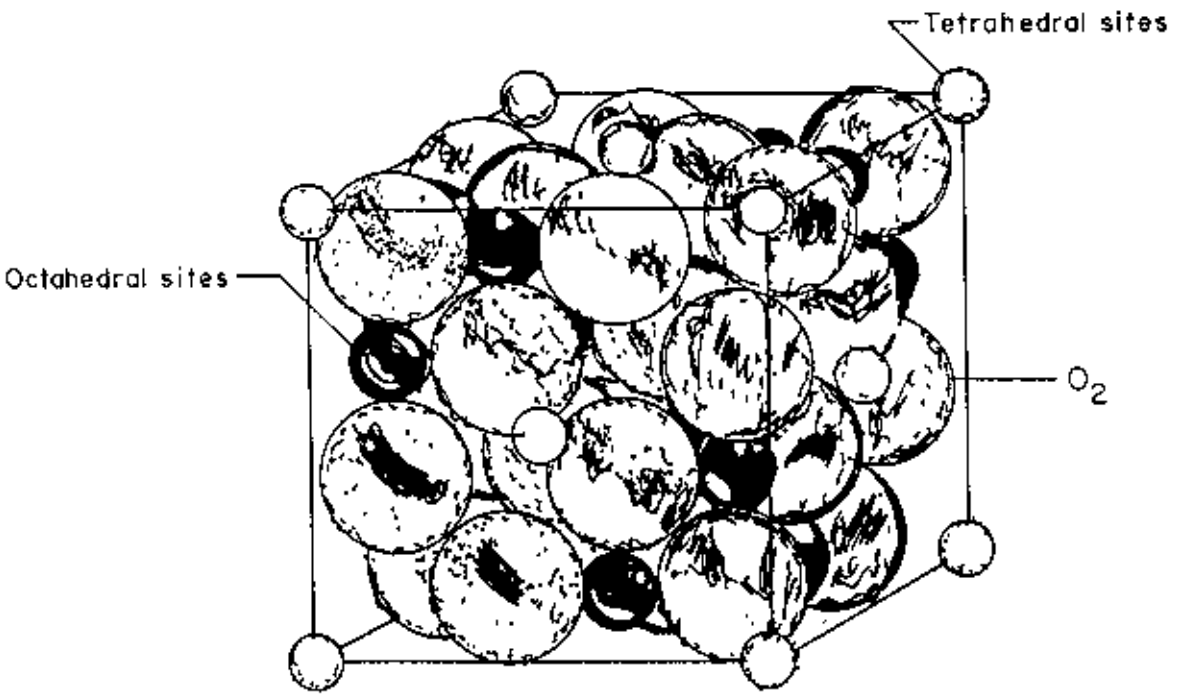

Fig.1.4 Unit cell of spinel structure.

expansion of the tetrahedral interstices at the expense of the octahedral sites. For small displacements the radii of the ions on tetrahedral sites (A sites) and octahedral sites (B sites) r_A and r_B respectively, are

$$r_A = (u - \tfrac{1}{4})\, a\sqrt{3} - r_{O^{2-}}$$
$$r_B = (5/8 - u)\, a - r_{O^{2-}}$$

regarding the distribution of the divalent and trivalent cations on the B (octahedral) and A (tetrahedral) sites experiment shows that there is a wide range of possible distributions [2], which can be represented in general terms by

$$Me_{\delta}^{II}\ Fe_{1-\delta}^{III}\ [Me_{1-\delta}^{II}\ Fe_{1+\delta}^{III}]O_4$$

Where the bracket indicates octahedral B sites. The limiting case $\delta = 1$ is called normal spinel and $\delta = 0$ is called inverse spinel. Ionic radius, electronic configuration, electrostatics energies & polarization effects are found to be the factors which determine the distribution of cations on A and B sites [3-5].

The single spinel ferrite are seldom used in actual applications. In most cases mixed compounds are prepared to obtain more favorable magnetic properties which can be adopted to various applications. In general a substitution is possible

if the ionic radius of the entering ion is of the right size and if the appropriate charge compensation is provided for cations of deviating valency. Some of the crystallographical possible substitutions for Fe^{III} that have actually been employed a to alter the magnetic moment and produce ferrites with a compensation point can be represented by [6]

$$Me_{1+\delta}^{II}\ Fe_{2-2\delta}^{III}\ Me_{\delta}^{III}\ O_4$$

Where Fe^{III} (r = 0.64A°) is replaced by Me^{III} was Al^{III} (r= 0.51A°), Cr^{III}(r = 0.63 A°) and Ga^{III}(r = 0.62A°), Fe^{III} can also be replaced by Ti^{IV}(r = 0.68A°) according to $Me_{1+\delta}^{II}\ Fe_{2-2\delta}^{III}\ Ti_{\delta}^{IV}\ O_4$. Frequently Mn^{III}(r = 0.66A°) is substituted for Fe^{III} to prevent the formation of Fe^{II} ions and thus reduce dielectric losses. If the ferric ions are partly replaced by one of the tetravalent ions Ti or Ge, the valency of an equal part of the ferric ions is lowered by one. Thus a great variety in the chemical composition of ferrimagnetic oxides with spinel structure is possible.

The garnet minerals include a quite a number of compounds characterized in general terms by the formula $Me_3^{II}Me_2^{III}\ Si_3^{IV}O_{12}$, where, Me^{II} is Ca, Fe, Mg, or Mn and Me^{III} is Al, Cr, Fe, or Mn. The magnetic iron garnets are derived from these compounds [7] by substituting $Me^{III}Fe^{III}$ for $Me^{II}\ Si^{IV}$, where Me^{III} is Y or rare earth Sm to Lu. The magnetic garnets have the general formula $Me^{III}\ Fe_5^{III}\ O_{12}$. They crystallizes in the b.c.c lattice with a

lattice constant of 12.5A°. The unit cell contains eight formula units

$$Me_3^{III}Fe_5^{III}O_{12}.$$

Magneto plumbite is a mineral of approximate formula $PbFe_{7.5}$ $Mn_{3.5}$ $Al_{0.5}$ $Ti_{0.5}$ O_{19}. The hexagonal ferrites were discovered and investigated at the Philips Research Laboratories. Their structure was determined by Braun [8]. Most of the investigations have been carried out on compounds originating from three component system $BaO\text{-}Me^{II}OFe_2O_3$ where Me^{II} is Ni, Mg, Co, Fe, Zn, Mn or Cu. and on substituted compounds. The most important substitution of Pb and Sr for Ba and that of trivalent ion Al, Ga, Cr and Mn for Fe^{III} [9]. The compounds $BaFe_{12}O_{19}$ is the most widely used ceramic permanent magnet material [10]. The sample under inrestigation in the present work is the nickel deficient spinel $Ni_{1-x}Fe_2O_4$ ferrites.

Gorter [11,12] has pointed out that solid solutions of spinels can occur with compounds which either do not exist themselves or possess a different crystal structure. The ferrite $CaFe_2O_4$ has an orthorhombic structure, but in $ZnFe_2O_4$ at high temperatures up to 35% of the Zn ion can be replaced by calcium ion with out altering the structure. The valency of the metal ions in ferrites can be determined by an analysis of the oxygen concentration. Ii appears that the sum of the valencies of the

metal ions per formula unit is greater than eight, this points to unoccupied metal ion sites, which means that the ferrite is a mixed crystal with γFe_2O_3.

1.2 Crystal structure of the spinel ferrites :

The crystal structure of $NiFe_2O_4$ was first determined by Bragg [13] and by Nishikawa [14]. The unit cell of the spinel lattice that has cubic symmetry contains eight molecules of $NiFe_2O_4$. In this cubic close packed structure two kinds of interstitial sites occur, the tetrahedral and the octahedral sites (called A and B sites respectively) Fig.1.5. In the tetrahedral sites the Fe^{3+} and the octahedral sites Fe^{3+} & Ni^{2+} are occupied. The oxygen ions are surrounded by tetrahedral & octahedral sites.

To describe the structure we can subdivide the unit cube with edge 'a' into eight octants with edge $\frac{1}{4}$ a . The oxygen ions are positioned in the same way in all octants. Each octant contains four oxygen ions (anions) which form the corners of a tetrahedron. as in Fig.1.5. The edge of the f.c.c. oxygen lattice is $\frac{1}{4}$ a. As regards the positions of the cations, the octants in the elementary cube that have only one edge in common are identical.In Fig.1.5 the positions of the ions are indicated in two adjacent octants.

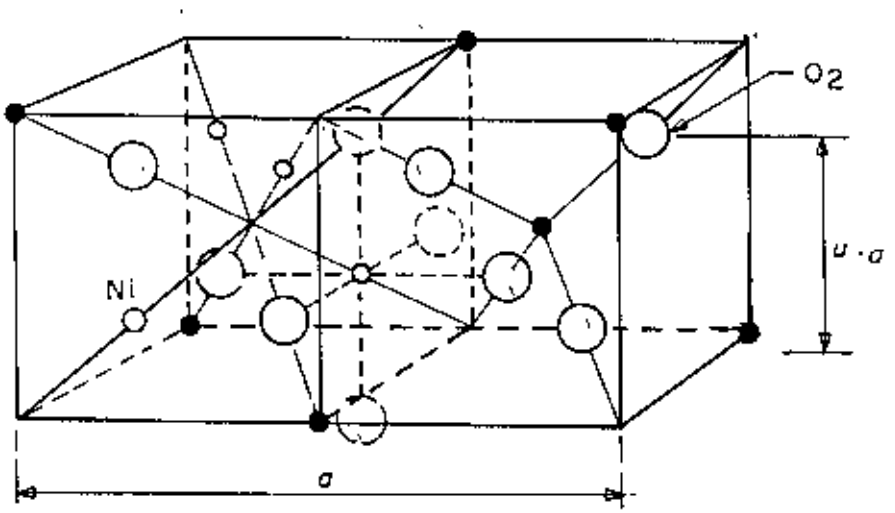

Fig.1.5 Two octants of the spinel structure, the large spheres represent the oxygen ions. The small black and white spheres represent the metal ions on tetrahedral and octahedral sites, respectively.

The occupied tetrahedral sites of one of the octants are thus in the center and on four of the eight corners of the octant. In the adjacent octant the central site is not occupied by a metal ion but, owing to translation symmetry, half of the corner sites are again occupied. It can be seen that the occupied tetrahedral sites (A sites) form two inter-penetrating f.c.c. lattices having an edge a. which are displaced with respect to each other over a distance $(1/4)a\sqrt{3}$ in the direction of the body diagonal of a cube. The occupied octahedral sites (B sites) are found only in the other type of octant. The four metal ions are situated at sites analogous to those of the oxygen ions that is on one quarter length of the diagonal from the other ends of the four body diagonals of the octant. Consequently the oxygen and (octahedral) metal ions in this octant together span a cube with edge $\frac{1}{2}$ a. All octahedral ions together lie on four inter-penetrating f.c.c. lattices with edge a, which are displaced with respect to each other over a distance in the direction of the face diagonals of the cube.

The surrounding of a tetrahedral ion by the other ions has strictly cubic symmetry. This is not the case for an individual octahedral ion. The octahedral ions, of course, are cubically surrounded as far as concerns the oxygen ions in their ideal lattice, but not as regards their environment by the neighboring metal ions. Fig.1.6 shows the environment of B ions by other B ions. The two cubes shown do not lie each in one octant of

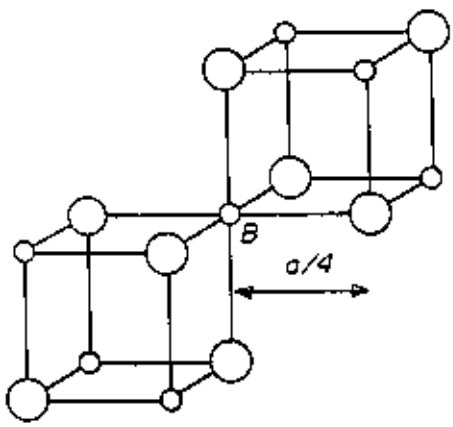

Fig.1.6 The nearest neighbours of a cation on octahedral (B) site in the spinel structure,large spheres are oxygen ions, small spheres are metal ions on octahedral (B) sites.

Fig.1.5 four B ions lie in one particular octant, the three other B ions belong to three different octants. It can be seen from this that the symmetry of the environment of an octahedral site by nearest metal neighbors is lower than cubic, and that only one of the (111) directions is an axis of symmetry. However in the whole lattice cell all (111) directions occur equally as symmetry axis, so that the overall symmetry never the less remains cubic.

1.3 Brief survey of the ferrite materials:

High magnetic permeability and high electrical resistivity and lower eddy current loss allows ferrites use to higher frequencies then possible with metals. The ferrites used at frequencies from audio to about 500 MHz are generally termed as non-microwave ferrites (r.f. ferrites), or soft ferrites and the ferrites used at frequencies between 100 MHz and the highest microwave frequencies now in use i.e. 500 GHz are termed microwave ferrites. The r.f. ferrite materials can be divided into the following classes with respect to their application.

(i) Ferrites for application at frequencies below about 1 MHz as core materials for transformers and for coils in filter circuits (μ ferrites): The primary requirement for ferrites used in transformers is high permeability. Other factors, such as losses and

temperature stability are less important. In cases where high-frequency signals have to be handled, a high value of saturation magnetization is desired. In filter circuits for carrier telephony equipment ferrites are required with a small loss factor and a permeability which is approximately constant for changes of ambient temperature.

(ii) Ferrites as core materials in coils and transformers and for antenna rods, to be used at frequencies above 1 MHz in radio and television equipment, in general high permeability and low losses are desired.

(iii) Ferrites used as nonlinear circuit elements: Such applications as magnetic amplifiers are based on the phenomenon that the induction is a non-linear function of the field amplitude.

Two categories of ferrite devices are in use in the microwave frequency range. The first category comprises non-reciprocal devices viz: isolators or circulators which is essentially used in radar. The second category comprises reciprocal devices viz: electrically controlled phase shifters. The first microwave device using ferrites was by Hogan from Bell Labs in 1952. This was a circulator based on Faraday rotation effect, working at about 9 GHz. All the application of

ferrites to microwaves since then have used the same basic principle. In all cases, the techniques in microwave applications used a ferrite structure whose permeability is controlled by the gyromagnetic phenomena. This permeability depends, firstly, on the values of magnetization and static applied magnetic field (basis for electrically controlled phase shifters) and, secondly, on the polarization of the electromagnetic waves relative to the direction of magnetization (basis for non-reciprocal devices)[15-21]. The three main classes of ferrite compounds are garnet ferrites, spinel ferrites and hexagonal ferrites.

1.3.1 Garnet ferrites:

The garnet microwave ferrites were discovered by Bertaut and Forrat [22]. Following the work of Geller [23,24] who designed and developed various types of substitution, the importance of substituted garnet in microwave application has been constantly growing. They were derived from Yttrium-iron-garnet $Y_3Fe_5O_{12}$. The characteristics of garnets are their low magnetization value (300 to 1900 G) and small line widths, these materials are suitable for the devices operating at frequencies any where between a few hundred MHz and 9000 MHz [25-29]. In Yttrium iron garnet (YIG) the Fe ions occupy two types of crystallographic sites; for one molecule, there are three Fe^{3+} ions in the tetrahedral sites and two Fe^{3+} ions in the

octahedral sites. The magnetization

$$M_s = | M_{tetra} - M_{Octa} |$$

Two methods of reducing M_s of YIG have been in use:

(a) The first is substituting for Fe-ions, non-magnetic aluminium ions which will occupy tetrahedral sites.

viz: $Y_3Fe_{5-5y}\ Al_{3y}\ O_{12}$, ($0 \leq y \leq 0.27$)

(b) The second is substituting for non-magnetic Yttrium ions, gadolinium ions whose magnetization counteracts the resultant of the magnetization of Fe-ions.

In the aluminium substituted garnet, as the curie temperature T_c also decreases, the stability with temperature is lower for these ferrites. The line width in these materials remain very low.

Gadolinium substituted garnets have the chemical formula:

$$Y_{3-3x}\ Gd_{3x}\ Fe_5\ O_{12}$$

In these ferrites the magnetization decreases without practically changing T_c. This results in a stabilization of M_s with temperature. For $x \geq 0.4$ this type of garnet is seldom used, because of the comparatively broad linewidth.

Since Al and Gd substitutions in Yttrium iron garnet (YIG) decrease M_s, having opposite effects on stability with temperature, and line width an intermediate compromise have been found in compositions.

$$Y_{3-3x}\ Gd_{3x}\ Fe_{5-5z}\ Al_{5z}\ O_{12}.$$

In general, microwave poly crystalline ferrites cannot be used when the microwave field exceeds a critical field, beyond which non-linear effects appear. One of the solutions to raise the value of this critical field consists in increasing the spin-wave linewidth. A very simple way of increasing linewidth consists in substituting partly for Yttrium, in the conventional garnets, a small quantity of rare-earth ions. This gives the chemical formula.

$$Y_{3-3x-3m}\ Gd_{3x}\ Me_{3m}\ Fe_{5-5z}\ Al_{5z}\ O_{12}.$$

The effect of various rare-earth, Me (Ce, Nd, Sm, Eu, Tb, Dy, Ho, Er, Yb) has been studied by many authors [30-33] and substitution of Dy or Ho is found to be most effective. The substitution of Dy or Ho for Y leads to decrease in magnetization. However, as m is very low $< 5\times10^{-2}$, the effect on Ms at room temperature and Tc is almost negligible. The line width increases linearly with m for this low level of

substitution.

The hysteresis loop of conventional, well densified garnets is fairly rectangular. The coercive force is typically of the order of 0.5 to 1.2 Oe. These characteristics made this ferrite suitable for use in controlling hysteresis loops in switching devices involving residual magnetization (latching devices).

1.3.2 Spinel ferrites:

Spinel ferrite were the first type of ferrites to be used for microwave applications (1952); they had previously been used for h.f. applications. The advantage of spinel ferrites is that their magnetization are higher than those of garnets. Properties of the some of the spinel ferrites of technical importance is described below.

Mn-Mg ferrites:

The basic chemical composition is $Mn_x\ Mg_y\ Fe_z\ O_4$ with $x + y + z = 3$. Although they were the first ferrites used for microwave applications, these ferrites are fairly complex. The Mn^{2+} ion has the same electronic configuration as Fe^{3+}. However, part of the manganese can exist in the Mn^{3+} state. In addition, the metallic ions are distributed between tetrahedral and

octahedral sites in a manner which depends upon the heat treatment applied; thus x, y and z are determined experimentally, in optimizing the characteristics, for each of the synthesis techniques used. Magnetization of from M_s =160 to 190 kA/m ($4\pi J_s$=2000-2400 G), with Curie temperatures between 270 and 300°C, are obtained. The linewidths ΔH due mainly to broadening by anisotropy, are of the order of 25 kA/m (300 Oe), while spin wave linewidths are low, of the order of 0.3 kA/m (3.5 Oe). These ferrites are therefore applicable to low-power microwave usage in the 7 to 15 GHz range, where temperature conditions are not severe. Useful compositions appear to be situated, in practice, in the intervals defined by

$$0.10 < x < 0.15 \qquad 0.4 < y < 0.5 \qquad 0.7 < z < 0.9.$$

Magnetization can therefore be reduced by substituting aluminium for part of the iron (usually between 0 and 10%) to the detriment of the Curie temperature and temperature coefficient.The hysteresis loop of this type of material is rectangular in shape: the coercive force field is fairly weak (0.1 kA/m approximately 1 Oe).

Nickel ferrites:

The nickel ferrite [34] $NiFe_2O_4$ has a curie temperate of about 570°C and the magnetization M_s = 255 kA/m ($4\pi J_s$ = 3200 G) is therefore much more stable with temperature ($\alpha_{-40}^{+85} \approx 0.43$

x 10^{-3}) than those of the former materials. However, the Ni ion, having an orbital magnetic moment, is a relaxing ion; it follows that the Ni ferrite is not suitable for devices with very low insertion losses, but rather for those required to withstand a certain peak power. The effect of the magnetocrystalline anisotropy on ΔH of the Ni ferrite is fairly high, but it can be reduced by low substitutions of Co^{2+} whose anisotropy is very high and is of sign opposite to that of their iron ions. This cobalt ion further increase ΔH_k. This leads to a composition of the $N_{1-x}Co_xFe_2O_4$ type (with $x \approx 0.02$). However, for physicochemical reasons, it is difficult to obtain a dense product with no dielectric losses. In order to reduce these as much as possible, a small percentage of manganese is added. This yields a material with ΔH=20 kA/m(250 Oe), ΔH_k = 2 kA/m (25 Oe) and $\tan \delta < 10^{-3}$, all these quantities being measured at 9 GHz.

Materials with a lower magnetization are obtained by substitution of aluminium for a particular quantity of iron [35]. The Al^{3+} ions preferably occupy octahedral sites in spinel structures, but a certain quantity of Al^{3+} ions occupy tetrahedral sites in a manner which depends upon the heat treatment.

Magnetization can be raised by partial substitution of zinc for the nickel, as expressed by the formula $Ni_{1-x}Zn_xFe_2O_4$ in a

substitution interval $0 < x < 0.5$. The Curie point decreases with x [36].

Lithium ferrites:

The lithium ferrite [37,38] $LiFe_5O_8$ or $Li_{1/2}Fe_{5/2}O_4$ has a magnetization of approximately M_s = 285 kA/m ($4\pi M_s$ = 3600 G) with a high Curie temperature, approximately 645^{0}C [39,40] so that its stability with temperature is similar to that of the Ni ferrite. It should be noted that, like the yttrium-iron garnet, the Li garnet is a substance which only has trivalent iron ions as magnetic ions. This results in a very narrow spin wave linewidth ΔH_k, of the order of 0.25 kA/m (3 Oe). This makes the lithium ion ferrites more suitable for uses at low microwave power levels with low direct losses.

1.3.3 Hexagonal ferrites:

Apart from those having garnet and spinel structures, the ferrites those are in use at microwave frequencies has a hexagonal structure. These materials have an axis of symmetry, c, and a high magnetocrystalline anisotropy. They are prepared by the ceramic techniques similar to that of spinels and garnets, subject to a few variants. In particular, during pressing the grains are oriented by a magnetic field in order to align the c-axes of all the crystallites in the same direction.

This yields a sample similar to a permanent magnet. When a microwave field is applied in a plane perpendicular to the magnetization direction, a gyro-resonance effect is observed. The resonance frequency f_r is related to the applied field Hz (in the direction of magnetization) by

$$f_r = (\gamma\mu_0/2\pi)\{[H_z + H_a + (N_x-N_z)M_z][H_z + H_a + (N_y - N_z)M_z]\}^{1/2}.$$

where H_a is the anisotropy field. N_x, N_y, N_z are the demagnetizing factors Owing to the high values of H_a, which may be up to 2780 kA/m (35 kOe), resonance may occur at millimetric frequencies in the absence of a continuous field, H_z, or with a weak field, H_z, which is therefore easy to handle. This is the main advantage of this type of material. Composition of hexagonal ferrites [41] which are suitable for microwave applications can be classiffied as M-type and W-type [42-50].

M-type hexagonal ferrites:

These ferrites are derived from barium or strontium ferrites, whose formulae are $BaFe_{12}O_{19}$ and $SrFe_{12}O_{19}$, by partial substitutions of Al^{3+} ions (or Ga^{3+} or Cr^{3+} ions) for Fe^{3+} ions, which causes the magnetization to increase and the magneto-crystalline anisotropy field to increase; by substitutions of the groups Ti^{4+} Me^{2+} or Ge^{4+} Me^{2+} (with Me^{2+} = Co, Ni, Zn....) for Fe^{3+} ions, which cases both the magnetization and the

anisotropy field to decrease; by combined substitutions of both of the above types, which results in better stability of H_a with temperature.

W-type hexagonal ferrites:

These are derived from barium ferrites, whose formula is $Ni_2BaFe_{16}O_{27}$, by partial substitution of Al^{3+} ions for Fe^{3+} ions, which causes the magnetization to increase and the anisotropy field to increase; by partial substitution of Co^{2+} ions for Ni^{2+} ions, which causes the anisotropy field to decrease, while the magnetization remains unchanged. Lastly, the W-type ferrites can be used to produce devices such as circulators with resonance frequencies lower than those of the M-type.

1.4 Present work:

$NiFe_2O_4$ is one of the first ferrites to be developed. The chemical and magnetic structures are well known for the compound $NiFe_2O_4$. It is ferrimagnetic and its structure is cubic. The structural and magnetic transformatiou of the degradingNi_x Fe_2O_4 (x = 1.0 to 0.10 in steps of 0.10) has been reported by Subramanyum et al [50]. From the initial magnetic susceptibility measurements on these specimens at a fixed microwave frequency of 9.5 GHz they concluded that a sharp ferrimagnetic - antiferromagnetic transition occurs in $Ni_{0.1}$ Fe_2O_4 that is at x =

0.10. From the X-ray diffraction study they also indicated that at x=0.10 there also occurs a change in crystal symmetry. They indicated that at x = 0.90 the sample remains cubic and for x = 0.80 down to x = 0.10 the structure was cubic plus rhombohedral; and at x = 0.00 i.e. for αFe_2O_4 the structure is rhombohedral.

In the present work our aim is to investigate the structural and magnetic properties of Ni_{1-x} Fe_2O_4 in a finer detail in the range x=0.00 to 0.10. For this purpose samples with x = 0.00 to 0.10 in steps of 0.01 have been prepared. The X-ray diffractometer study has been performed to study the crystal structure and homogeneity of the samples. The finding is given in chapter 2. Measurements of magnetization have been performed on these specimens to study the spin arrangements in the specimens with the decrease in nickel content. The result is given in chapter 3. The initial permeability of the nickel deficient ferrite specimens that is the magnetic spectra of the real and imaginary part of the initial permeability μ' and μ'' and loss tangent tanδ of these nickel deficient samples have been investigated in the frequency range of 100KHz to 13MHz. The findings are given in chapter 4. It is beleived that the investigations on these nickel deficient ferrites will reveal the mechanism responsible for their behaviour.

CHAPTER-2

PREPARATION AND IDENTIFICATIONOF $Ni_{1-x}Fe_2O_4$.

2.1 Methodology of the ferrite preparation:

Nearly all ferrites, the spinels the garnet, and the magnetoiplumbite type decomposes if it is attempted to melt them under normal conditions. This is because the oxygen splits off at higher temperature, reducing Fe^{III} to Fe^{II}. This implies that the ferrites cannot be prepared by melting as is the case with metals. The normal technology for processing ferrite materials is thus a ceramic technology. The starting materials mostly oxides or compounds (such as carbonates, oxalates, or sulphates) which are easily convertible into oxides by thermal decomposition are mixed and converted into the desired products by a solid state reaction at higher temperature between 800 and 1500°C. These prefired powders are then pressed into desired shapes and densified by a sintering process at elavated temperature. The three processing steps-reaction, molding, and densification some times overlap. Some starts with molding. They press an unreacted mixture and carry out the reaction and sintering in one operation during a single firing process.

2.2 Preparation and identification of the $Ni_{1-x}Fe_2O_4$ samples:

The $Ni_{1-x}Fe_2O_4$ ferrites for x= 0.01 to 0.10 were synthesized using the solid state reaction method. The starting materials NiO and Fe_2O_3 used were of purity 99.99% in the form of powders supplied by BDH, England. The stoichiometric proportion of the

constituent component were weighed within an accuracy of 100 micro-grams using an Sartorius electric digital analytical balance. The powders were then thoroughly mixed using a ceramic mortar and a pestle for 3 to 4 hours in presence of acetone. The resultant powders were then ball milled for 6 to 8 hours to produce fine powders of the mixed constituents. These mixed powders were then spread on a clean ceramic boat washed with acetone and then with distilled water. Boats with the powders were fired for 2.5 hours at a temperature of 1350°C in air atmosphere in a programmable furnace NABER (Model-HT 08/16 Germany). The temperature of the furnace could be maintained with in an accuracy of ±1°C. In heating and cooling the specimen the following cycle was used. The sample was first heated from room temperature of 24°C to 300°C in one hour then the temperature was raised to 1350°C in another sixty minutes. The sample was heated at this temperature for half an hour. The sample was then cooled to 900°C in sixty minutes then to 600°C in another twenty minutes. When the temperature of the fnrnace reached the set temperature of 600°C, the furnace was switched off to cool down to room temperature. The same procedure was applied for all the samples. The furnace cooled samples were then crushed and made to fine powders. Part of these powder specimens ground to powders of less than 100 micron size were put to x-ray investigation for their identification. X-ray diffraction pattern of these powders were taken in an X-ray diffarctometer using CuK_{α} radiation.

2.3 Results and discussion

The diffraction patterns obtained for the samples of different compositions are shown in Fig.2.1 to 2.5. The 2θ values of the diffraction peaks obtained for the different specimens i.e. for different concentration of x along with the corresponding indexing of the planes (hkl) are given in Table 1. The lattice parameter 'a' of the samples were then calculated from the relation:

$$a = \sqrt{n}d^2$$

where $n = h^2+k^2+l^2$ and $d = \lambda/2\sin\theta$; λ is the wave length of the Cuk_α radiation. Table 2 shows the [redacted] values of the lattice parameter 'a' calculated from the 2θ values obtained for different crystallographic planes. To reduce the error in the lattice parameter 'a' due to the uncertainty in the angle of scattering which is significant at low diffraction angle the values of 'a' were extraplotated against the Taylor, Sinclair [1] Nelson Riley function [2]

$$f(\theta) = \frac{1}{2}\left(\frac{\cos^2\theta}{\sin\theta} + \frac{\cos^2\theta}{\theta}\right)$$

The curves are given in Fig. 2.6a to 2.6e. The extrapolated value of 'a' corresponding to 2θ=180 degree is shown at the last

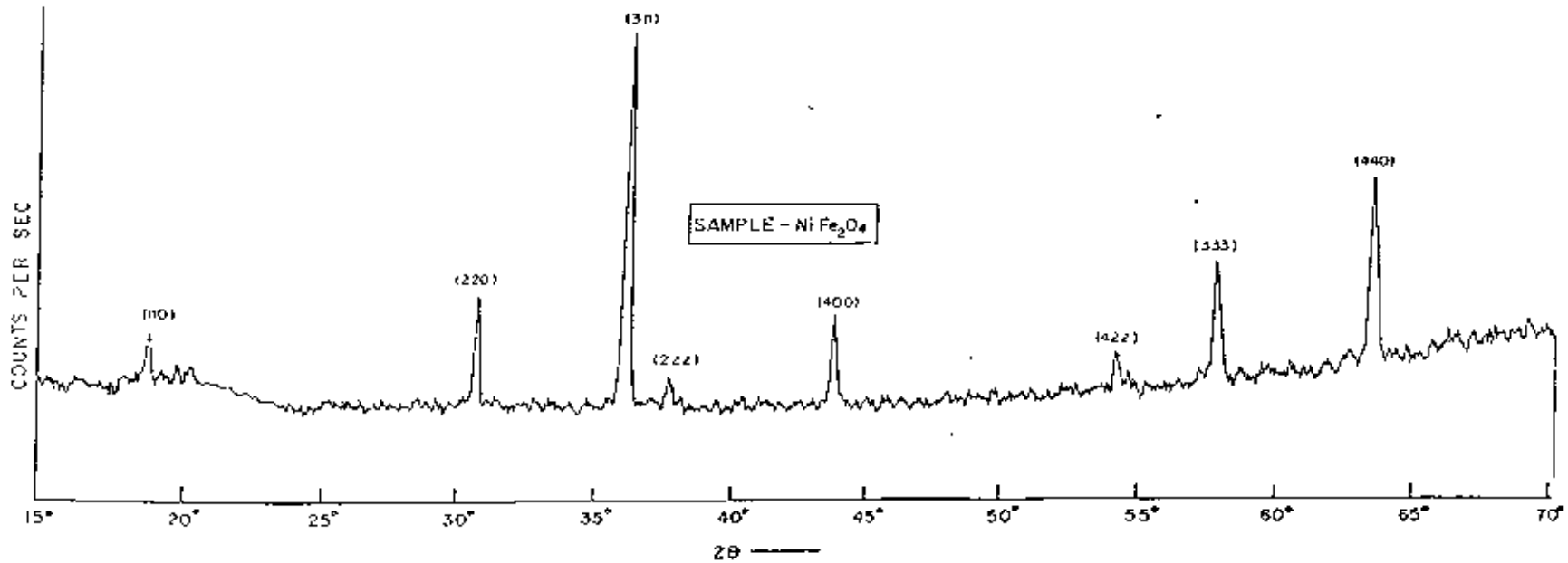

Fig.2.1 X-ray diffraction pattern of $NiFe_2O_4$ sample.

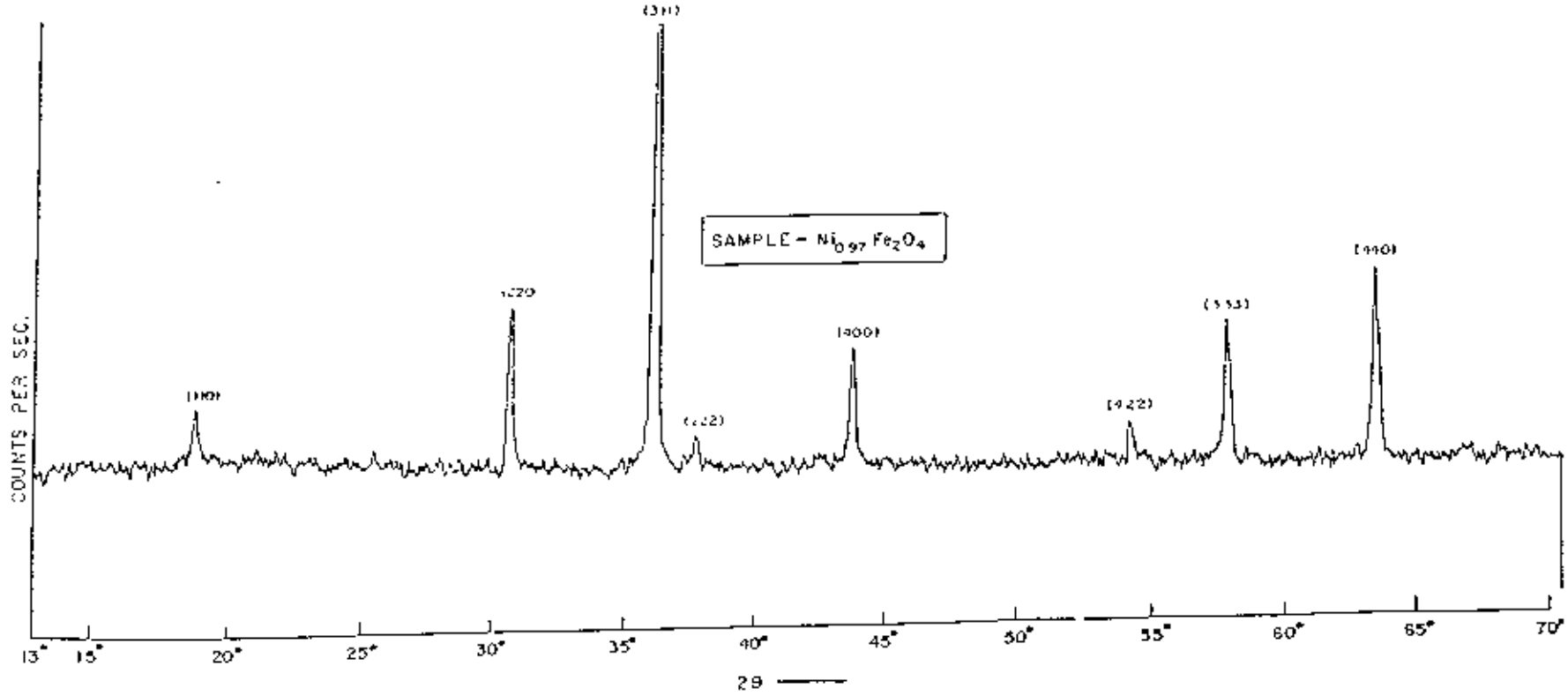

Fig.2.2 X-ray diffraction pattern of $Ni_{0.97}Fe_2O_4$ sample.

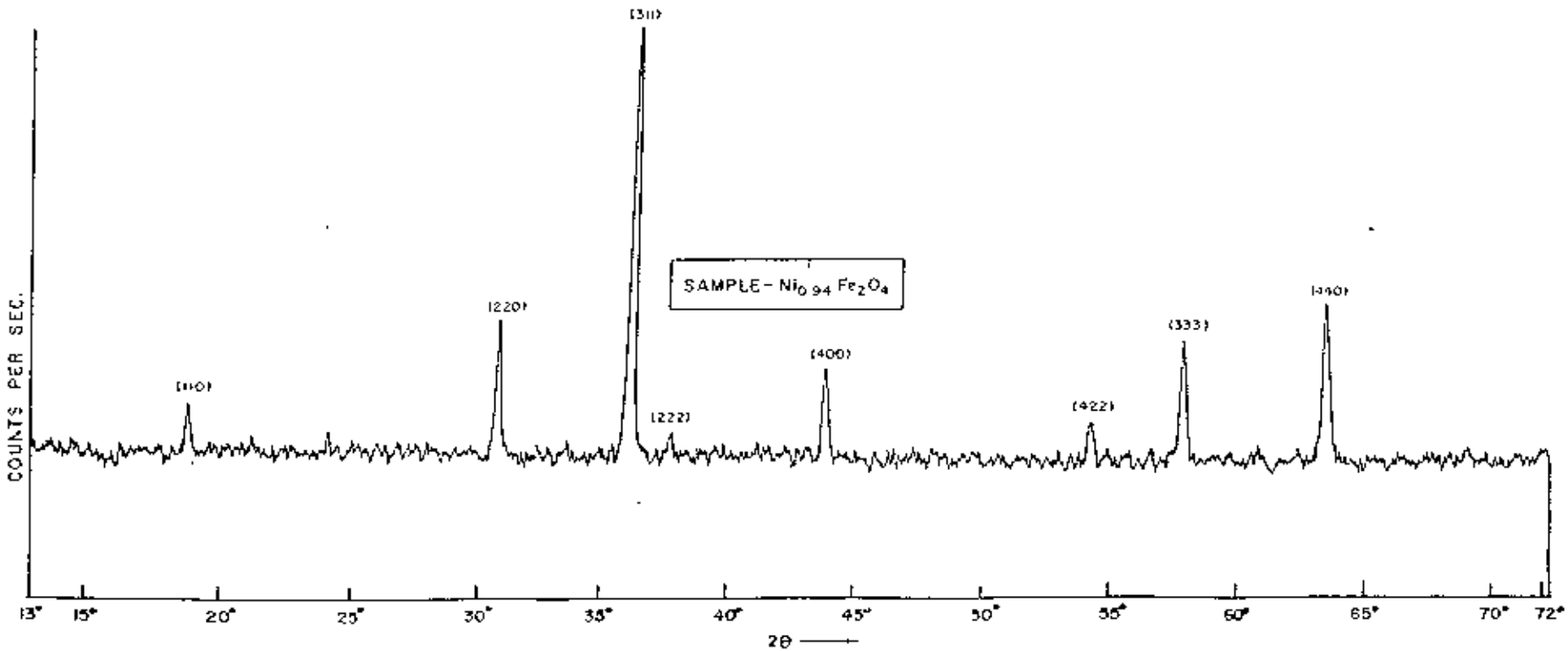

Fig.2.3 X-ray diffraction pattern of $Ni_{0.94}Fe_2O_4$ sample.

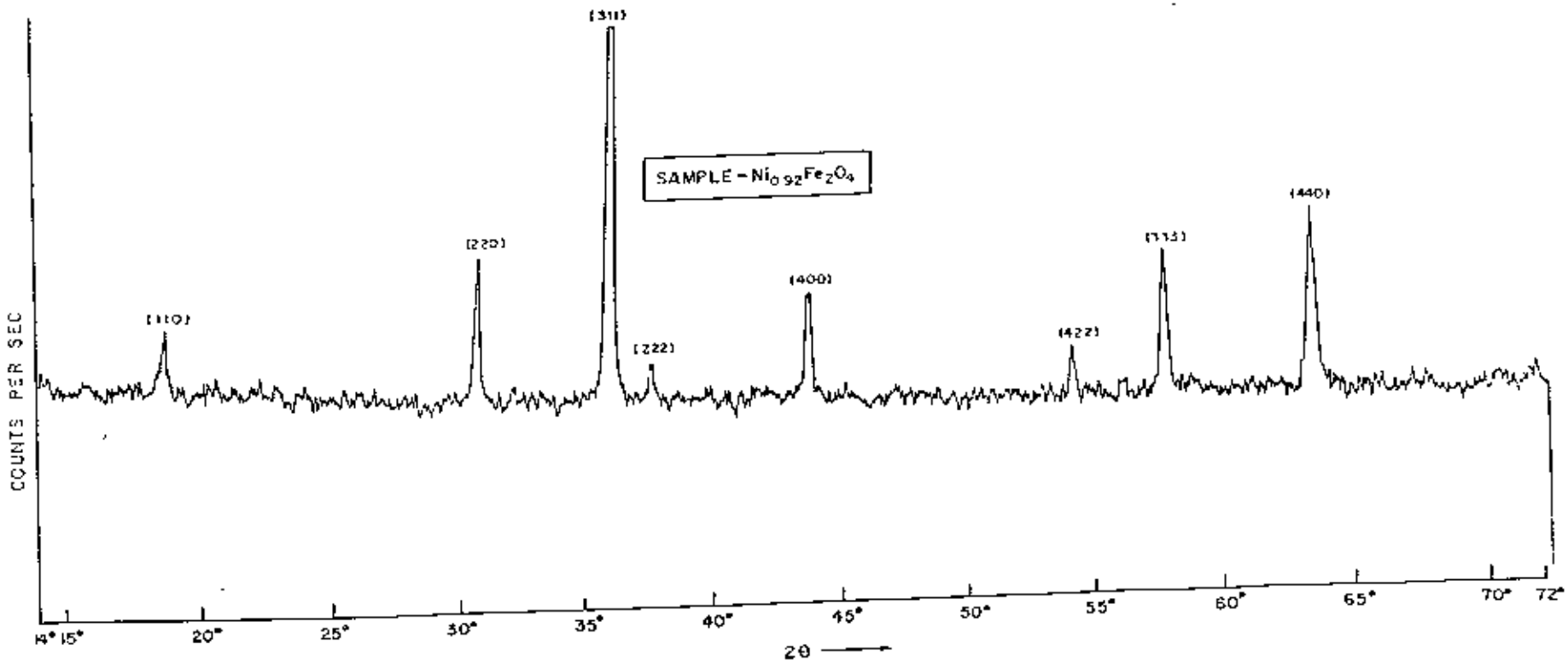

Fig.2.4 X-ray diffraction pattern of $Ni_{0.92}Fe_2O_4$ sample.

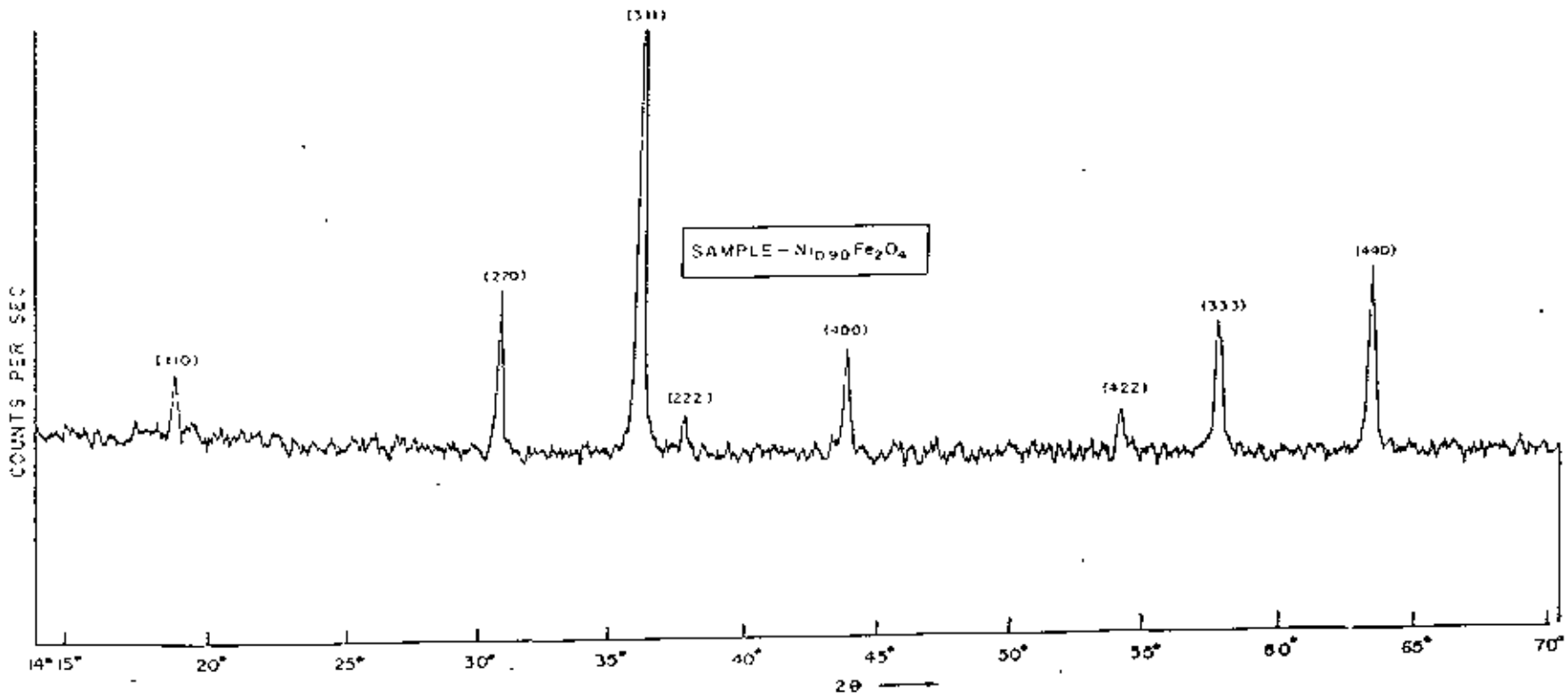

Fig.2.5 X-ray diffraction pattern of $Ni_{0.90}Fe_2O_4$ sample.

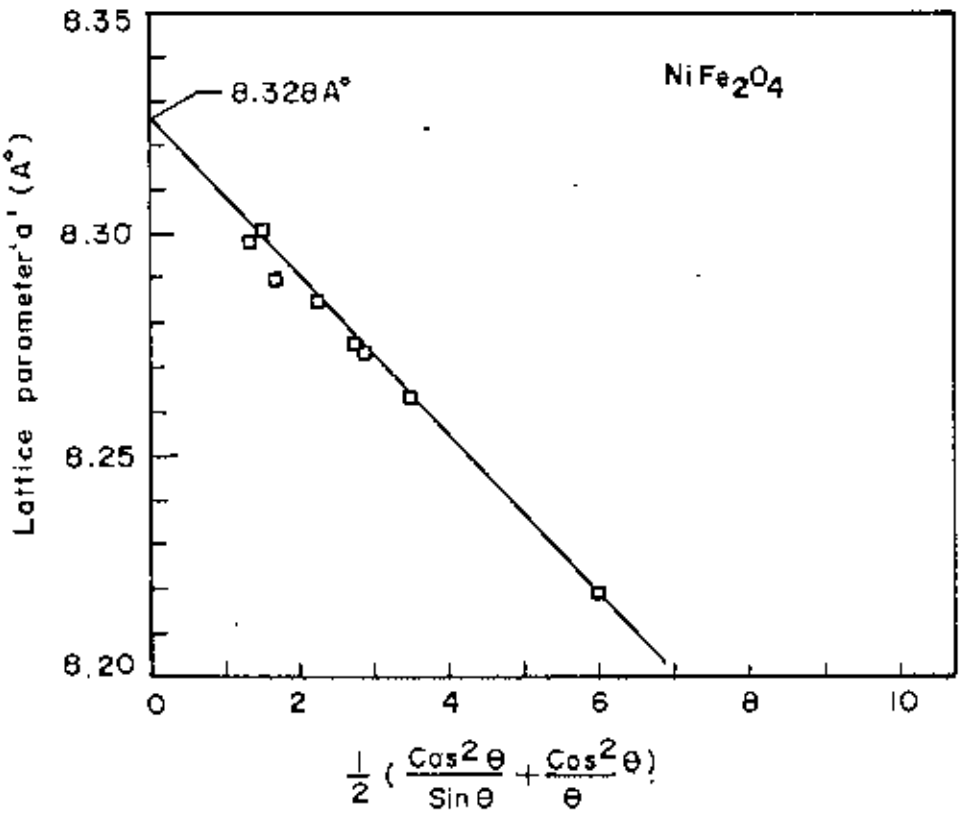

Fig.2.6a Lattice parameter 'a'(A') against Nelson-Rileys extrapolation function.

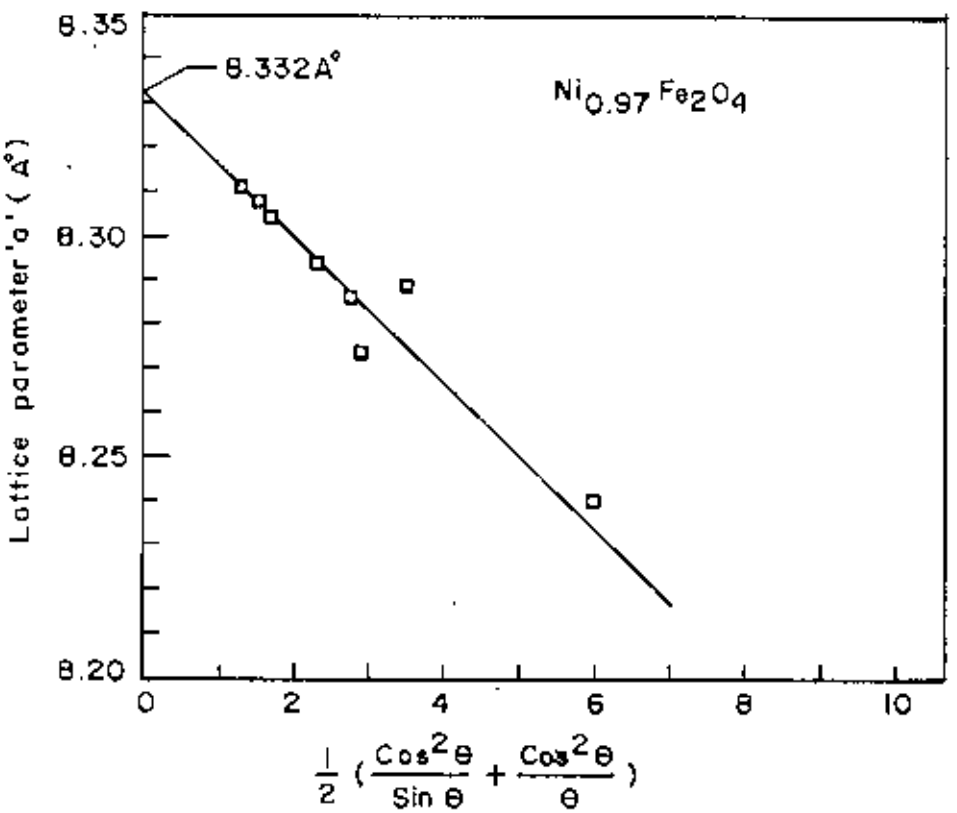

Fig.2.6b Lattice parameter `a'(A°) against Nelson-Rileys extrapolation function.

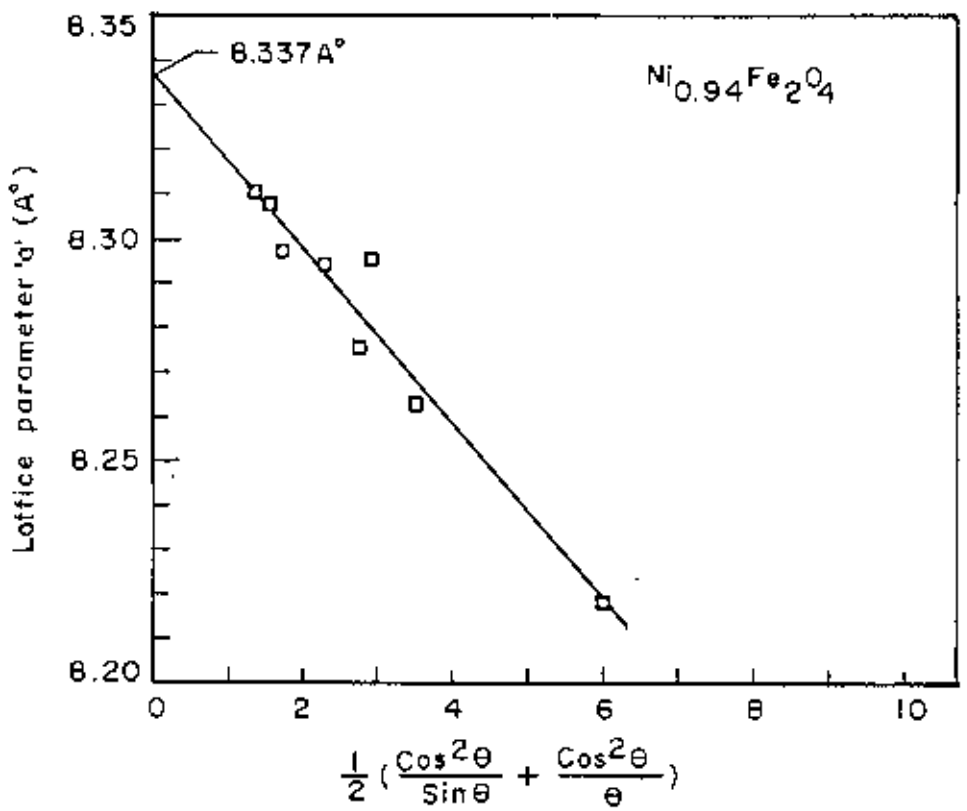

Fig.2.6c Lattice parameter `a'(A') against Nelson-Rileys extrapolation function.

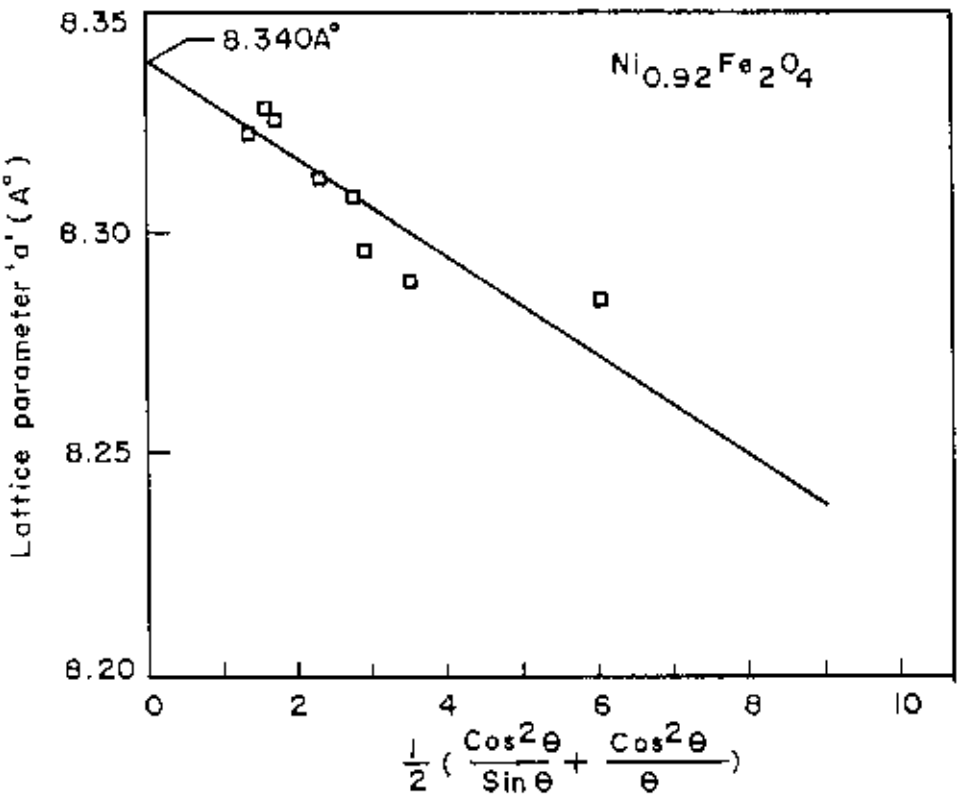

Fig.2.6d Lattice parameter 'a'(A°) against Nelson-Rileys extrapolation function.

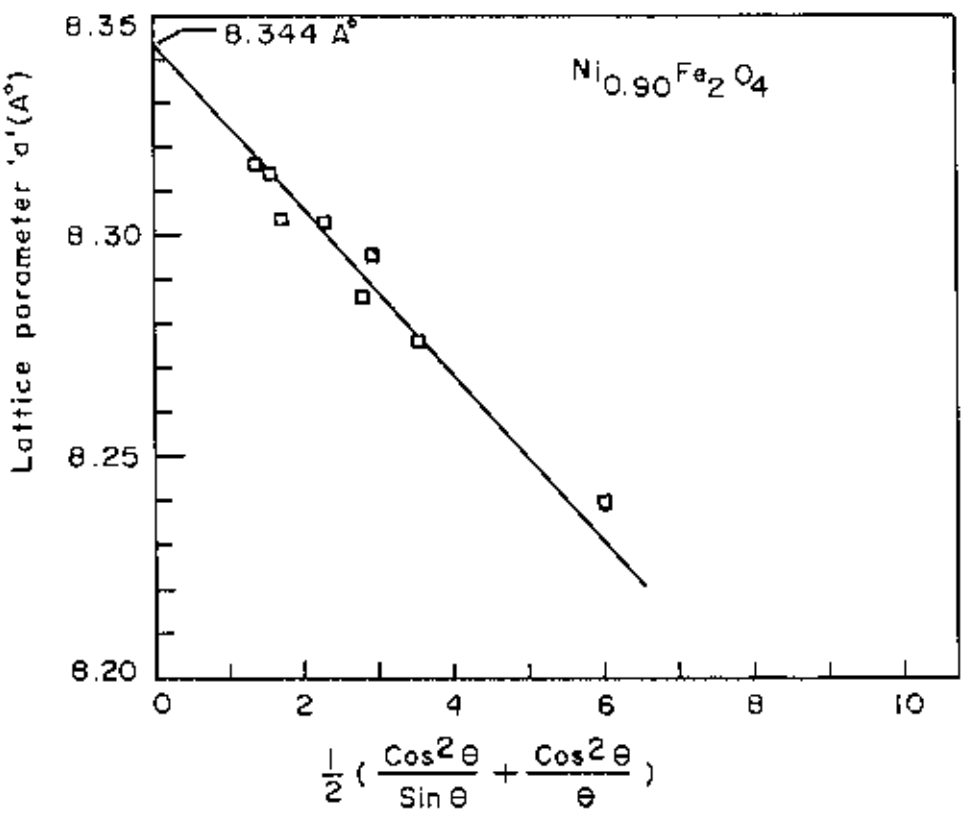

Fig.2.6e Lattice parameter `a'(A') against Nelson-Rileys extrapolation function.

row of Table 2. The variation in the value of 'a' for different nickel concentration in $Ni_{1-x}Fe_2O_4$ is shown in Fig.2.7 . The lattice parameter obtained for the $NiFe_2O_4$ is in close agreement with the reported value of 8.325 [3]

It is seen that the diffration peaks occur almost at the identical angles for all the compositions and no additional peaks is seen to appear for the nickel deficient samples . This suggests that the crystal structure of the specimens remains unchanged and there is no trace of second phase. However the value of the lattice parameter 'a' is found to increase slightly with the increased value of x.

It is to be mentioned that sintered powders prepared thus were used for preparing specimens for the measurements of magnetization and permeability.

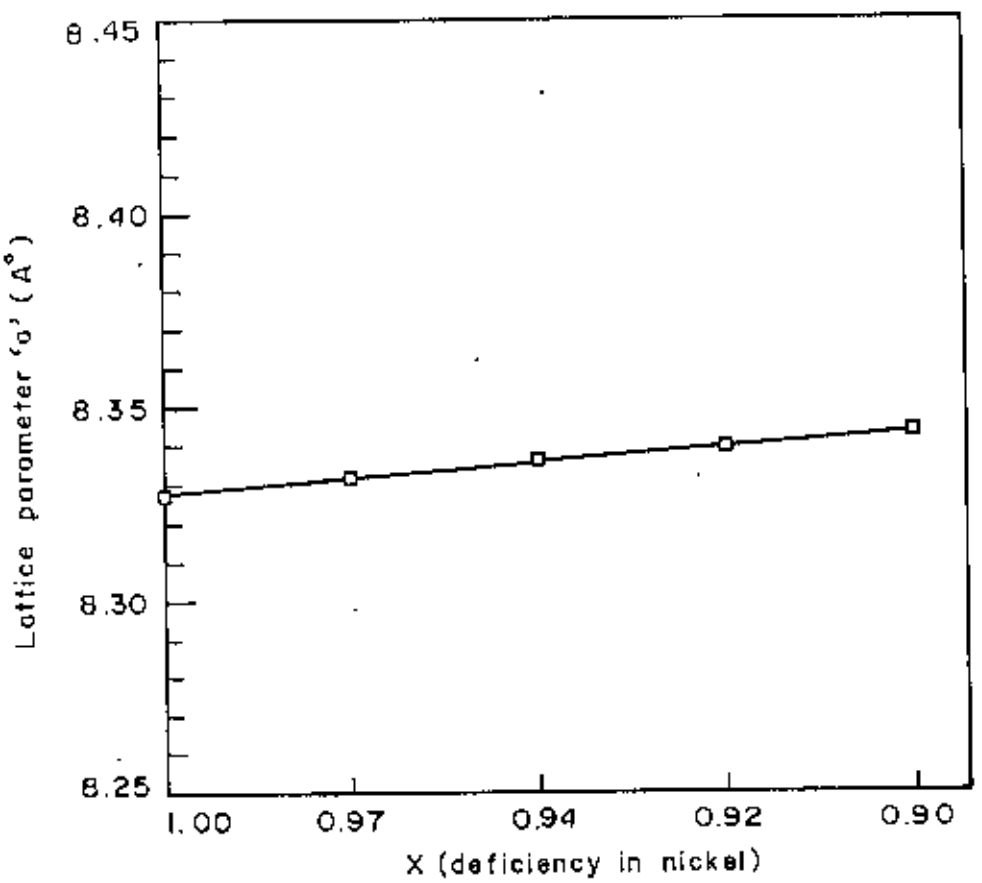

Fig.2.7 The lattice parameter of the $Ni_{1-x}Fe_2O_4$ samples as a function of x

Table-1

Peak numbers	2θ values of the diffraction peaks				(hkl)
1	18.65	18.70	18.55	18.65	(111)
2	30.50	30.60	30.50	30.55	(220)
3	36.00	35.90	35.90	35.90	(311)
4	37.60	37.65	37.50	37.60	(222)
5	43.65	43.65	43.55	43.60	(400)
6	54.10	54.15	53.95	54.10	(422)
7	57.65	57.65	57.50	57.60	(333)
8	63.30	63.30	63.20	63.25	(440)
X in $Ni_{1-x}Fe_2O_4$	00.03	00.06	00.08	00.10	

Table-2

(hkl)	Value of the lattice parameter 'a' from $a=\sqrt{(nd^2)}$ for different specimens				
	$NiFe_2O_4$	$Ni_{0.97}Fe_2O_4$	$Ni_{0.94}Fe_2O_4$	$Ni_{0.92}Fe_2O_4$	$Ni_{0.90}Fe_2O_4$
110	8.2186	8.2405	8.2186	8.2845	8.2405
220	8.2632	8.2896	8.2632	8.2896	8.2764
311	8.2739	8.2739	8.2962	8.2962	8.2962
222	8.2760	8.2866	8.2759	8.3079	8.2866
400	8.2853	8.2943	8.2943	8.3124	8.3034
422	8.2903	8.2903	8.3045	8.2974	8.3045
333	8.3017	8.3083	8.3083	8.3281	8.3149
440	8.2990	8.3107	8.3107	8.3225	8.3166
Extrapolated Value of 'a'	8.328	8.3320	8.3370	8.3400	8.3440

CHAPTER – 3

MAGNETIZATION MEASUREMENTS OF $Ni_{1-X}Fe_2O_4$

3.1 Introduction to the theory of magnetism:

Magnetic properties of solids is of atomic origin. An atom with an unfilled shell will have the uncompensated spin in its orbit and spin magnetic moment along with the orbital angular momentum of the electron give rise to magnetism. Generally the magnetic contribution due to outermost electrons called Pauli [1] paramagnetism are negligible and temperature independent .The magnetism that are of importance arises from the unfilled inner shell electrons of the atoms as 3d electrons in transition metals and 4f electrons in rare earths. If the magnetic atoms in a solid can be treated as non-interacting we speak of paramagnetism. The effect of an external field on such a material is to align the atomic magnetic moments along the field direction against thermal agitation. Theoretically perfect alignment is attainable only at absolute zero where the thermal energy is zero or at infinite external magnetic field. The susceptibility in this type of material is +ve but less than 1, and a function of temperature. If there exists an interaction between the magnetic atoms in a solid, we will find some degree of alignment of the magnetic moments even in absence of any external magnetic field. This type of material are termed as ordered magnetic material. Ferromagnetism, Ferrimagnetism, Antiferromagnetism belong to this class. The characteristic of these ordered materials are an orderly arrangement of the magnetic cores of the elementary magnets is achieved with little

external field. It therefore appears that a very high internal field or its equivalent must in some way spontaneously come into existences. In 1907 Weiss [2] postulated that a high internal field existed in any ferromagnetic material. Weiss theory is centered about the following two hypothesis.

(i) A ferromagnetic specimen contains in general, a number of small regions called domains which are spontaneously magnetized. The magnitude of the spontaneous magnetization of the specimen is determined by the vector sum of the magnetic moments of individual domains. In absence of any external field the domain magnetizations are arranged in such a way that the net magnetization becomes zero.

(ii) Within each domain the spontaneous magnetization is due to the existence of a molecular field which tends to produce a parallel alignment of the atomic moments (despite the effect of thermal energy).

In an applied field the magnetization takes place initially due to domain wall displacement and at higher fields due to rotation of the magnetization vector.

3.2 Ferromagnetism :

For ferromagnetic material the susceptibility χ is positive and permeability is also positive and large compared to unity that is $\chi >> 0$ and $\mu' >> 1$.

Ferromagnetism arises due to the alignment of the atomic magnetic moment within a solid in the same direction. The alignment is caused by a quantum mechanical exchange field which is also known as molecular field . In ferromagnetism the spins are aligned parallel to one another below T_c. Above the curie point ,T_c, the susceptibility obeys the curie-weiss law, which states that $1/\chi$ rises from zero at the curie point and increases linearly with temperature shown in Fig.3.1. If an external field is applied , the apparent magnetization finally reaches the saturation magnetization, which is equal to the spontaneous magnetization.

3.3 Curie-Weiss law for ferromagnetism

For spontaneous magnetization Weiss assumed that the molecular field B acting on a atomic magnetic dipole is

$$B = B_0 + N_w M \qquad (1)$$

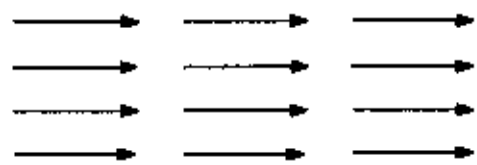

Spin alignment of ferromagnetism

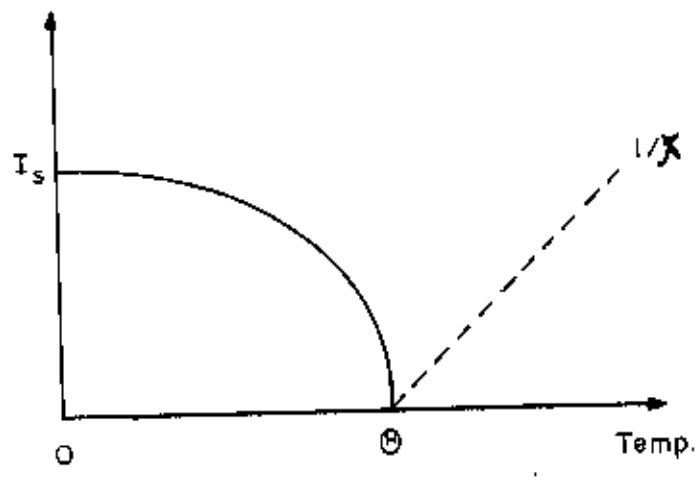

Fig.3.1 Temperature dependence of spontaneous magnetization for ferromagnetism

Where B_0 is the applied field and M is the magnetization and N_w is the molecular field or weiss constant. For a solid containing N atom per unit volume and the total angular momentum quantum number J the magnetization M can be written as

$$M = N g \mu_B J B_J(\alpha) \qquad (2)$$

Where B_J is the Brillouin function is defined by

$$B_J(X) = \frac{2J+1}{2J} \operatorname{ctnh}\left[\frac{(2J+1)x}{2J}\right] - \frac{1}{2J} \operatorname{ctnh}\left(\frac{x}{2J}\right)$$

and $\operatorname{ctnh}\ x = 1/x + x/3 - x^3/45 + \ldots\ldots\ldots$

For ferromagnetism

$$\alpha = \frac{g \mu_B B J}{K T}$$

$$\alpha = \frac{g \mu_B (B_0 + N_w M) J}{K T} \qquad (3)$$

Now for spontaneous magnetization $B_0 = 0$

$$\alpha = \frac{g\ \mu_B\ N_w\ M\ J}{K\ T}$$

or
$$M = \frac{\alpha\ K\ T}{g\ \mu_B\ N_w\ J} \qquad (4)$$

Fig.3.2 shows the curves drawn for equation (2) and straight line equation (4). It can be seen that at $T \geq \theta_f$ the spontaneous magnetization vanish but at $T < \theta_f$,only one non-vanishing value of M can be found at the intersection point P.

For this condition ($T < \theta_f$) θ_f increase with N_w ; because the tendency for parallel alignment increases as N_w becomes larger, so α must be less than 1 i.e., $\alpha << 1$, then the Brillouin Function will be

$$B_J(\alpha) \approx \frac{(J+1)\alpha}{3J} \qquad (5)$$

Putting this value in equation (2)

$$M = \frac{N\ g\ \mu_B\ J(J+1)\ \alpha}{3\ J}$$

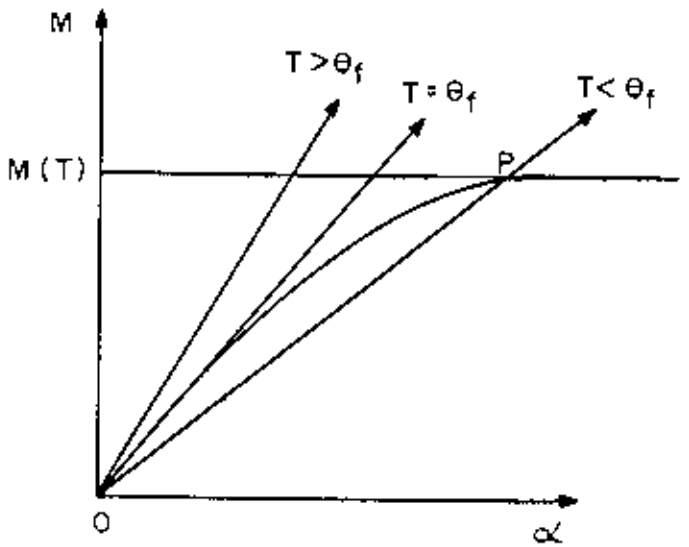

Fig.3.2 Schematic representation of the method for finding the spontaneous magnetization at a temperature T. A point of intersection such as p determines M(T).

$$\text{or} \quad M = \frac{N\, g\, \mu_B\, (J+1)\, \alpha}{3}$$

Now put the value of α from equation (3).

$$M = N\, g\, \mu_B\, (J+1)\, g\, \mu_B\, (B_0 + N_W\, M)\, J/3KT$$

$$= \frac{N\, g^2 \mu_B^2\, J(J+1) B_0}{3KT} + \frac{N\, g^2\, \mu_B^2\, J(J+1)\, N_W\, M}{3KT}$$

$$\frac{M[3\, K\, T - N\, g^2 \mu_B^2\, J(J+1)\, N_W\,]}{3KT} = \frac{N\, g^2\, \mu_B^2\, J(J+1)\, B_0}{3KT}$$

$$\frac{M}{B_0} = \frac{N\, g^2\, \mu_B^2\, J\, (J+1)}{3KT - N\, g^2\, \mu_B^2\, J(J+1)\, N_W}$$

Let us consider $C = Ng^2\mu_B^2 J(J+1)/3K$ and $\theta = CN_W$

$$\text{then} \quad \frac{M}{B_0} = \frac{C}{T - \theta}$$

$$\text{or } \chi = \frac{C}{T - \theta}$$

(3.3) is the Curie Weiss law for ferromagnetism. The origin of the Weiss molecular field was explained by Heisenberg [3]. He showed that the molecular field is of quantum mechanical origin. The exchange field E_{ex} is related to the atomic spins S by

$E_{ex} = -2JeS_i.\Sigma S_j$ Where J_e is the exchange integral.

3.4 Ferrimagnetism :

In ferrimagnet, like ferromagnetic material the atomic moments are aligned without the action of any external field, that is the material is spontaneously magnetized except that there are two oppositely directed sublattices each of which are spontaneously magnetized. The magnetization of one sublattice differs from the other resulting in a net magnetization. As the temperature increases the arrangement of the spins is disturbed by thermal agitation; which decreases the spontaneous magnetization. At curie point the arrangement of spins becomes random and the spontaneous magnetization vanishes. Above curie point Ferrimagnetism behave paramagnetism and the susceptibility decrease with increase of temperature as in Fig.3.3.

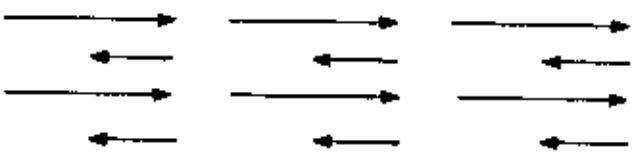

Spin alignment of ferrimagnetism

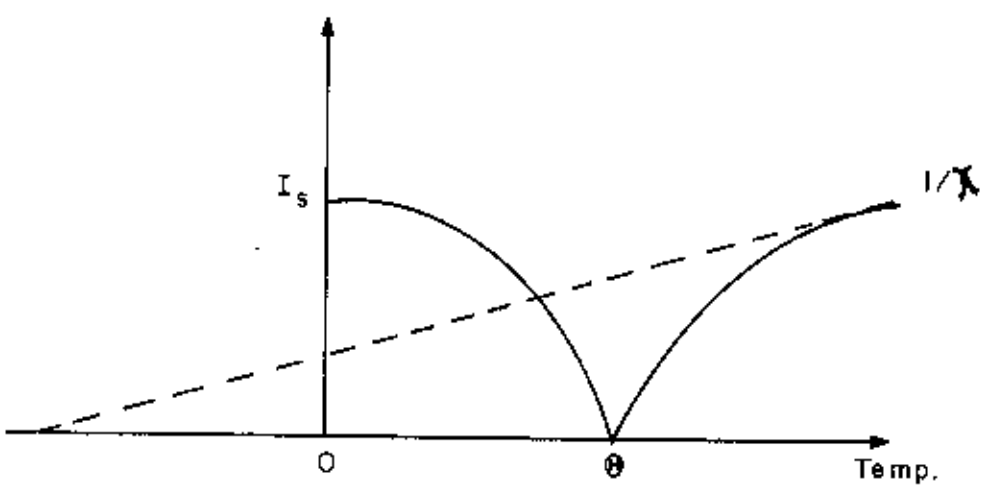

Fig.3.3 Temperature dependence of spontaneous magnetization for ferrimagnetism

In ferrimagnetic crystal the saturation magnetization at T = 0°K does not correspond to parallel alignment of the magnetic moment of the constituent paramagnetic ions, even the crystals for which there is strong evidence that the individual paramagnetic ions have their normal magnetic moments. The most familiar example is magnetic Fe_3O_4 or $FeO.Fe_2O_3$. The ferric (Fe^{3+}) ions are in a state with spin S = 5/2 and zero orbital moment. Thus each ion should contribute $5\mu_B$ to the saturation moment. The ferrous (Fe^{2+}) ions have a spin of 2 and should contribute $4\mu_B$. Thus the effective number of Bohr magnetons per Fe_3O_4 formula unit should be about 2 x 5 + 4 = 14 if all spins were parallel. The observed value is about $4\mu_B$ [4]. This discrepancy is accounted if the moments of the Fe^{3+} ions are antiparallel to each other. Thus the observed moment arises only from the Fe^{2+} ions is S = 2 as in Fig.3.4

A systematic discussion of the consequences of this type of spins order was given by L. Neel [5] with reference to an important class of magnetic oxides known as ferrites. The usual chemical formula of a ferrite is ($MO.Fe_2O_3$) where M is a divalent cation often Zn, Cd, Fe, Ni, Cu, Co, or Mg.

The cubic ferrites have the spinel crystal structure shown in Fig.3.5 . There are eight occupied tetrahedral (or A) Sites and 16 occupied octahedral (or B) sites in a unit cube. A remarkable feature of the spinels is that all exchange

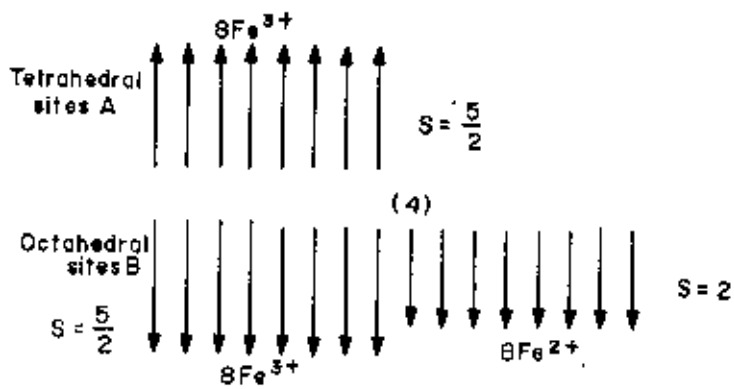

Fig.3.4 Spin arrangements in magnetite, $FeO.Fe_2O_3$, Showing that the moments of the Fe^{3+} ions cancel out, leaving only the moments of the Fe^{2+} ions.

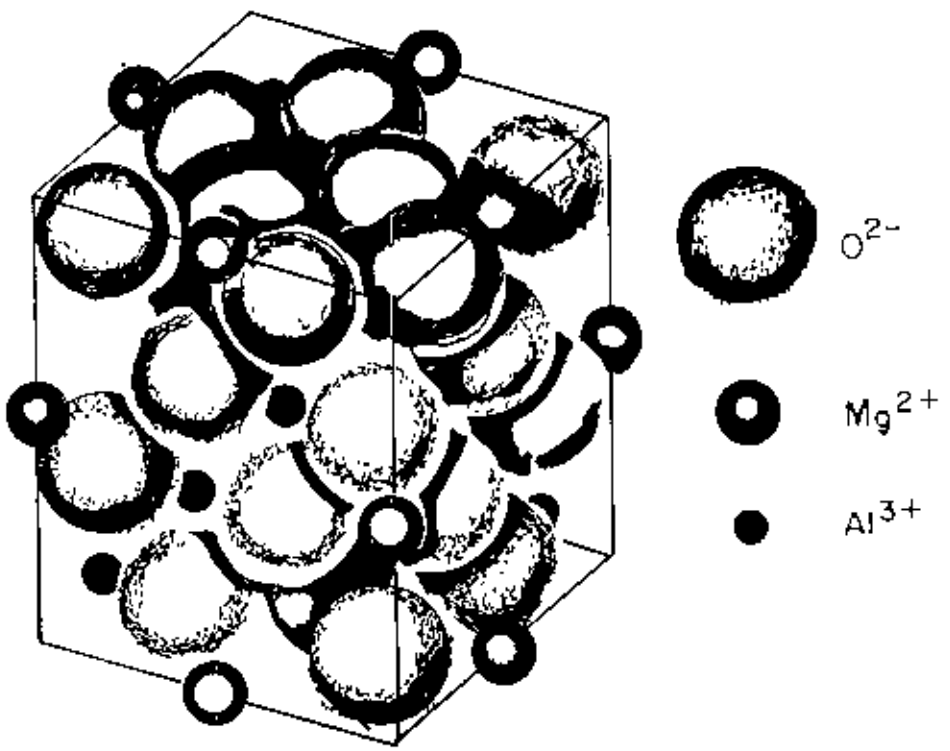

Fig.3.5 Crystal structure of the mineral spinel $MgAl_2O_4$, the Mg^{2+} ions occupy octahedral sites.

interaction (AA,AB and BB) favor antiparallel alignment of the spins connected by the interaction. But the AB interaction is the strongest, so that the A spins are parallel to each other and the B spins are parallel to each other, just in order that the A spins may he antiparallel to the B spins. It is believed that all exchange integral J_{AA}, J_{AB} and J_{BB} are negative. If J in $U= -2J\ S_i.S_j$ is positive, we say that the exchange integral is ferromagnetic; if J is negative, the exchange integral is antiferromagnetic. Now the three antiferromangetic interaction can result in ferrimagnetism. The mean exchange fields acting on the A and B spin lattices may be written

$$B_A = - \lambda M_A - \mu M_B$$

$$\text{and} \quad B_B = - \mu M_A - \nu M_B \qquad (6)$$

Where λ, μ, ν all are positive constants. The minus sign then corresponds to an antiparallel interaction. The interaction energy density is

$$U = - \tfrac{1}{2} (B_A.M_A + B_B.M_B)$$

$$= \tfrac{1}{2} \lambda M_A^2 + \mu M_A.M_B + \tfrac{1}{2} \nu M^2_B \qquad (7)$$

this is lower when M_A is antiparallel to M_B than when M_A is parallel to M_B. The energy when antiparallel should be compared

with zero, because a possible solution is $M_A = M_B = 0$

Thus when

$$\mu M_A M_B > \tfrac{1}{2}(\lambda M_A^2 + \nu M_B^2) \qquad (8)$$

The ground state will have M_A directed oppositely to M_B. Under certain conditions there may be noncollinear spin arrays of still lower energy.

3.5 Curie temperature and susceptibility

Let us consider C_A and C_B are the curie constant for the A and B sites. If all the interactions be zero except for an antiparallel interaction between the A and B sites; Then

$$B_A = - \mu M_B \quad \text{and} \quad B_B = - \mu M_A \qquad (9)$$

where μ is positive. The some constant μ is involved in both expressions because of the form of eqn. (7). In analogy to the argument and the mean field approximation.

$$M_A T = C_A (B_a - \mu M_B) \; ; \quad M_B T = C_B (B_a - \mu M_A) \qquad (10)$$

where Ba is the applied field. These equations have a nonzero solution for M_A and M_B in zero applied field if

$$\begin{vmatrix} T & \mu C_A \\ \mu C_B & T \end{vmatrix} = 0 \qquad (11)$$

So that the ferrimagnetic curie Temperature is given by $T_C = \mu(C_A\ C_B)^{\frac{1}{2}}$. We solve eqn. (10) for M_A and M_B to obtain the susceptibility at $T>T_C$

$$\chi = \frac{M_A + M_B}{B_a} = \frac{(C_A + C_B)T - 2\mu C_A C_B}{T^2 - T_C^2} \qquad (12)$$

3.6 **Magnetism in ferrites:**

The magnetism in ferrites is due to (i) unpaired 3d electrons (ii) the super exchange between adjacent metal ions and (iii) non-equivalence in number of A and B sites. In the free state the total magnetic moment of an atom containing 3d electrons is the sum of the electron spin and orbital moments. In an oxide compound such as ferrite, the orbital magnetic moment is mostly quenched by the crystalline electric field caused by the surrounding oxygens about the metal ion. The atomic magnetic moment then becomes the moment of electron spin. According to Anderson [6], Indirect exchange interaction (super-exchange) takes place between adjacent metal ions separated by oxygen ions. The strength of this interaction depends on the degree of orbital overlap of oxygen p-orbitals and transition

metal d-orbitals. The interaction will decrease as the distance between the metal increases as the angle of Me-O-Me decreases from 180° to 90°. The only important interaction in ferrites is the AB interaction since the angle is 125° while BB is negligible because the angle is 90°. This interaction is such that antiparallel alignment of moments results between the two metal ions when both ions have 5 or more 3d electrons or 4 or fewer 3d electrons. Parallel alignment occurs when one ion has ≤4 electrons and second has ≥ 5 electrons. Since the common ferrite ions (Mn^{2+}, Fe^{2+}, Ni^{2+}, Co^{2+}) have more than 5d electrons, the magnetic moments are aligned anti-parallel between A and B sites. Since there are twice as many B sites occupied as A sites, the B site will dominate over A site resulting in ferri-magnetism as proposed by Neel and verified by Pauthenet [7].

3.7 The technique of measurement of magnetization

The measurement of magnetization is usnally performed by measuring the magnetic moment of a specimen and dividing this quantity by the specimen volume or mass. The techniques for the measnrements of magnetic moment by the direct methods can be conveniently classified into two categories:

a) The measurement of the force exerted on the magnetic moment of the specimen by an inhomogeneous field and
b) The measurement of the emf induced in a suitable coil

system by changing relative position of the magnetic moment with respect to the coil system or by varying the magnetic moment.

The technique of vibrating sample magnetometer (VSM) used in the present measuremeut falls in the second category .

The vibrating sample magnetometer (VSM) is a highly sensitive and versatile equipment for measuring the magnetic moment, maguetization and magnetic susceptibility. The vibrating sample magnetometer was invented by Van Oesterhout [8] and simultaneously and independently by S. Foner [9,10]. The basic principle of the VSM developed by Foner is based on the flux change in a coil when the sample is vibrated near it. The sample, usually a small disc, is cemented to the end of a rod, the other end of which is fixed to a loudspeaker cone(Fig.3.6) or to some other kind of mechanical vibrator. Current through the loudspeaker vibrates the rod and sample at about 80 cycles/sec and with an amplitude of about 0.1mm in a direction at rightangles to the magnetic field. The oscillating magnetic field of the sample induces an alternating emf in the detection coils. The vibrating rod also carries a reference specimen, in the form of a small permanent magnet, near its upper end, the oscillating field of this induces another emf in two reference coils. The voltages from the two sets of coils are compared, and the difference is proportional to the magnetic moment of the

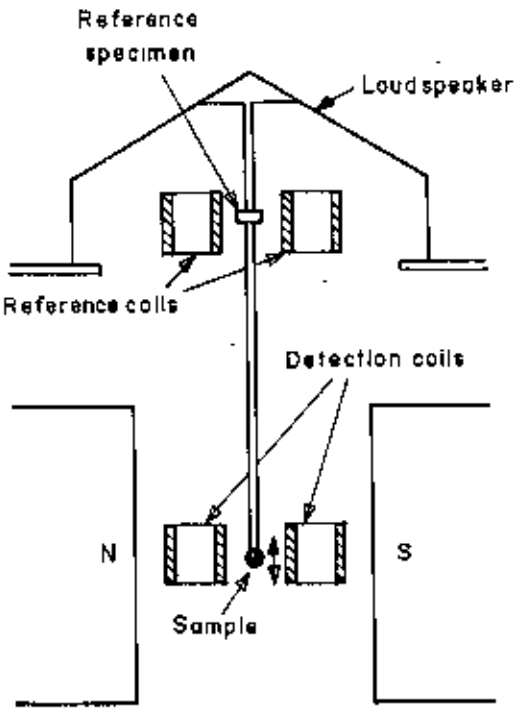

Fig.3.6 Vibrating sample magnetometer, after Foner [9].

sample. This procedure makes the measurement insensitive to changes in, for example, vibrating amplitude and frequency. The VSM used in the present work to take the magnetization measurements is of Foner type. The magnetic Material division, AEC, Dhaka designed and constructed this Foner type VSM in 1986. The measurement of magnetization for all the samples were taken with the help of this Foner type VSM.

3.8 Working principle of the magnetometer:

A schematic diagram of the VSM used in the present work, including the various mechanical and electronic parts is shown in Fig.3.7. The signal generator (SG) feeds a sine wave signal of 80 Hz frequency to the audio amplifier (AA) which in turn drives the speaker (SP). The output of the signal generator is also connected to reference channel input of the lock-in-amplifier (LA) model 124A. The drive-rod assembly (R) tightly coupled to the vibrating paper cone of the speaker vibrates in a vertical direction along its length. The amplitude of vibration may be varied at will by changing the gain of the audio amplifier. A permanent BaO $6Fe_2O_4$ magnet (P) of cylindrical shape is fitted to the drive-rod at its lower end with the help of a sample holder (H). Two cylindrical sample coils (SC) with their axes kept vertically are placed on the opposite sides of the sample and along the line joining the centers of the pole faces (NS.) of the electromagnet. They are

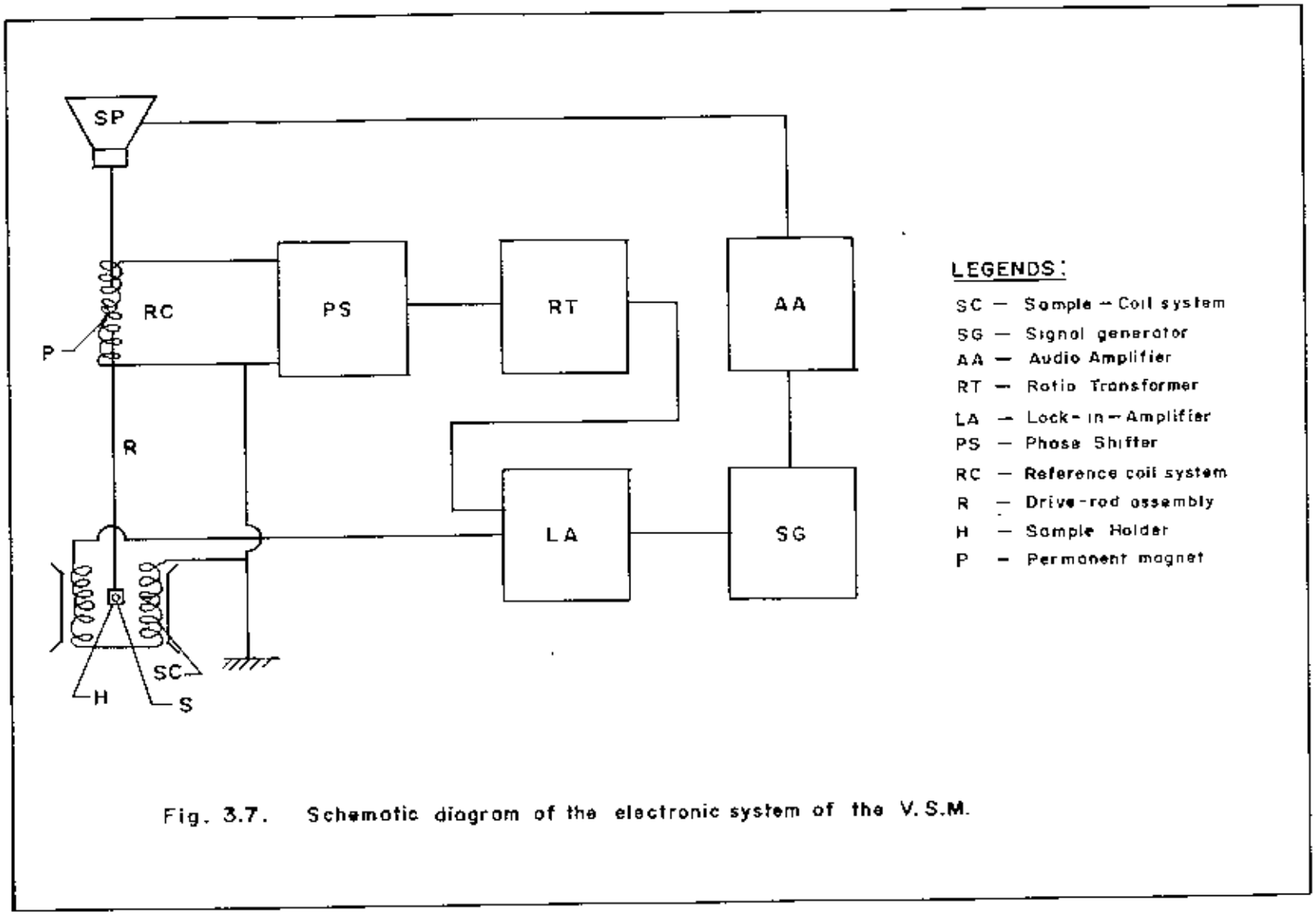

Fig. 3.7. Schematic diagram of the electronic system of the V.S.M.

connected in series opposition and the net out-put signal is fed iuto the lock- in-amplifier through a shielded cable. This pair of coils is referred to as the sample coil system. Another pair of coaxial coils (RC) also connected to each other in series opposition is placed symmetrically around the permanent magnet (P). This coil pair is the reference coil system. As the drive-rod assembly is vibrated with a particular frequency and amplitude, the sample (S) induces a signal of the same frequency in the sample coil system. This signal is proportional to the diploe moment of the sample. As the field in the pole-gap is gradually increased by increasing the current through the electromagnet, the sample becomes increasingly magnetized more and more and induces a larger signal in the sample coil system till the sample reaches the state of saturation magnetization. This signal directly goes to one of the inputs of the lock-in-amplifier. Similarly, another signal of the same frequency is induced in the reference coil system due to vibration of the permanent magnet (P). Since the moment of the permanent magnet is fixed, the signal it produces is also of fixed amplitude for a particular frequency and vibration of amplitude. This signal is termed as the reference signal and it is first fed to a unity gain phase-shifter unit. The phase-shifter capable of continuously changing the phase from 0^0 to 360^0, is used to bring the reference signal in phase with the sample signal.

From the phase-shifter the reference signal passes on to the decade ratio transformer (RT) of a constant input impedance. The output of this transformer then goes to the other input of the lock-in -amplifier. The output to input ratio of the decade transformer can be accurately varied from 10^{-3} to 1. By adjusting the decade transformer the amplitude of its output is made equal to that of the sample signal. The lock-in-amplifier is operated in the differential input mode and is used as a signal detector. When the sample signal and the output signal of the decade transformer are of equal amplitude and are in the same phase the d.c. meter of the lock-in-amplifier gives a null-reading. The whole electronic system then correctly measures the ratio of the sample signal to the reference signal. Since the sample (S) and the permanent magnet (P) are vibrated with the same drive-rod assembly, the sample signal and the reference-signal have a direct phase and amplitude relationship. As a result the ratio of the sample signal to the reference signal is proportional to the magnetic moment of the sample. The measurement is insensitive to small changes in the amplitude and frequency of vibration and the gain of the amplifier. The accuracy of the equipment depends mainly on the accuracy of the ratio transformer and the gain of the amplifier.

3.9 Description of mechanical design of the VSM:

The various mechanical parts of the magnetometer are shown in detail in the Fig.3.8. The base B of the VSM is a circular brass plate of 8mm thickness and 250mm diameter. A brass tube T of 25mm outer diameter and 0.5mm thickness runs normally through the base such that the axis of the tube and the center of the plate coincide. The tube extends 60mm upward and 24mm downward from the base. There is a vacuum port on the lower part of the tube 120mm below the base. The lower end of the tube T is joined to a brass extension tube L by a threaded coupling and an o'ring seal. Another thin tube K made of german silver and of 8mm inner diameter runs through the extension tube L from the coupling point C to about 50 mm below the sample position. Above the base there is a hollow brass cylinder M of 180mm length and 130mm inner diameter and having 40mm wide collars at its both ends. The lower collar seats on an O'ring seal which is situated in a circular groove in the base plate. On the upper collar, there rests an aluminum top N with an O'ring seal. The brass cylinder M has a side port VP. This is again a brass tube of 41mm diameter and 43mm length. The port has a collar at the end away from the cylinder. A perspex vacuum feed-through is fitted at its end with O,ring seal. This port is connected to the cylinder by soft solder.

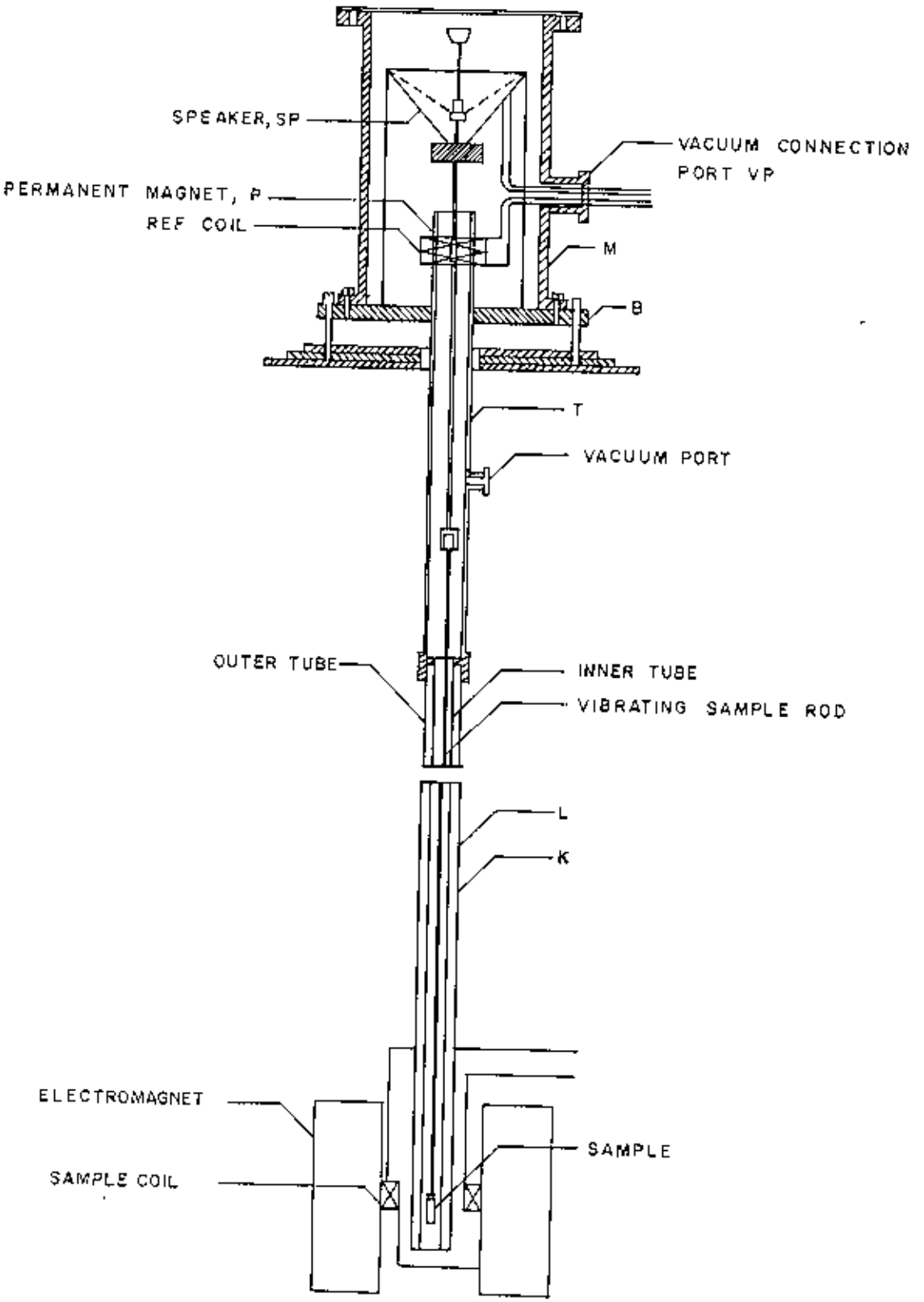

Fig. 3.8. MECHANICAL CONSTRUCTION OF THE V S M .

Electrical connections from the audio amplifier to the speaker and from the reference coil system to the phase-shifter are taken via the perspex feed-through. By connecting the vacuum port of the tube T to a vacuum pump the sample environment can be changed. The speaker (sp) is fitted 25mm above the tube T with the help of brass stands. The lower ends of stands are screwed to the base plate while the rim of the speaker is screwed on the tops of the stands. The speaker has a circular hole of 10 mm diameter along it axis . An aluminium disc having female threads in it is fitted to the papercone with araldite. The aluminium connector having male threads on it and attached to the drive rod assembly fits in the aluminium disc and thus the drive rod assembly is coupled to the speaker. The drive rod assembly consists of two detachable parts which are joined together by means of aluminium threaded connectors. Each part is thin Pyrex glass tubing of 4mm diameter. The upper part has a small permanent magnet (P) situated 100mm below the aluminium connector attached to it. At the lower end of the drive rod assembly a perspex sample bolder having quite thin wall can be fitted tightly with the sample in it. A few perspex spacers are also attached to the driver-rod throughout its length. The spacers guide the vibration of the sample only in the vertical direction and stops side wise or motion. The total length of the drive rod assembly is 920 mm.

The base plate of the VSM rests on three levelling screws above a brass frame which in turn rests on an iron angle bridge. The bridge is rigidly fitted to the sidewall of the room. The brass frame is provided with arrangements with the help of which it can be moved in two perpendicular directions in the horizontal plane. The levelling screws are used to make the drive rod vertical and to put the sample at the center of the pole-gap between the sample coils. The sample can also be moved up and down by the levelling screws.

3.10 Design and construction of sample & references coils:

Both the sample coil system and the reference coil system are each a double coil system. The reference coil system consists of two coils wound oppositely side by side on the two grooves of a former. The former is made of bakelites. Each coil is 4mm long, 2mm thick and its inner diameter is 25mm. The wire is super enamelled BICC copper wire of 0.02mm diameter. Total number of turns in each coil is 6000. Since the two coils are connected in series opposition the output signal is only due to the vibrating permanent magnet P. Any noise induced in it due to background will be minimum. The coil system fits over the brass tube T about 25mm above the base. It is positioned by moving it up and down the tube T while vibrating the permanent magnet so that the output signal is a nice sine-wave. The sample coil (SC)

system is also a two-coils system and each coil is wound on a cylindrical bakelite former. The length of the coil is 6mm and its diameter is 4mm. The same super enamelled BICC wire of 0.02 mm diameter has been used in these coils. The number of turns of each coil is 6000 again. The coils stand on a platform of thin bakelite sheet and are equidistant from the nearby poletips. The brass tube T passes through the gap in the platform and the sample is at equal distance from the sample coils on opposite sides of it. The sample and the sample coils are put on the same horizontal plane visually. The final and optimum position of the sample is obtained by maximizing the sample signal by moving the sample slightly up or down.

The signal due to the sample moment induced in the sample coil system is, in principle, given by the relation

$$V_s = K_s \omega A \exp(\omega it) M_s \qquad (13)$$

Where k_s is a constant dependent on the coil geometry, ω the angular frequency of vibration, A the amplitude of vibration and M_s the magnetic moment of the sample. Similarly, the emf induced in the reference coils is given by

$$V_r = K_r \omega A \exp(\omega it) M_r \qquad (14)$$

Taking the rms value of V_s and V_r it is seen that the ratio of the two signals is independent of frequency and amplitude. The ratio is

$$V_{out} = (V_s)_{rms} / (V_r)_{rms}$$

$$= K_s M_s / K_r M_r$$

$$\text{or, } M_s = K_r M_r V_{out} / K_s$$

$$M_s = K V_{out} \qquad (15)$$

Where K is a constant since K_s, K_r and M_r are constant. Here V_{out} is actually the ratio transformer reading. The coils have been prepared depending mainly on the considerations of (i) maximization of area-turns, (ii) minimization of size and (iii) making the shape compatible to accommodate an one inch diameter tube between them and also to put them as far as possible form the poletips.

3.11 Calibration of the VSM:

There are usually two methods of calibration of a vibrating sample magnetometer:

(i) by using a standard sample and

(ii) by using a coil of small size whose moment can be calculated for d.c. current through it.

The VSM has been calibrated using a 300mg spherical sample of 99.9% pure nickel. The sample was made spherical with the help of a sample shaping device. It was then annealed in helium atmosphere at about 900^{0}c. The samples saturation magnetic moment has been calculated using the available standard data. The ratio-transformer reading is obtained by actual measurements and thus from the eqn.15 the value of the calibration constant K is obtained. The accuracy of this calibration, however, depends on the reliability of the standard nickel sample, the accuracy of the ratio transformer and the gain of the amplifier. The equipment has been operated repeatedly with the same standard sample and stability has been found to be within 1 in 1000.

3.12 Sensitivity of the VSM:

The sensitivity of a VSM is usually determined by the signal to noise ratio. But because of comparatively low sensitivity of the lock-in-amplifier used in this equipment, the noise level could not be measured. The maximum sensitivity of the lock-in-amplifier is 10 microvolt (rms). So the differential method has been used to measure the sensitivity. It is found to be about 10^{-4} emu. It may be mentioned here that the sensitivity

of a commercial VSM made by PARC(Pronceton Applied Research Corporation, USA), is $5x10^{-5}$ emu. With the sensitivity so far achieved of this VSM can be used for investigation of only ferromagnetic, ferrimagnetic and strongly paramagnetic materials at room temperature. In order to extend its usefulness, a more sensitive lock-in-amplifier, a sample oven and a cryostat are needed. Under the present conditions, however, routine measurements at room temperature can be performed for the materials mentioned above.

3.13 Working Procedure of the VSM:

The sample is fitted to the drive rod assembly and then positioned at about the mid-point of the sample coils by eye estimation. The switches of the electromagnet power supply unit, the signal generator, the audio amplifier and the phase-shifter are turned on. Nearly half an hour is spent for the warm-up of all the component units. The frequency of the sine wave from the signal generator is set at 80Hz. The gain of the audio amplifier is adjusted to make the output signal driving the speaker about 3 volts peak to peak. This signal makes the rod assembly vibrate with sufficiently large amplitude. The signal produced in the reference coil-system is found to be about 5mV peak to peak. The rod-assembly is made vertical by adjusting the levelling screws. About 2 amperes or more current is passed through the electromagnet depending on the size and material of

the specimen. The sample signal alone is first seen on the D.C. meter of the lock-in-amplifier. The meter reading is maximized by changing the phase of the locking signal in the reference channel. The sample signal is then optimized i.e. it is maximized by moving the sample in the Z-direction (vertical) and in the Y-direction, and then minimized by moving it in the X-direction (field direction).

The locking signal in the reference channel is brought in exact quadrature with the sample signal to give a correct null-reading on the meter. The two signals are then brought in the same phase to give a maximum reading on the meter to the right. Similarly, the reference coil signal alone is next seen on the meter. This signal is first brought in quadrature with the locking signal with the help of the external phase-shifter in such a manner that it gives a deflection to the left on the meter when it is again bronght in phase with the sample signal. The lock-in-amplifier is then set in the differential mode. The null-reading is obtained by correctly equalizing the decade transformer output with the sample signal. The reading on the decade transformer is then multiplied by the calibration constant to obtain the sample moment.

3.14 Measurements of Magnetization.

The measurements of magnetization on $Ni_{1-x}Fe_2O_4$ ferrite samples for x= 0.00,0.01,0.02 upto 0.10 were performed using a vibrating sample magnetometer as shown in Fig.3.8. Samples in the form of thin disc of diameter about 5mm were prepared from the disc shaped nickel ferrite samples. They were then weighed. The specimens were then glued to the lower end of the sample holder of the VSM. The measurements of magnetization were taken at room temperature for different values of the magnetic field in the range 0.1 KG to 4 KG . The strength of the applied magnetic field was simultaneously monitored with the help of a Digital Gauss-meter(Model 811A), keeping the tip of the Gauss-meter closed to a pole of the electromagnet. The accuracy in determining the field was estimated to be within one percent. The measurements as a function of temperature could not be performed due to the non-functioning of the vacuum pump and also due to the non-availability of a low-temperature cryostat. The measurements were therefore performed only at room temperature. The room temperature magnetization measurements on the specimens of $Ni_{1-x}Fe_2O_4$ for different concentration of x are given in Table-3.1 to 3.11 (appendix A). The magnetization curves drawn from these data obtained for different compositions for x=0.01 to 0.10 are given in Fig.(3.9a to 3.9k). The strength of the magnetization obtained for the different values of the magnetic field B for fixed value of x were then drawn against 1/B. The

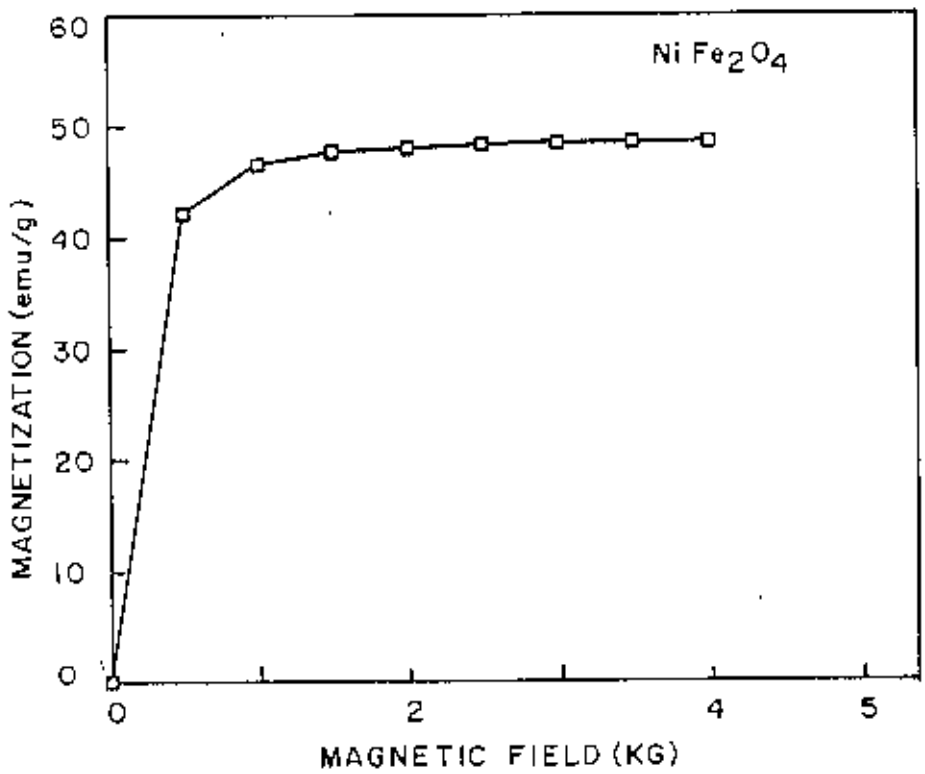

Fig.3.9a Magnetization curve of $NiFe_2O_4$ against magnetic field.

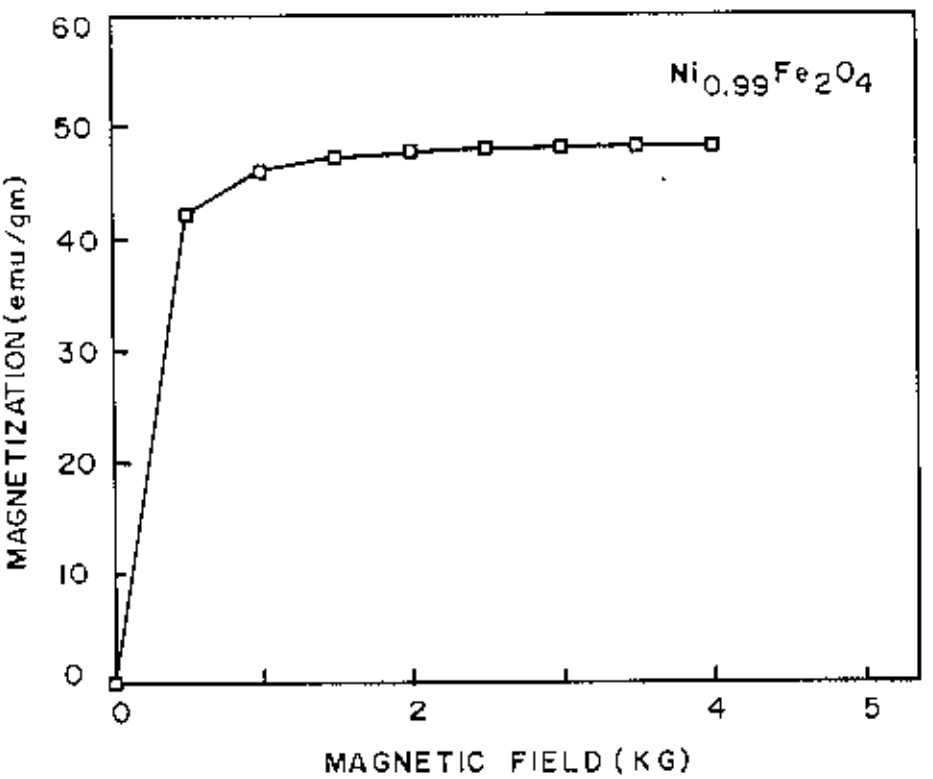

Fig.3.9b Magnetization curve of $Ni_{0.99}Fe_2O_4$ against magnetic field.

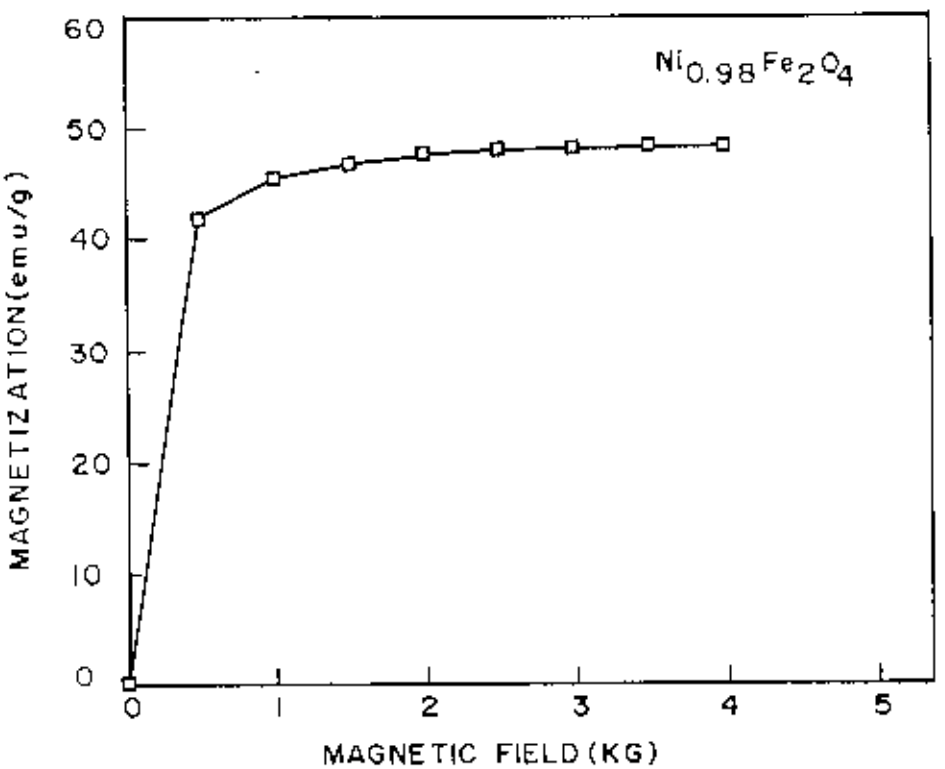

Fig.3.9c Magnetization curve of $Ni_{0.98}Fe_2O_4$ against magnetic field.

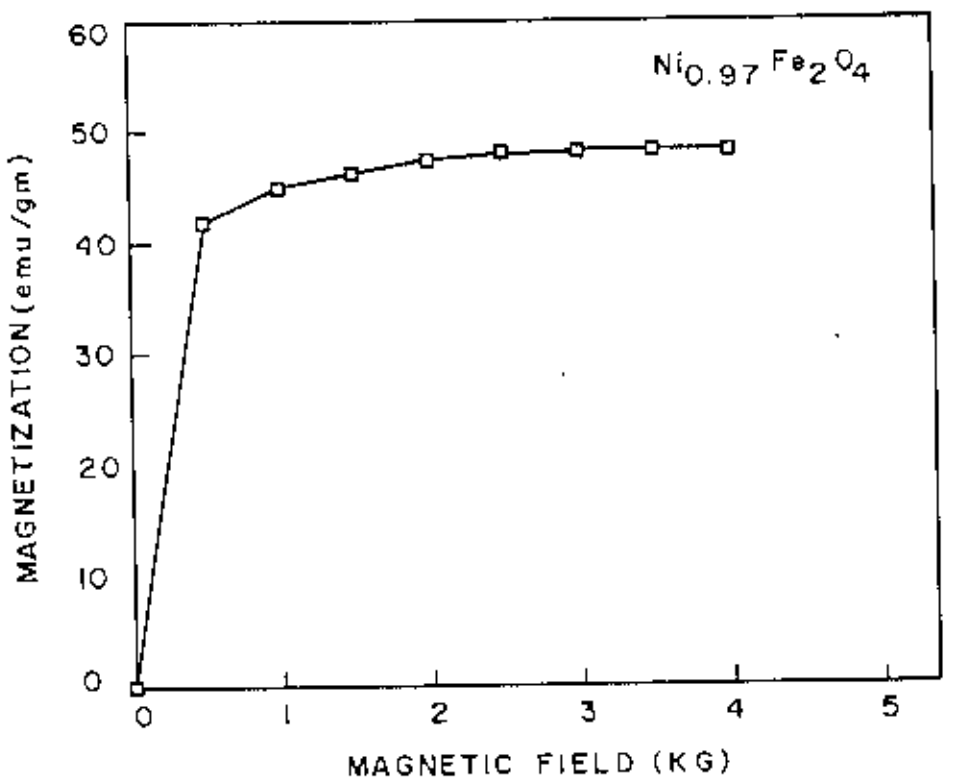

Fig.3.9d Magnetization curve of $Ni_{0.97}Fe_2O_4$ against magnetic field.

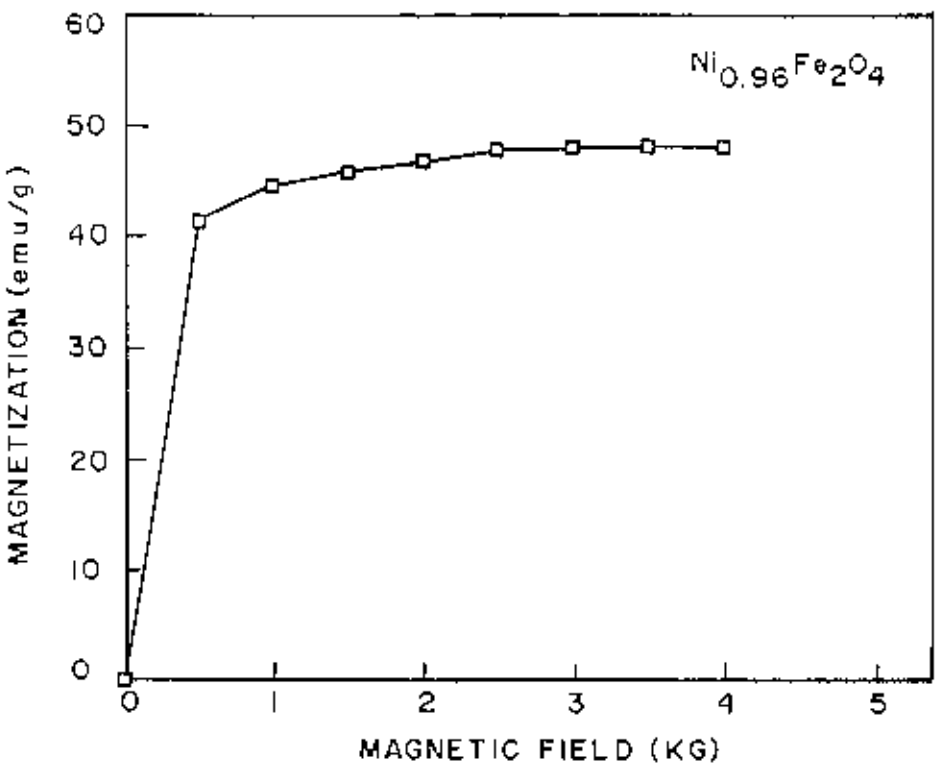

Fig.3.9e Magnetization curve of $Ni_{0.96}Fe_2O_4$ against magnetic field.

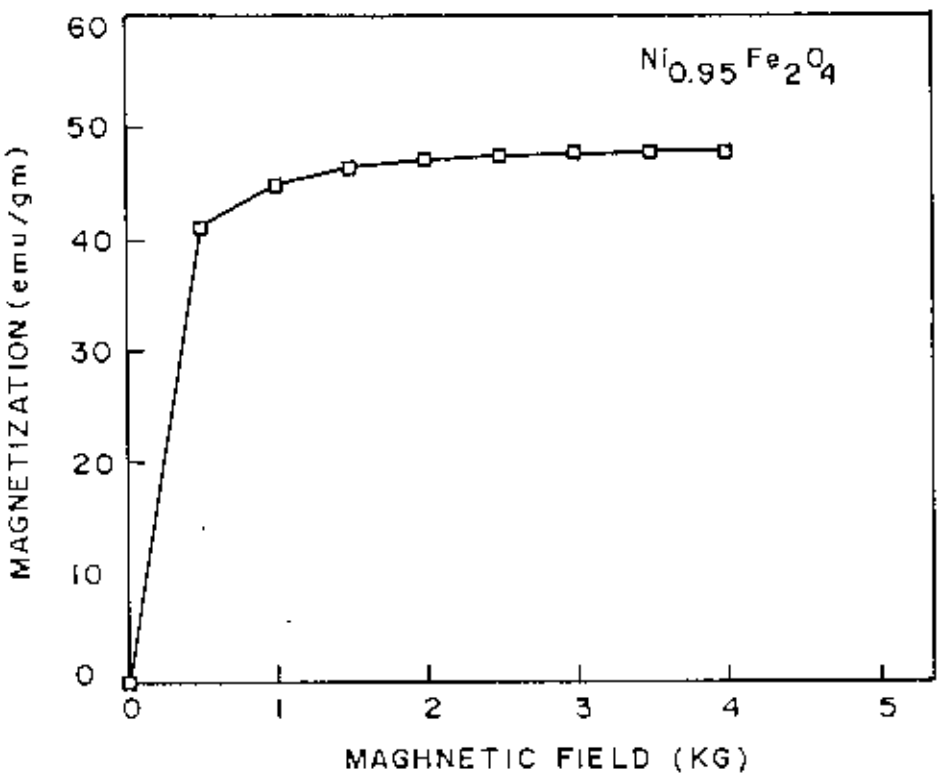

Fig.3.9f Magnetization curve of $Ni_{0.95}Fe_2O_4$ against magnetic field.

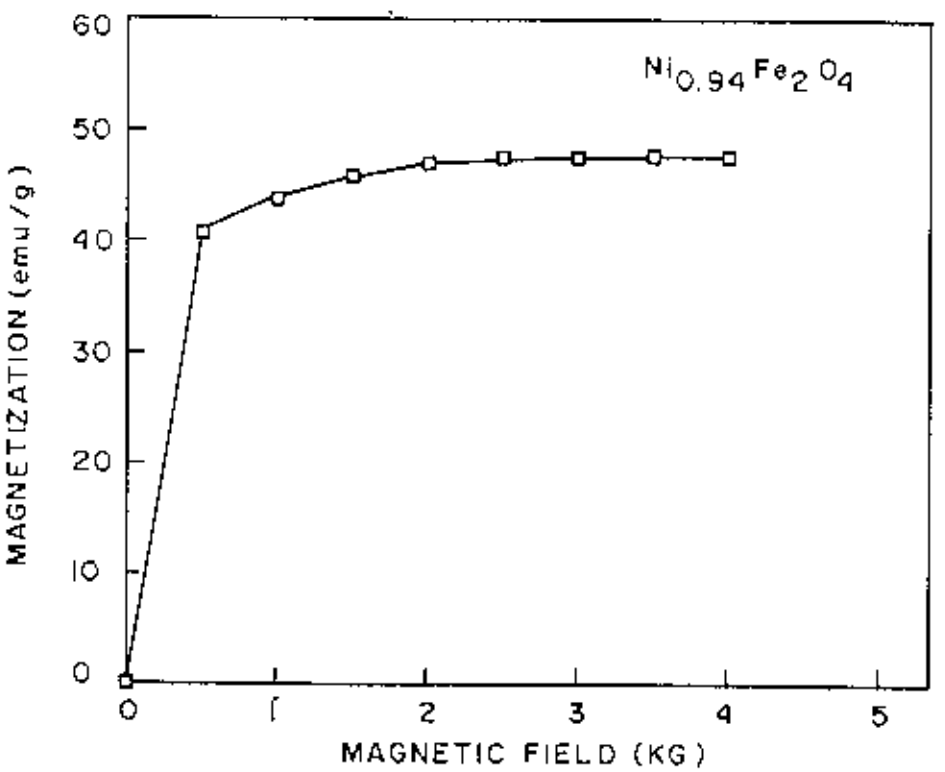

Fig.3.9g Magnetization curve of $Ni_{0.94}Fe_2O_4$ against magnetic field.

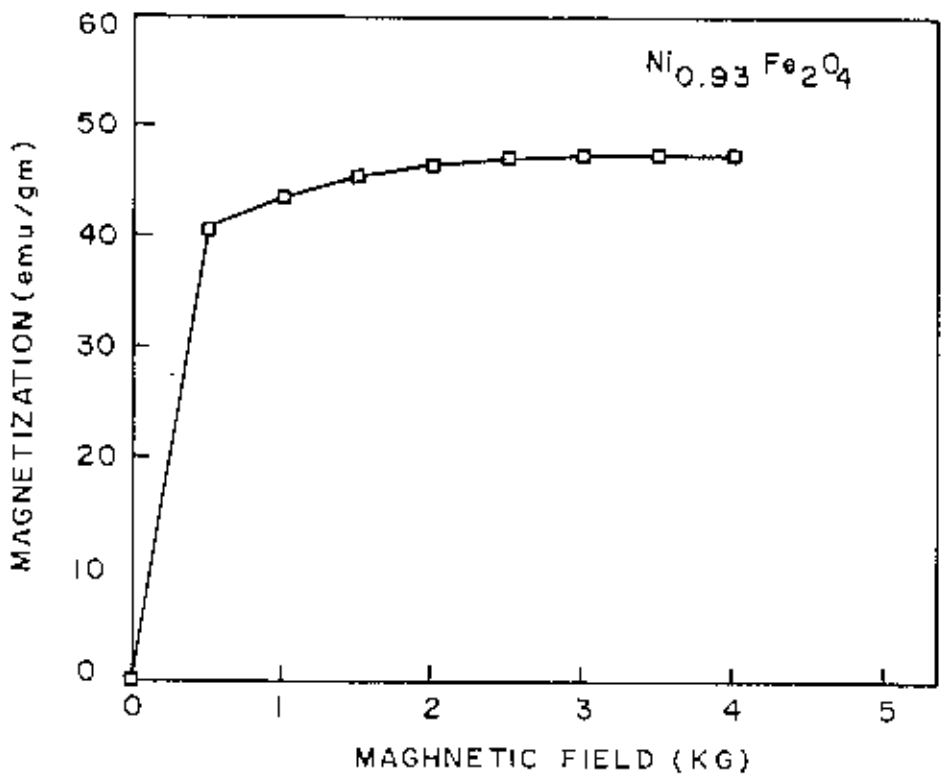

Fig.3.9h Magnetization curve of $Ni_{0.93}Fe_2O_4$ against magnetic field.

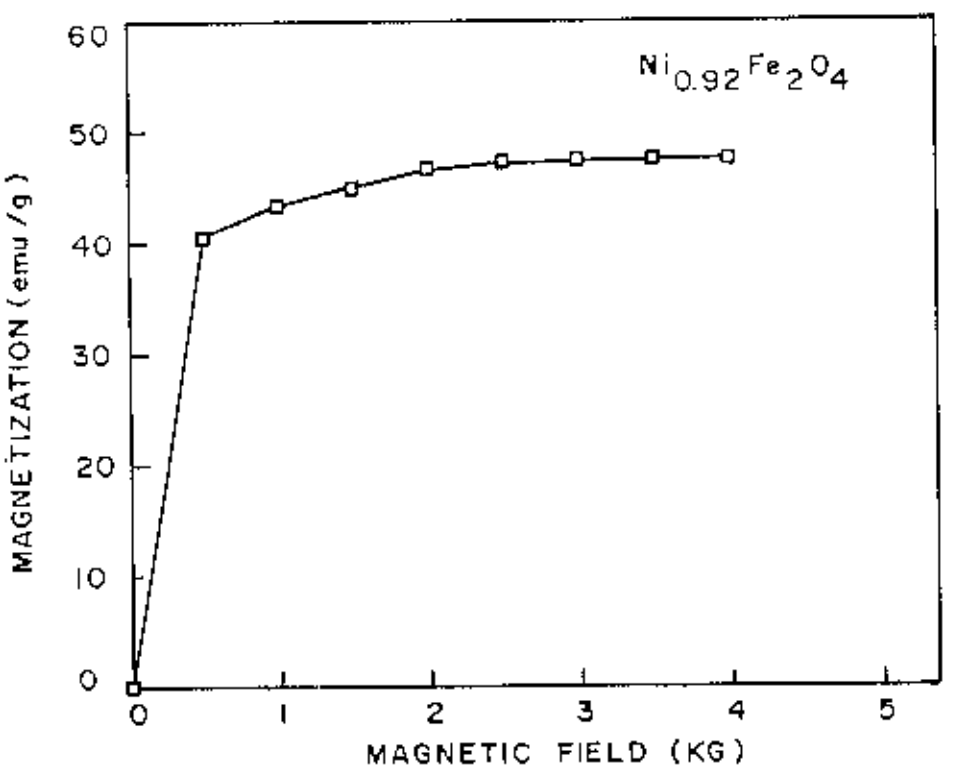

Fig.3.9i Magnetization curve of $Ni_{0.92}Fe_2O_4$ against magnetic field.

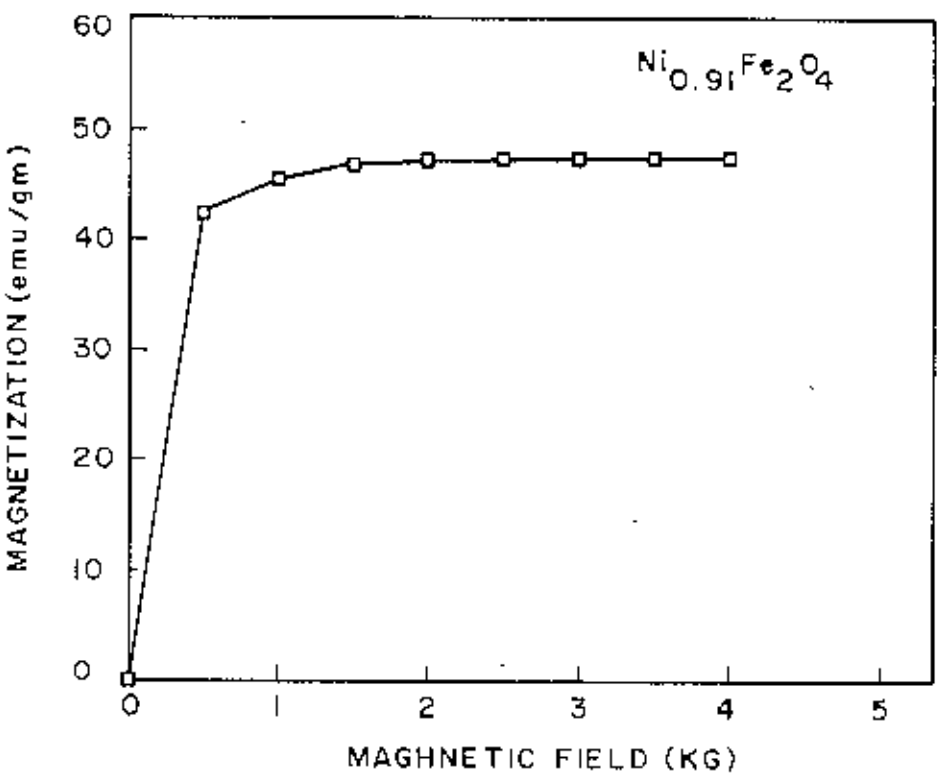

Fig.3.9j Magnetization curve of $Ni_{0.91}Fe_2O_4$ against magnetic field.

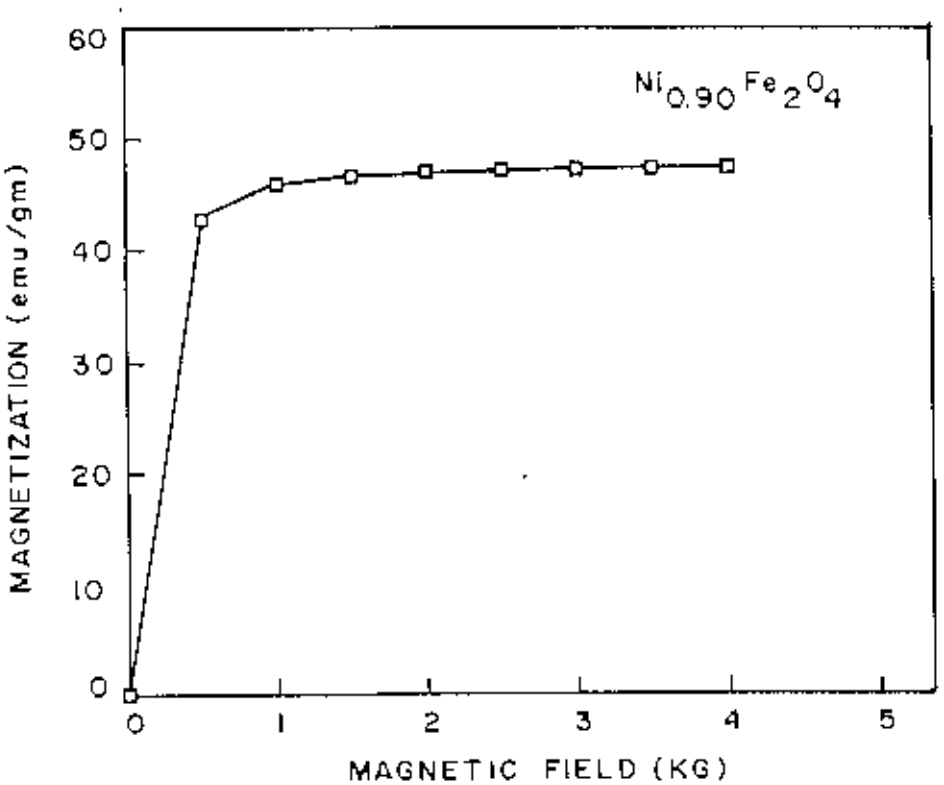

Fig.3.9k Magnetization curve of $Ni_{0.90}Fe_2O_4$ against magnetic field.

curves obtained thus are shown in Fig. (3.10a to 3.10k). The values of the magnetization at (1/B)=0 were taken as the values at saturation . The saturation magnetization thus obtained for different concentration of x is shown in Fig.(3.11).

3.15 Results and Discussion.

The measurements of magnetization shows that with the increased content of x in the compound Ni_{1-x} Fe_2O_4 the magnetization value decreases. This is expected, because the compound $NiFe_2O_4$ is inverse spinel and the arrangement of the magnetic ions in the octahedral B and tetrahedral A lattice sites are antiferro-magnetically coupled, which is represented by Fe^{III} $[Ni^{II}$ $Fe^{III}]O_4$, where the bracket indicated the octahedral B sites. Thus the Fe^{III} moment in the two sites cancel each other and the net moment is due to Ni^{II} ions only. Thus with the decrease of nickel content in $Ni_{1-x}Fe_2O_4$ one expects to observe a lower moment with the increased value of x, provided the cryatal structure and the spin arrangement of the Fe^{III} ions in the octahedral site B and tetrahedral site A remains uneffected. X-ray investigations carried out on the specimens suggests that the crystal structure of the samples of $Ni_{1-x}Fe_2O_4$ under investigation remains cubic similar to that of $NiFe_2O_4$ only except that the cell edges are slightly increased with the increased value of x. We realize that similarities in crystal

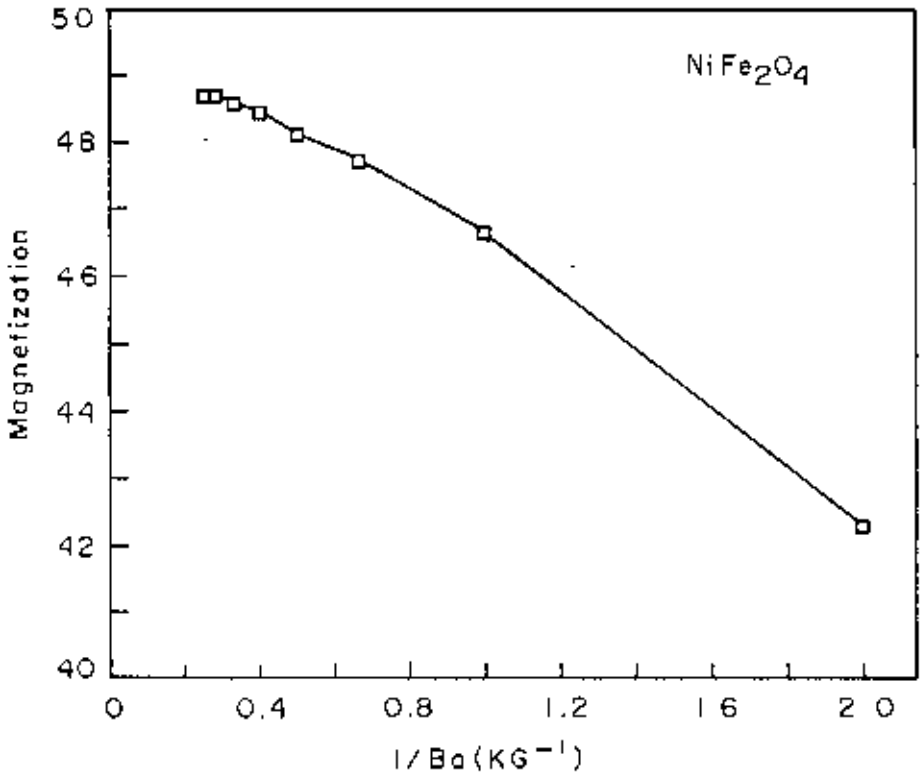

Fig.3.10a Values of the magnetization obtained at different field against 1/Ba. (Ba is applied field)

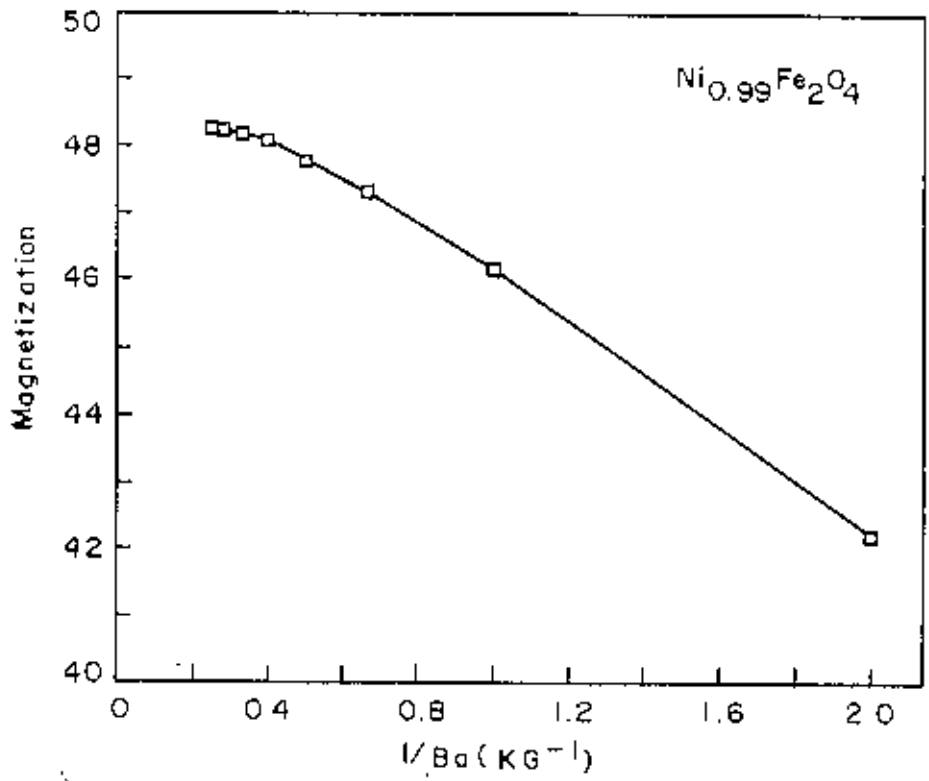

Fig.3.10b Values of the magnetization obtained at different field against 1/Ba. (Ba is applied field)

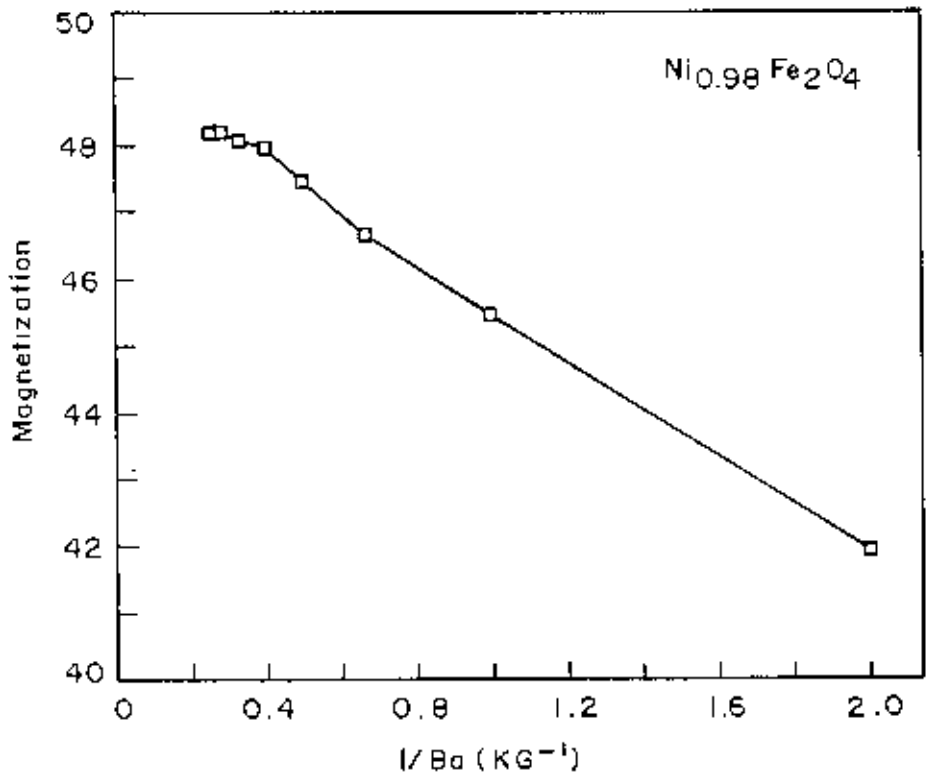

Fig.3.10c Values of the magnetization obtained at different field against 1/Ba. (Ba is applied field)

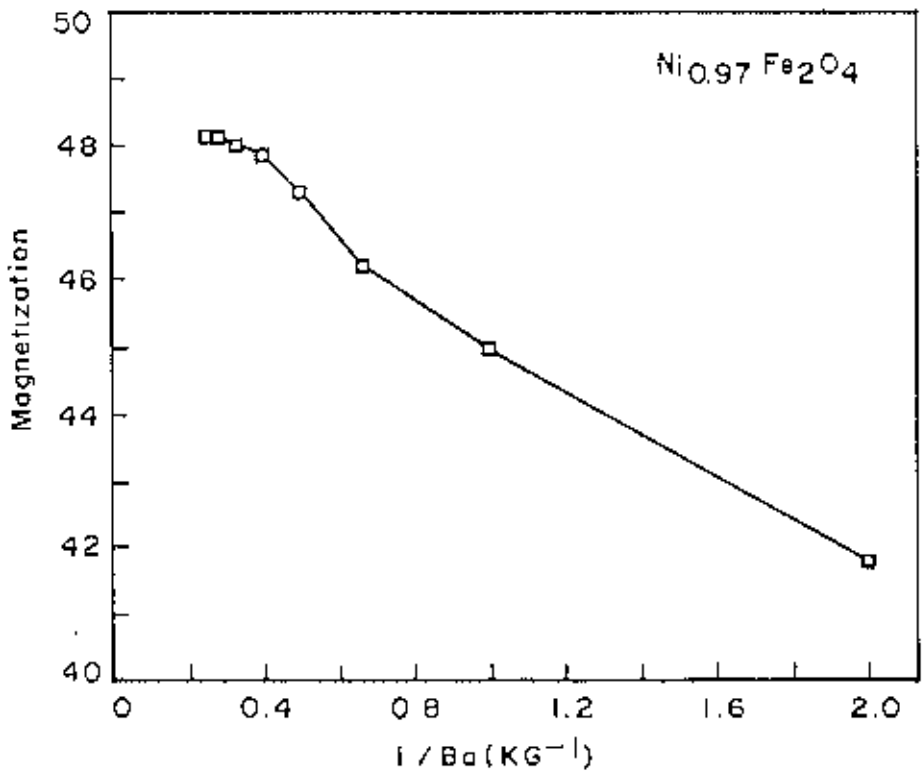

Fig.3.10d Values of the magnetization obtained at different field against 1/Ba. (Ba is applied field)

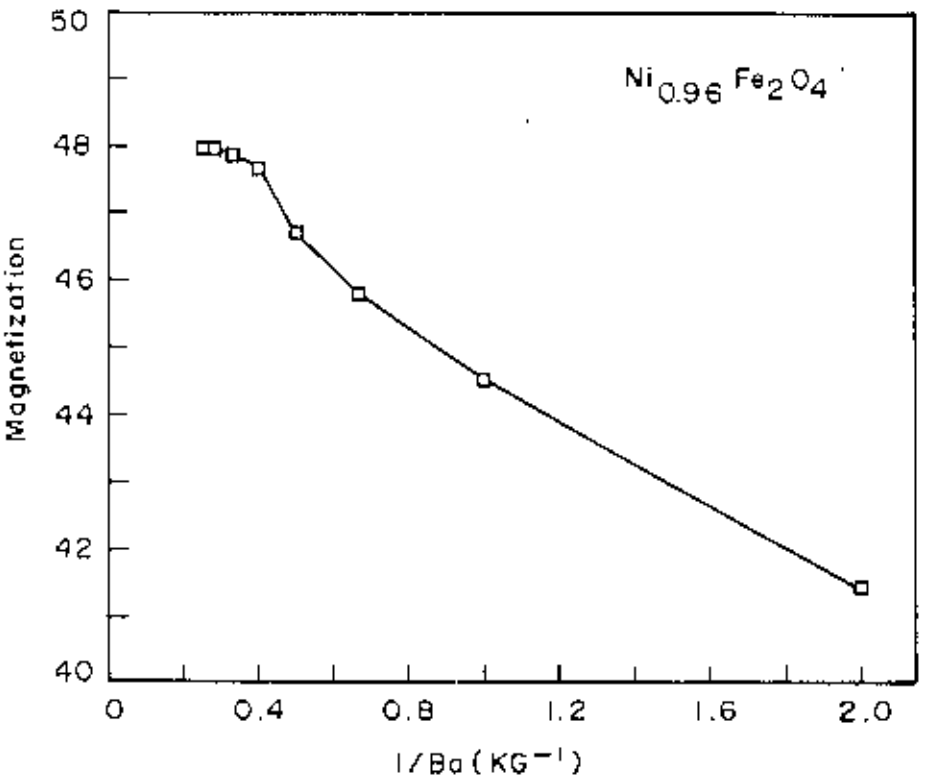

Fig.3.10e Values of the magnetization obtained at different field against 1/Ba. (Ba is applied field)

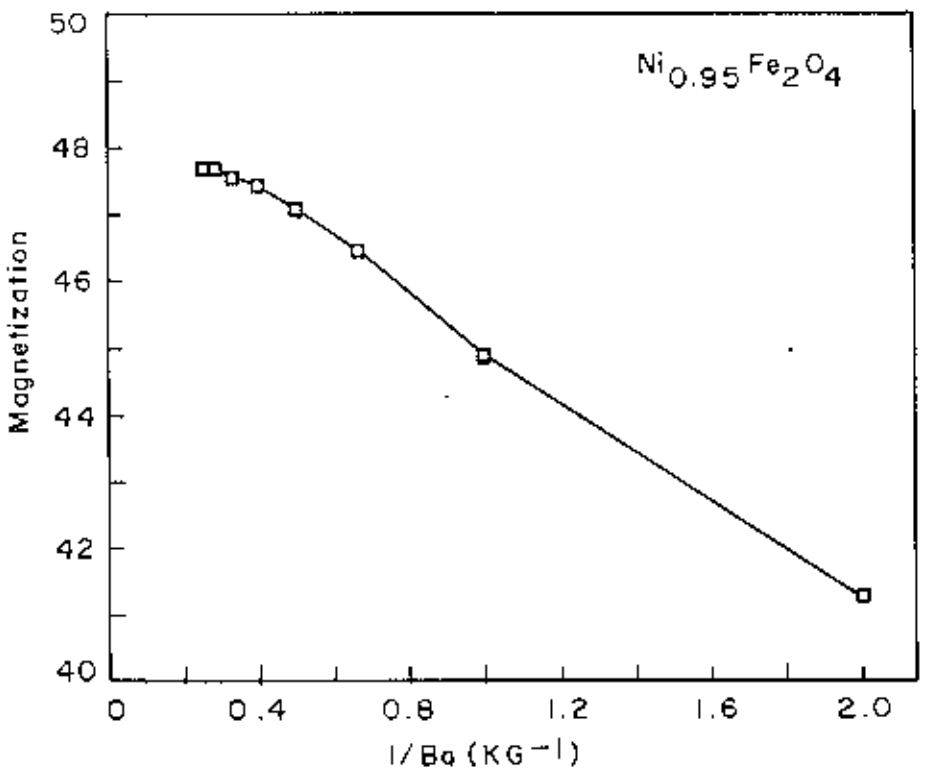

Fig.3.10f Values of the magnetization obtained at different field against 1/Ba. (Ba is applied field)

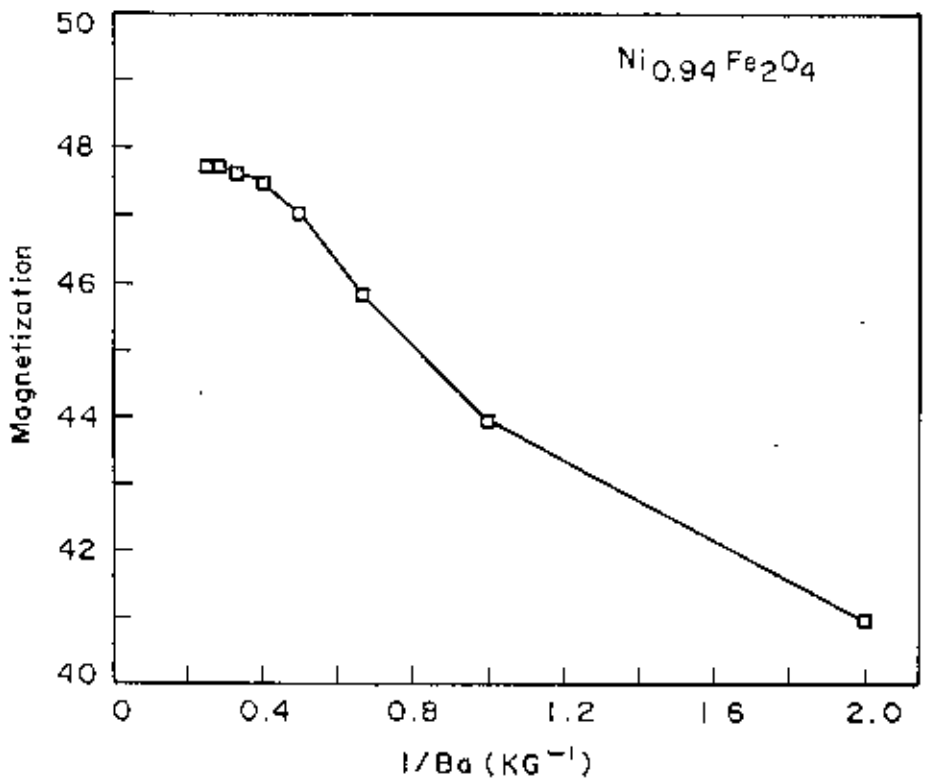

Fig.3.10g Values of the magnetization obtained at different field against 1/Ba. (Ba is applied field)

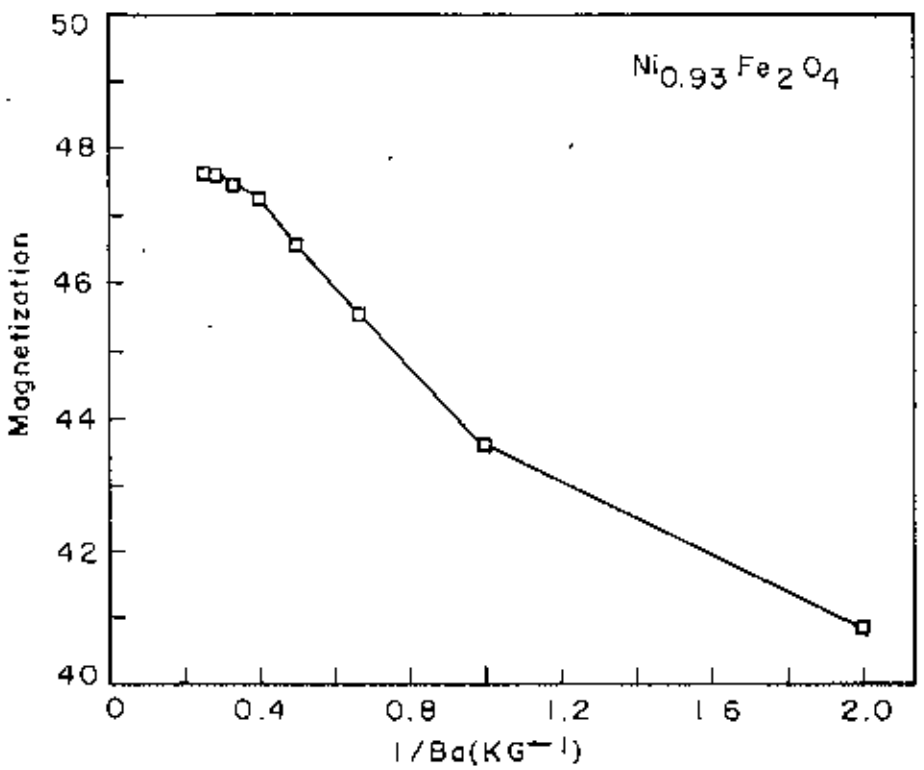

Fig.3.10h Values of the magnetization obtained at different field against 1/Ba. (Ba is applied field)

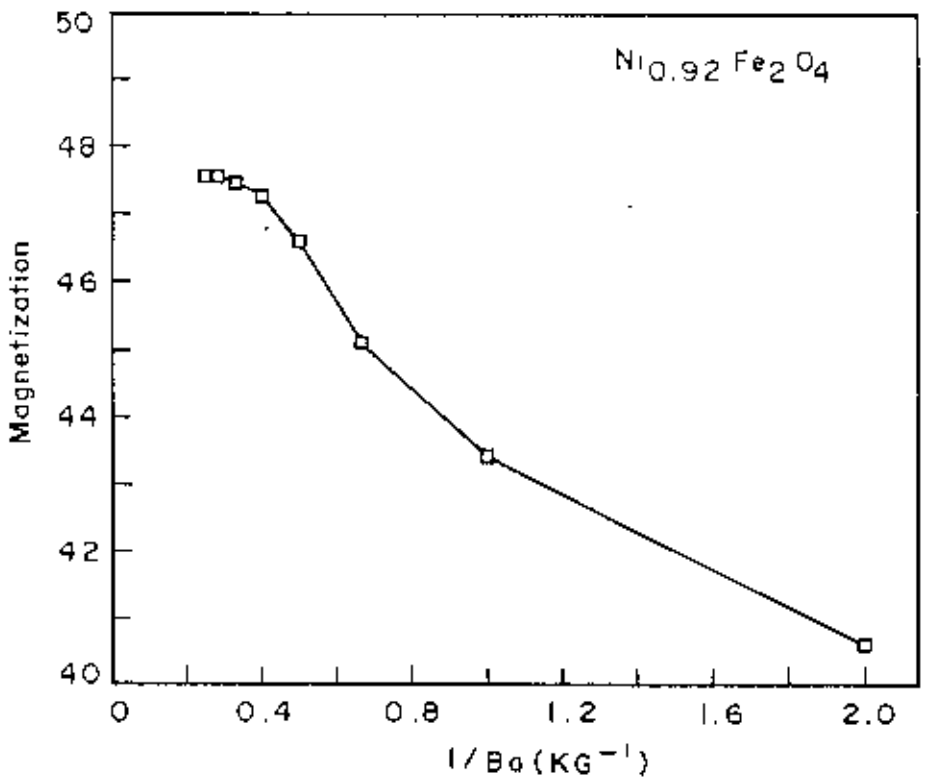

Fig.3.10i Values of the magnetization obtained at different field against 1/Ba. (Ba is applied field)

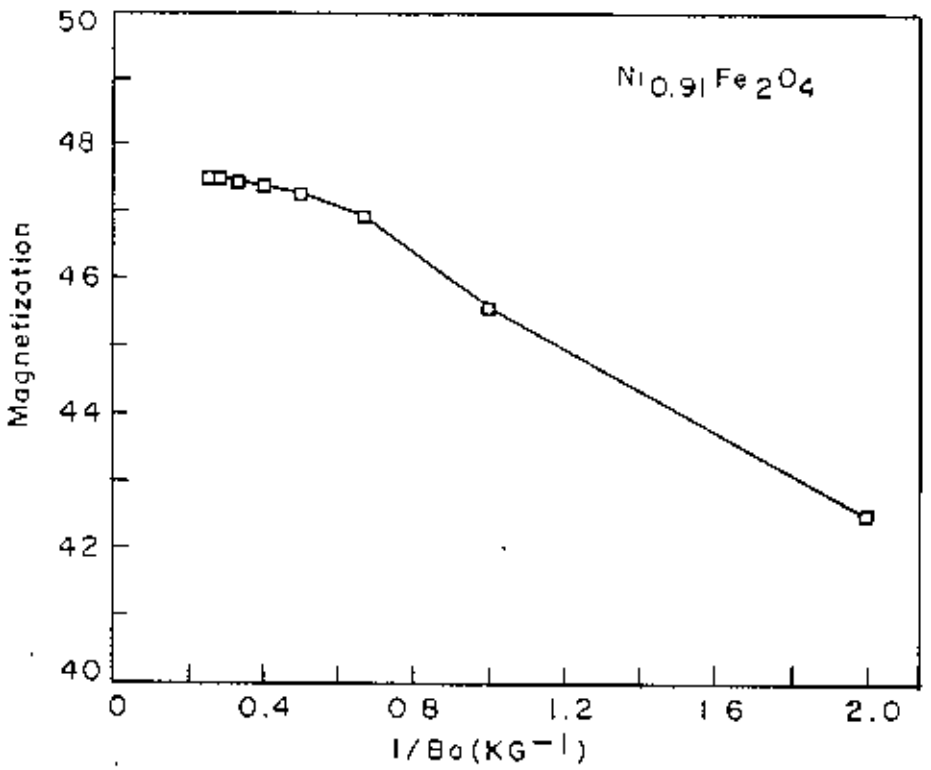

Fig.3.10j Values of the magnetization obtained at different field against 1/Ba. (Ba is applied field)

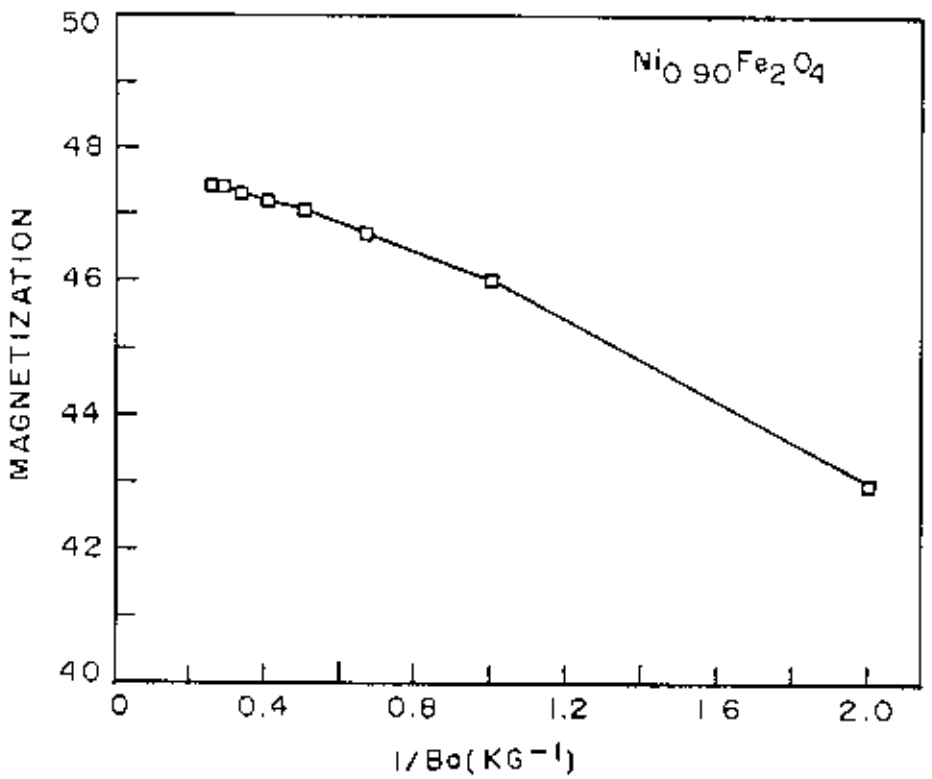

Fig.3.10k Values of the magnetization obtained at different field against 1/Ba. (Ba is applied field)

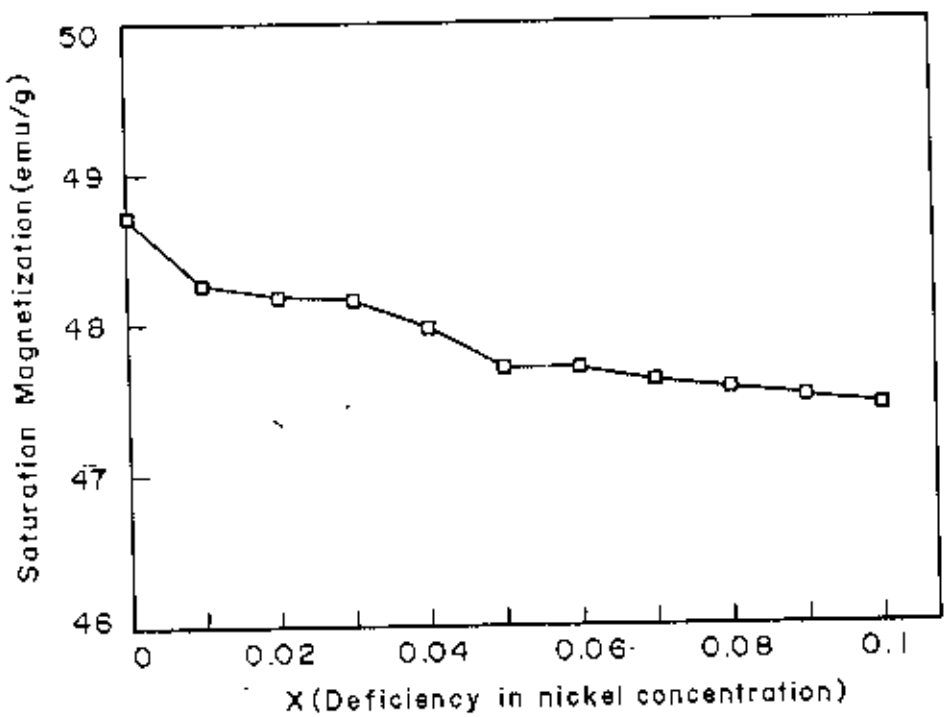

Fig.3.11 Saturation magnetization of $Ni_{1-x}Fe_2O_4$ as a function of x

structure does not necessarily suggest that the spin arrangement of the ions remains unaffected. With the decrease in nickel content, one would normally expect inhomogeneity in the specimens or the precipitation of excess iron in the nickel deficient samples . The precipitated iron phase will be very small compared to the bulk specimen. If we assume that the compound $Ni_{1-x}Fe_2O_4$ contains the stoichiometric compound ($Ni_{1-x}Fe_{2-2x}O_4$) and excess Fe_{2x} as precipitate, then the possible spin arrangements might be

$$Fe_{1-x}^{III}[Ni_{1-x}^{II}Fe_{1-x}^{III}]O_4\ Fe_{2x}.$$

The magnetic moment of the system will then be:

(i) sum of the moments of $\uparrow Ni_{1-x}^{II} + \uparrow Fe_{2x}$ if the Fe_{2x} iron ions are coupled parallel with the nickel ions.

(ii) difference of the moments of $\uparrow Ni_{1-x}^{II} + \downarrow Fe_{2x}$ if they are antiferromagnetically coupled ,or

(iii) the moments due to nickel ions only $\uparrow Ni_{1-x}\ \uparrow Fe_x\ \downarrow Fe_x$

This spin arrangement will give the same moment if we assume homogeneous compound of $Ni_{1-x}Fe_2O_4$ with the spin arrangement

$$\uparrow Fe^{II}[Ni_{1-x}\uparrow Fe^{II}\downarrow]\ O_4 \text{ like that in } NiFe_2O_4.$$

Theoretically calculated value of the three different spin distributions are given in Table-3.12. The moment for Ni^{2+} and Fe^{3+} was taken to be $4\mu_B$ and $5\mu_B$ respectively. Table-3.13 shows the normalized expected values

$$\frac{\text{moment of } Ni_{1-x}Fe_2O_4}{\text{moment of } NiFe_2O_4}$$

for the three different assumptions along with the experimental normalized values. The values thus obtained are drawn in Fig.3.12. It is clear that the experimental values are close to the value if only the moment due to nickel content is taken into account. Since no traces of extra-lines has been noticed in the x-ray diffraction pattern and the magnetization measurement supports the spin arrangement as in cubic $NiFe_2O_4$, it seems quite certain that nickel deficient ferrites, deficient upto 10% is capable of maintaining its cubic structure. The source of magnetic moment in these material is dominated by Ni^{2+} ions.

TABLE-3.12

Concentration	$\uparrow Ni_{1-x}$	$\uparrow Ni_{1-x} \uparrow Fe_{2x}$	$\uparrow Ni_{1-x} \downarrow Fe_{2x}$
0	4.1	4.1	4.1
0.01	4.059	4.159	3.959
0.02	4.018	4.218	3.818
0.03	3.977	4.277	3.677
0.04	3.936	4.336	3.536
0.05	3.895	4.395	3.395
0.06	3.854	4.454	3.254
0.07	3.813	4.513	3.113
0.08	3.772	4.572	2.972
0.09	3.731	4.631	2.831
0.10	3.690	4.690	2.690

Theoritical values of the magnetization (in Bohr magneton) for $Ni_{1-x}Fe_xO_4$ assuming three different passible spin arrangements of Ni and Fe in the system.

Table-3.13

Concentr a-tion x	Experimen-tal	$\uparrow Ni_{1-x}$	$\uparrow Ni_{1-x}\ \uparrow Fe_{2x}$	$\uparrow Ni_{1-x}\ \downarrow Fe_{2x}$
0.00	1.00	1.00	1.00	1.00
0.01	0.990	0.99	1.014	0.965
0.02	0.989	0.98	1.028	0.931
0.03	0.988	0.97	1.043	0.896
0.04	0.984	0.96	1.057	0.862
0.05	0.979	0.95	1.071	0.828
0.06	0.979	0.94	1.086	0.793
0.07	0.977	0.93	1.100	0.759
0.08	0.976	0.92	1.115	0.724
0.09	0.975	0.91	1.129	0.690
0.10	0.973	0.90	1.143	0.656

Normalized values of the magnetization ($M\ Ni_{1-x}Fe_2O_4$ / $MNiFe_2O_4$) of $Ni_{1-x}\ Fe_2O_4$ for the three different possible spin arrangement (claculated from the values in Table 3.12) along with the normalized experimental values.

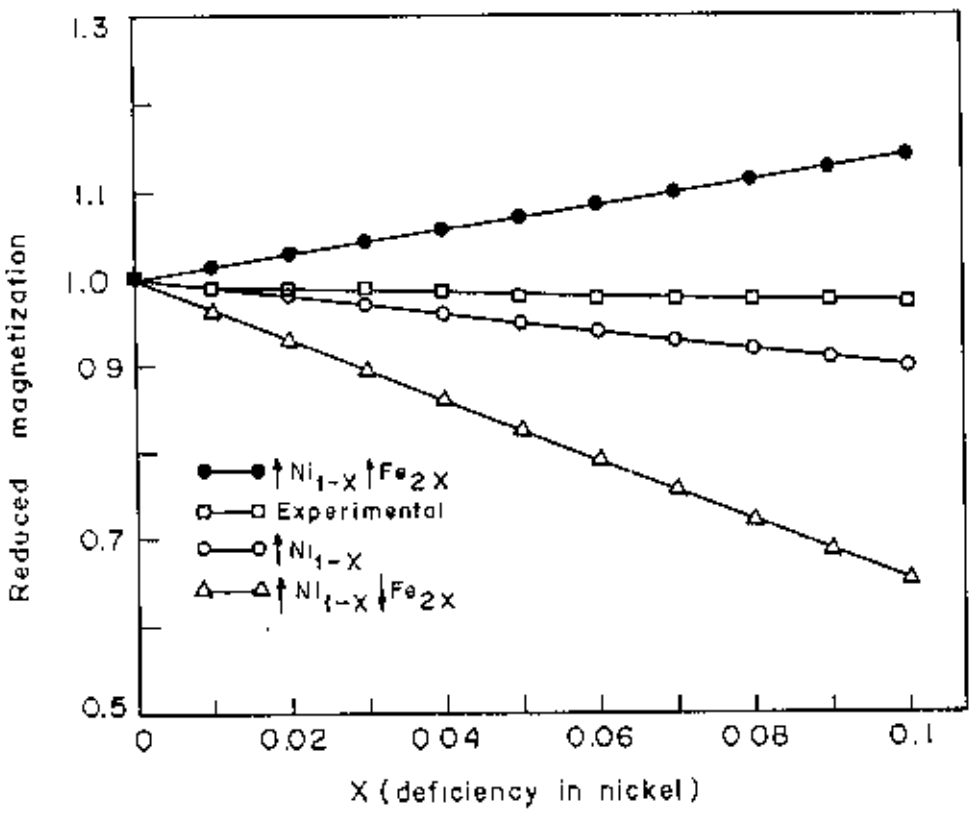

Fig.3.12 Reduced magnetization assuming different spin arrangements compared to the experimental values.

CHAPTER – 4

MEASUREMENTS OF PERMEABILITY AND LOSS TANGENT OF $Ni_{1-X}Fe_2O_4$

4.1 Introduction to permeability:

The technical importance of ferrites lies primarily in their high resistivity. Whereas in the metallic ferromagnetic materials the resistivity can not be made higher than 10^{-4} Ωm; technical ferrites have, depending on their applications, resistivities of 1 to 10^{12} Ω-cm. In magnetic materials a low resistivity gives rise to eddy-current losses. All other properties being equal, these losses are proportional $D^2 f/\rho$, where D is the thickness of the core, f is the frequency of the ac field, and ρ is the resistivity. Even at 50 Hz, iron cores must be divided into isolated shells of about 1mm thickness to avoid large losses. In a massive ferrite core 1 cm thick of 10Ω-cm resistivity similar eddy current losses would not occur below 0.5 MHz; a ferrite core of 10^{10} Ω-cm resistivity would not show such losses below 5×10^{14} Hz, the frequency of the visible light. It is thus clear, then, that the use of massive core effects considerable savings in magnetic components. Although the high resistivity ferrites show no eddy-current losses upto optical frequency, losses due to other mechanisms and dispersion of the permeability are found at lower frequencies. For r.f. applications most important property is permeability. The primary requirement is the highest possible permeability, together with low losses in the frequency range of interest. The initial permeability μ is defined as the derivative of the induction B with respect to the internal field H in the demagnetized state:

$$\mu = \frac{dB}{dH} \quad , \quad H \to 0, \; B \to 0$$

At microwave frequencies, and also in anisotropic crystals dB and dH may be in different directions the permeability then has a tensor character. In the case of poly-crystalline materials containing a large number of randomly oriented crystallites the permeability will be scaler, at least at low frequencies with

$$B = H + 4\pi M$$

the susceptibility

$$\chi = \frac{dM}{dH} = \frac{d}{dH} \frac{1}{4\pi} (B - H)$$

$$= \frac{1}{4\pi} (\mu - 1)$$

The magnetic energy density

$$E = \frac{1}{4\pi} \int H \, . \, dB \qquad (1)$$

For time harmonic fields $H = H \sin \omega t$, the dissipation can be described by a phase difference δ between H and B. In this case the permeability concept may be extended to include the losses. Therefore we can introduce the quantity

$$\mu = \frac{B}{H}$$

as the ratio of the amplitudes of B and H.

$$B = B \sin(\omega t - \delta) = \mu H \sin \omega t \cos\delta - \mu H \cos\omega t \sin\delta \qquad (2)$$

The component $\mu H \cos\delta$, which is in phase with H, is related to the maximum stored magnetic energy density E', by

$$E' = \frac{1}{8\pi} \mu H^2 \cos\delta \qquad (3)$$

The component $\mu H \sin\delta$ is 90° out of phase with H. This component is a measure for the losses. In the steady state the losses can be found by integrating

$$E = \frac{1}{4\pi} \int H.dB$$

over one period $T = \frac{2\pi}{\omega}$

The energy dissipation per unit volume per unit time is therefore,

$$P = \frac{1}{4\pi} \frac{1}{T} \int_0^T H \frac{dB}{dt} dt = \frac{\omega}{8\pi} \mu H^2 \sin\delta \qquad (4)$$

In the complex notation with the time factor $e^{j\omega t}$ expression (2) can be written as $B = \mu H$ by introducing the complex permeability.

$$\mu = \mu' - j\mu'' = \mu \cos\delta - j\mu \sin\delta \qquad (5)$$

from which it follows that $\mu = |\mu|$. The real part μ' describes the stored energy E' (eq.3) and μ'' describes the dissipation P according to eq.4. It is useful to introduce the loss factor or loss tangent tanδ. From eqn. (3), (4) & (5)

$$\tan\delta = \frac{\mu''}{\mu'} = \frac{\text{energy dissipated per period } 2\pi/\omega}{2\pi \times \text{stored energy}}$$

The behavior of μ' and μ'' versus frequency is called a permeability spectrum: The initial permeability of a ferromagnetic or ferrimagnetic substance is the combined effect of the wall permeability and rotational permeability mechanisms.

4.2 The mechanism of Permeability:

The mechanisms can be explained as follows: A demagnetized magnetic material is divided into number of weiss domains separated by Block walls. In each domain all the magnetic moments are oriented in parallel, and the magnetization has its saturation value M_s. In the walls the magnetization direction

changes gradually from the direction of magnetization in one domain to that in the next. The equilibrium positions of the walls result from the interactions with the magnetization in neighboring domains and from the influence of pores, crystal boundaries and chemical inhomogeneities which tend to favor certain wall positions.

4.2.1 Wall permeability

The mechanism of wall permeability arises from the displacement of the domain walls in small fields. Let us consider a piece of material in the demagnetized state, divided into weiss domains with equal thickness L by means of 180° Bloch walls (as in the Fig.4.1). The wall are parallel to the Y,Z plane. The magnetization M_s in the domains is oriented alternately in the +Z or -Z direction. When a field H with a component in the +Z direction is applied, the magnetization in this direction will be favored. A displacement dx of the walls in the direction shown by the dotted lines will decrease the energy density by an amount.

$$\frac{2\ M_s\ H_z\ dx}{L}$$

This can be described as a pressure $2\ M_s\ H_z$ exerted on each wall. This pressure will be counteracted by restoring forces,

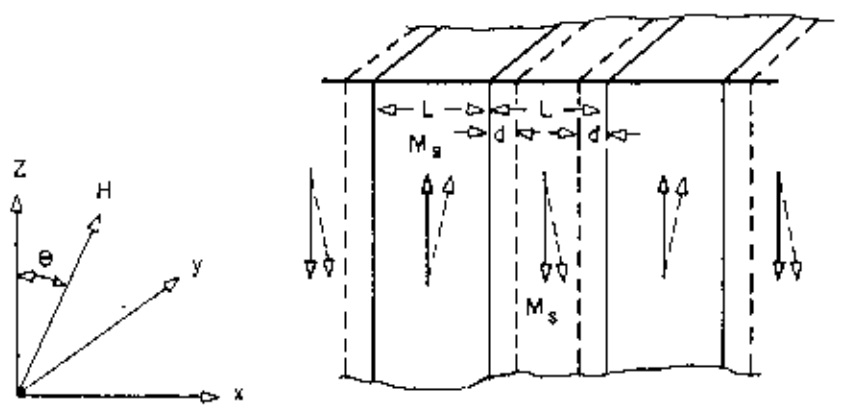

Fig.4.1 Magnetization by wall motion and spin rotation.

which for small deviations may assumed to be -Kdx per unit wall surface. The new equilibrium position is then given by

$$d = \frac{2M_s H_z}{K}$$

From the change in the magnetization

$$\Delta M = \frac{2M_s d}{L}$$

the wall susceptibility χ_ω may be calculated. Let H make the angle θ with Z direction. The magnetization in the θ direction becomes

$$(\Delta M)_\theta = \frac{2M_s d}{L} \cos\theta, \quad \text{and with } H_z = H \cos\theta \text{ and}$$

$$d = \frac{2M_s Hz}{K}$$

We obtain

$$\chi_\omega = \frac{(\Delta M)_\theta}{H} = \frac{4 M_s^2 \cos^2\theta}{KL} \qquad (6)$$

4.2.2 Rotational permeability

The rotational permeability mechanism arises from rotation of the magnetization in each domain. The direction of M can be

found by minimizing the magnetic energy E as a function of the orientation. Major contribution to E comes from the crystal anisotropy energy. Other contributions may be due to the stress and shape anisotropy. The stress may influence the magnetic energy via the magnetostriction. The shape anisotropy is caused by the boundaries of the sample as well as by pores, non-magnetic inclusions and inhomogeneities. For small angular deviations α_x and α_y or M, where

$$\alpha_x = \frac{M_x}{M_s} \quad \& \quad \alpha_y = \frac{M_y}{M_s}$$

from the equilibrium Z-direction may be expressed as

$$E = E_0 + \tfrac{1}{2}\,\alpha_x^2\, E_{xx} + \tfrac{1}{2}\,\alpha_y^2\, E_{yy}.$$

where it is assumed that x an Y are the principal axes of the energy minimum. Instead of E_{xx} & E_{yy}, the anisotropy field H_x^A and H_y^A are often introduced. Their magnitude is given by

$$H_x^A = \frac{E_{xx}}{2M_s} \quad \text{and} \quad H_y^A = \frac{E_{yy}}{2M_s}$$

H_x^A & H_y^A represent the stiffnesses with which the magnetization is bound to the equilibrium direction for deviations in the X

and Y direction, respectively. The rotational susceptibilities $\chi_{r,x}$ & $\chi_{r,y}$ for fields applied along X and Y directions, respectively are

$$\chi_{r,x} = \frac{M_s}{H_x^A} \qquad \chi_{r,y} = \frac{M_s}{H_y^A}$$

For cubic materials it is often found that H_x^A and H_y^A are equal. For $H_x^A = H_y^A = H^A$ and a field H which makes an angle θ with the Z direction (as shown in Fig.4.1) the rotational susceptibility, $\chi_{r,c}$ in one crystallite becomes

$$\chi_{r,c} = \frac{M_s}{H^A} \sin^2\theta \qquad (7)$$

A polycrystalline material consisting of a large number of randomly oriented grains of different shapes, with each grain divided into domains in a certain way. The rotational susceptibility χ_r of the material has to be obtained as a weighted average of $\chi_{r,c}$ of each crystallite, where the mutual influence of neighboring crystallites has to be taken into account. If the crystal anisotropy dominates other anisotropics, then H^A will be constant throughout the material, so only the factor $\sin^2\theta$ (eqn.7) has to be averaged Snoek [1] assuming a linear averaging of $\chi_{r,c}$ and found

$$\chi_r = \frac{2\ M_s}{3\ H^h} \qquad (8)$$

The total internal susceptibility

$$\chi = \chi_\omega + \chi_r = \frac{4M_s^2 \cos^2\theta}{KL} + \frac{2M_s}{3H^h} \qquad (9)$$

If the shape and stress anisotropics can not be neglected, H^h will be larger. Any estimate of χ_r will than be rather uncertain as long as the domain structure, the stresses, and the pore distribution in the material are not known. A similar estimate χ_ω would require knowledge of the stiffness parameter k and the domain width L. These parameters are influenced by snch factors as imperfection porosity and crystallite shape and distrbution and are essentially unknown. In few cases the motion of domain walls in polycrystalline samples has been studied by the Bitter techniques in the relatively large field [2]. In the small fields necessary for the measurement of the initial permeability the observation of wall motion would be extremely difficult. However if the anisotropy is known, an idea of the wall susceptibility can be obtained by subtracting from the total susceptibility the value of χ_r obtained from eqn. 8. The value of the μ_{rk} ($= 4\pi\chi_r+1$) obtained thus must be considered as a maximum of the rotation permeability. The total permeability is usually an order of magnitude larger than μ_{rk} [3-7] indicating

that the wall permeability is dominant in small fields.

4.3 Techniques of measurments of permeability

Measurements of permeability normally involves the measurements of the change in self inductance of a coil in presence of the magnetic core. The behavior of a self-inductance can now be described as follows. Suppose we have an ideal lossless air coil of inductance L_0. On insertion of a magnetic core with permeability μ, the inductance will be μL_0. The complex impedance Z of this coil can be expressed as

$$Z = R + j X = j\omega L_0 \mu = j\omega L_0(\mu' - j\mu'') \qquad (10)$$

where the resistive part is

$$R = \omega L_0 \mu'' \qquad (11)$$

and the reactive part is

$$X = \omega L_0 \mu' \qquad (12)$$

The r.f. permeability can be derived from the complex impedance of a coil Z (eqn.10). The core is usually toroidal to avoid demagnetiziug effects. The quantity L_0 is derived geometrically.

The methods of measurement listed below can be generally categorized as bridge measurements, direct impedance measurements and measurements of the properties of a resonance circuit incorporating the material.

Methods of measurement those are commonly used are :

1. The Maxwell bridge.
2. Resonance circuits.
3. The standing-wave method.

4.3.1 The Maxwell bridge.

The principle of operation of the Maxwell type of rf bridge is shown schematically in Fig.4.2. The conditions of balance are, with an unknown impedance

$$Z_x = R + j\omega L$$

$$R = R_1 R_2 / R_4 \quad \text{and} \quad L = R_1 R_2 C$$

The advantage of this type of bridge is that the setting of C is constant as long as μ' is independent of frequency. However, some difficulties are encountered in bridge measurements. One problem arises from the finite resistivity R_c of the coil wiring. Because $\mu'' = R/\omega L_0$ according to Eq. (11), R may be very small compared with R_c especially at low

frequencies. Attempts to decrease R_c have led to the permeameter [8], which is essentially an impedance transformer. It has a wound toroidal core of a ferrite with known properties as a primary winding and a coaxial shorting enclosure as a secondary winding. The latter contains both the primary and the toroidal test sample.

Another problem is the stray impedance. The influence of the capacitance to earth of the bridge edges may be removed by employing highly symmetrical bridge arms and a Wagner earth, as described by Kohler and Koops [9]. Also, at high frequencies the reactive parts of the precision resistors become important and may give rise to serious errors. A method for decreasing the reactance of resistors in a bridge up to 60 MHz is described by Mulhall [10]. He replaced the bulky wire-wound precision resistors by tiny thermistors with negligible reactance. The resistance of these thermistors can be controlled by means of an auxiliary low-frequency bridge circuit. The same principle is applied in some commercial measuring equipment such as the Siemens bridge Rel 3 R 218, which operates between 60 kHz and 30 MHz.

If μL_0 is sufficiently high, a "single-turn" coaxial system, like S in Fig.4.2, may be connected directly to the bridge, and a zero balance may be made by removing only the sample. With this procedure the quantity μ-1 is measured.

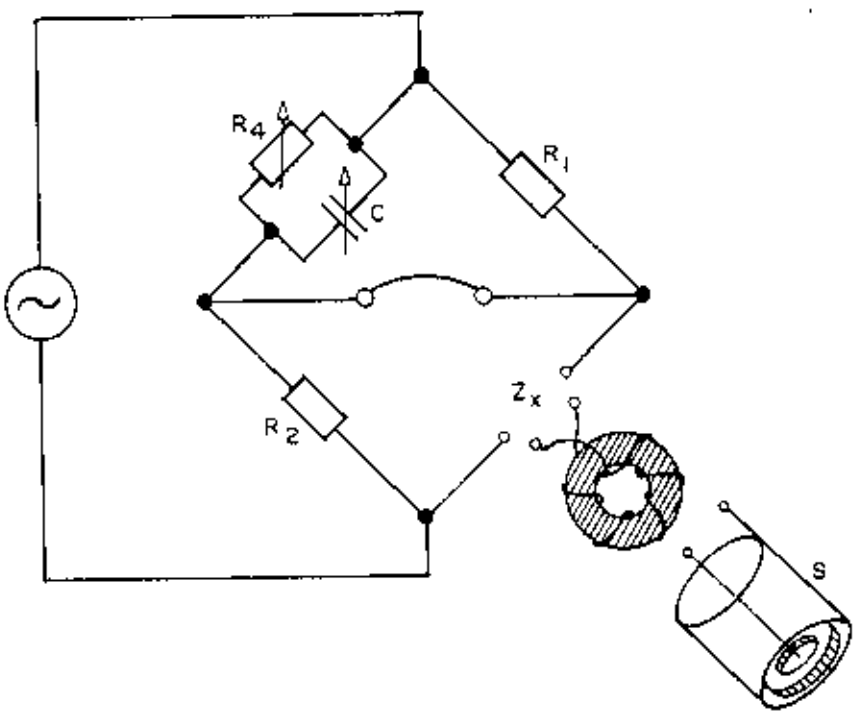

Fig.4.2 The Maxwell bridge.

4.3.2 Resonance circuits

A particularly useful method of impedance measurement is based on the detuning of a resonance circuit. The principle of operation is shown in Fig.4.3. By varying the frequency of a constant-voltage generator, the resonance frequency and the quality factor of a resonance circuit may be obtained from the frequency characteristic of the current. In the unloaded circuit of Fig.4.3a, for small losses the resonance frequency and quality factor are

$$\omega_0=(LC)^{-\frac{1}{2}} \qquad Q_0 = \frac{\omega_0 L}{R}$$

On loading the circuit with an impedance $Z_x = R_x + j\omega L_x$ we obtain

$$\omega_1=[(L+L_x)C]^{-1/2} \qquad Q_1 = \frac{\omega_1 (L+L_x)}{R+R_x}$$

The value of R_x and L_x may be calculated from ω_0, ω_1, Q_0 and Q_1 if either L or C is unknown.

This method may be used in a large frequency range, from 10 kHz up to microwave frequencies. From 50 to 2000 MHz short-circuited coaxial lines of quarter- or three-quarter-wave

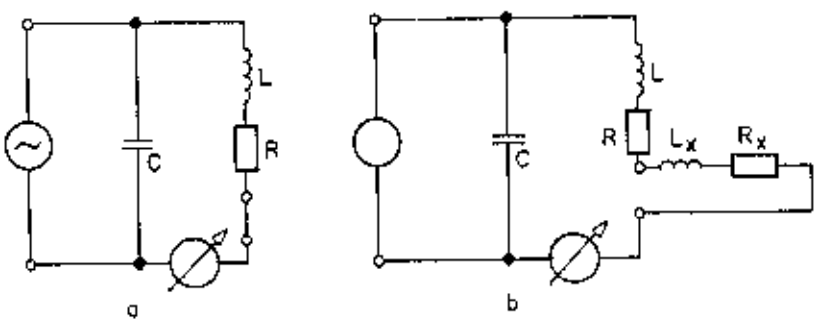

Fig.4.3 Detuning of a resonant circuit.

lengths are used. The toroidal samples are inserted concentrically, with the inner and outer conductors near the short circuit of the line. Therefore the measured quantity is μ-1. With coaxial-line resonators measurements can also be taken at constant frequency by varying the length of the inner conductor [11]. Without exact knowledge of the properties of the resonator, the calibration may be obtained as follows. At frequencies above 30 MHz the magnetic field does not penetrate in a metallic sample. A copper ring therefore effectively shows $\mu = 0$, and the insertion of such a ring gives the frequency shift due to $\mu - 1 = -1$ for the cross section of the ring.

4.3.3 The standing-wave method

In a transmission line which is terminated by a closely fitting ferrite sample the permeability as well as the dielectric constant may be measured. In this method, which was developed by Roberts and Von Hippel [12], the complex reflection co-efficient of the line is measured at two positions in a short circuit, immediately behind the sample and a quarter-wave distance away. The calculation is rather complicated. Serious errors may result from air gaps between the sample and the transmission line.

4.4 Preparation of the samples for permeability measurements:

To perform the investigation of permeability on $Ni_{1-x}Fe_2O_4$ samples, specimens of anchor ring shaped were prepared from the presintered powder samples prepared for the measurements of magnetization. The presintered powders were first crushed to fine powders prior to the preparation of anchor ring shaped specimens. The anchor ring shaped specimens of internal diameter 16 to 17 mm, exterual diameter 21 to 22 mm and thickness 4 to 5 mm were then made from the resultant fine powders at a pressure of about 100 bar in a hydraulic press using a dye. The components of the dye are shown in Fig 4.4. The samples thus prepared were then sintered at 1350 °C. The heating and cooling procedure for the anchor ring shaped samples were exactly smilar to that used for sintering specimens for magnetization measurements. While measuring the permeability of ferrite cores at high frequency, the high electric resistance of these materials generally precludes the troublesome skin effect found with metals. However, the cross-section of the ferrite core to be measured may have to be kept small in order to avoid dimensional resonance phenomena . The reason is that, owing to the high dielectric constant of some ferrits, it is possible that at the measuring frequency the wave length in the ferrite will be of the order of magnitude of a linear dimension, which can give rise to standing-wave phenomena iu the core. To avoid an increase in resistance owing to skin effect , braided copper

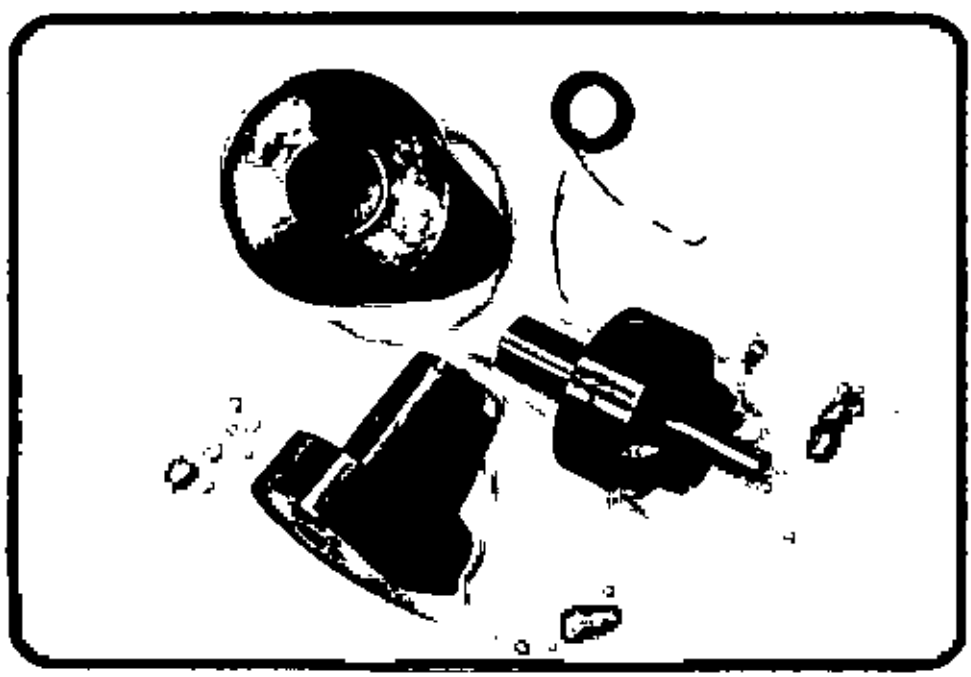

Fig.4.4 The components of the dye and the anchor ring shaped specimen.

wire needed to be used at frequencies higher than 100 KHz. The thickness of the separate wire strands being adapted in the measuring frequency of up to about 10 MHz the rule of thumb is that the wire thickness in microns must be smaller than the wavelength in meters.

At higher frequencies the capacitance arising from the winding gives inaccurate values R_s and L_s. It is therefore necessary to keep the capacitance of the winding as low as possible. Keeping this in minds a special low capacitance winding of thirty turns of 42 SWG gauze enameled copper wire were then wound on the anchor ring shaped samples. Frequency response characteristics were then investigated on these anchor ring shaped specimens as a function of frequency.

4.5 Measurements of frequency characteristics of $Ni_{1-x}Fe_2O_4$ samples

The frequency characteristics of the anchor ring shaped Ni_{1-x} Fe_2O_4 ferrite, samples for x = 0.00 to 0.10 that is their permeability spectra were investigated using an Hewlett Packart Impedance analyzer of Model No 4192ALF. The mean diameter and thickness of the samples used are given in Table 4.5a. The measurement of inductance and resistance were taken in the frequency range 100 KHz to 13 MHz. The values of the measured parameters obtained as a function of frequency are shown in Table 4.5b. The real and imaginary part of the permeability μ',

μ'' and tanδ given in Table 4.5c to 4.5k are calculated using the formula

$$L_s = L_0 \mu' \quad \text{and} \quad R_s = \omega L_0 \mu''$$

$$\text{and} \quad \tan\delta = \mu''/\mu'$$

Where L_s and R_s are the self inductance and resistance of the sample core and

$$L_0 = (\mu_0 N^2 A/\pi D_m)$$

is the inductance of the winding coil without the sample core and N is the number of turns of coil; A is the area of cross-section and D_m is the mean diameter of the sample. Fig.(4.5a to 4.5i) shows the permeability spectra at room temperature of the $Ni_{1-x}Fe_2O_4$ ferrites of different x. In the Fig.(4.5a to 4.5i) double logarithm scale is used because of the large span of the measured permeability and frequency values. The permeability scale is logarithmic for $\mu>1$ and linear for $\mu<1$.

4.6 Results and discussion

The behavior of μ' and μ'' versus frequency i.e. the permeability spectra at room temperature of the $Ni_{1-x}Fe_2O_4$ ferrites is shown in Fig 4.5a to 4.5i. In the figures double logarithmic scale is used because of the large span of measured permeability

and frequency values.This scale is also useful in distinguishing between a resonance and a relaxation process. In case of a relaxation the quantity

$$| d \log \mu'' / d \log f |$$

is always less than unity. A further characteristic difference between a resonance and a relaxation is that a minimum and maximum value of μ' always indicates resonance character, whereas for a relaxation process μ' decreases monotonically with frequency. In Fig. 4.5a to 4.5i the permeability scale for $\mu<1$ was taken linear.

In the reported measurement [13-14] of $NiFe_2O_4$, μ' was found to remain constant and upto the frequency of 100 MHz, and μ'' also maintains a constant value of less than 1 upto 10MHz beyond which an increase was observed, suggesting that in $NiFe_2O_4$ the permeability spectrum in the frequency range upto 10MHz is due to relaxation process & the permeability mechanism arises mainly due to the displacement of the domain walls beyond 10MHz the rotation of the magnetization starts taking place indicating a contribution to permeability from the resonance phenomena.

The permeability values of μ' and μ'' obtained in the present measurement is in close agreement with the reported value. We observed a similar behavior for μ' and μ'' for all the

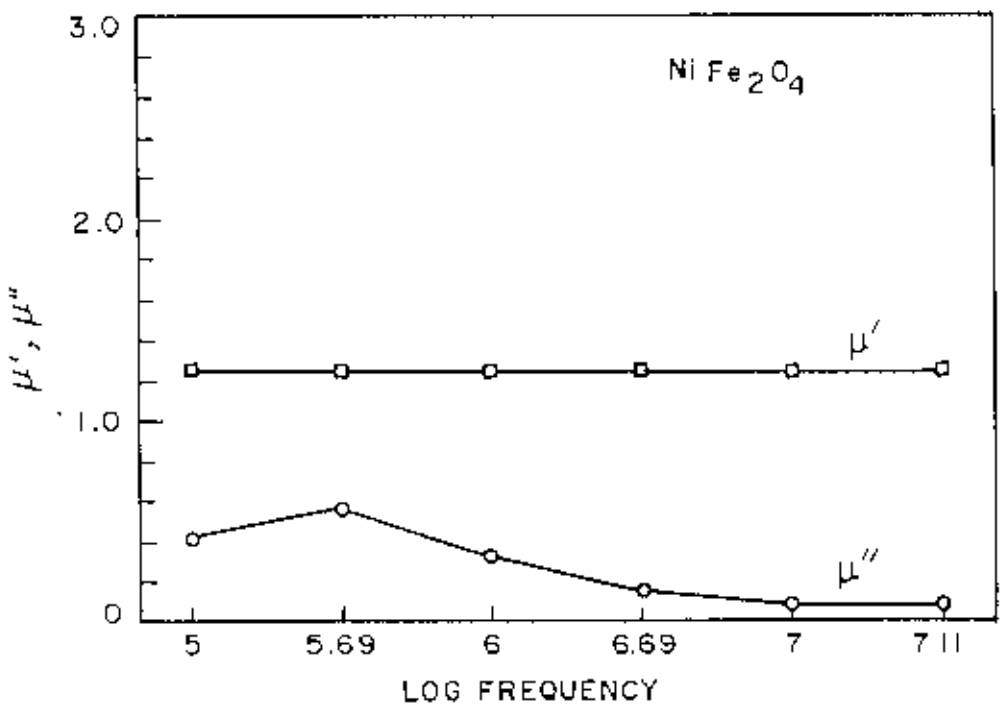

Fig.4.5a Permeability spectra at room temperature of $NiFe_2O_4$ ferrites. The μ scale is logarithmic for μ>1 and linear for μ<1.

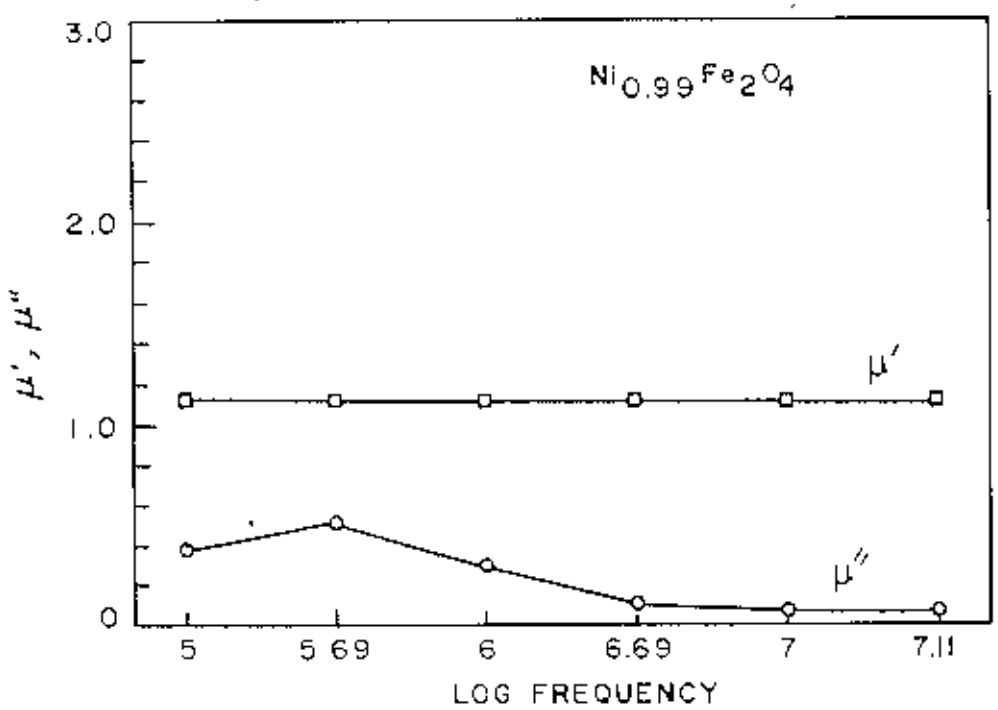

Fig.4.5b Permeability spectra at room temperature of $Ni_{0.99}Fe_2O_4$ ferrites. The μ scale is logarithmic for μ>1 and linear for μ<1.

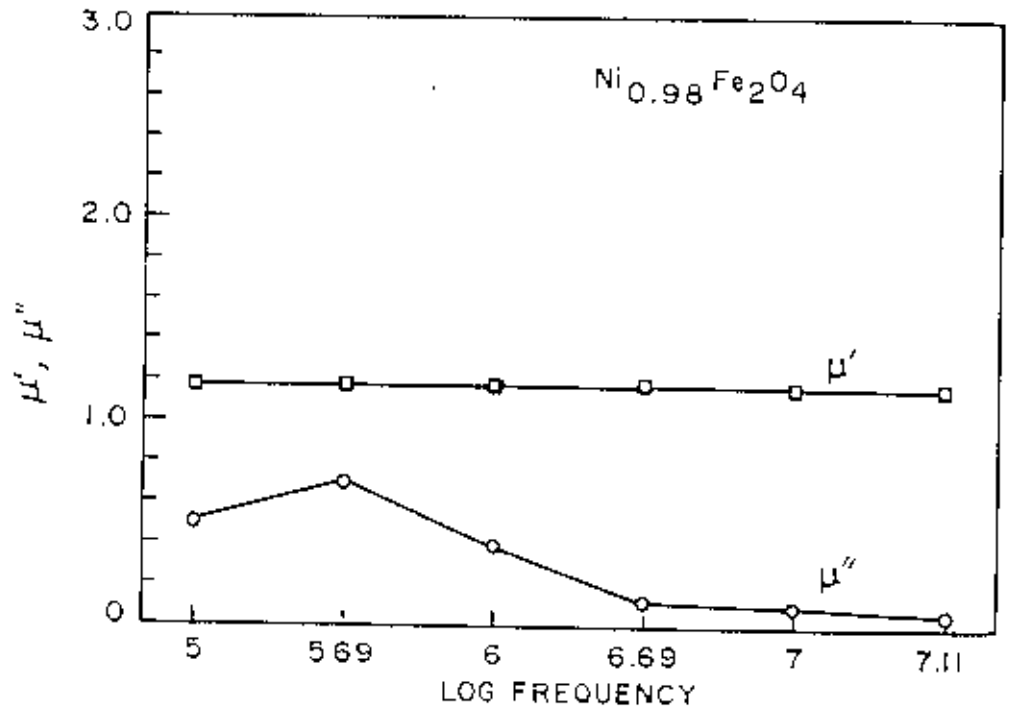

Fig.4.5c Permeability spectra at room temperature of $Ni_{0.98}Fe_2O_4$ ferrites. The μ scale is logarithmic for $\mu>1$ and linear for $\mu<1$.

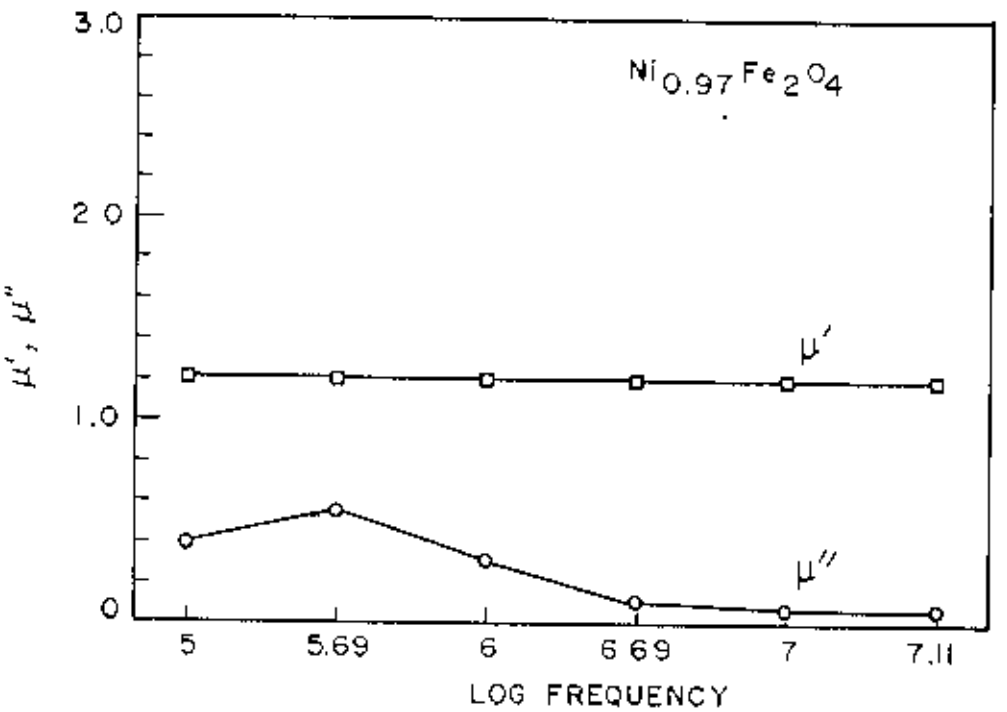

Fig.4.5d Permeability spectra at room temperature of $Ni_{0.97}Fe_2O_4$ ferrites. The μ scale is logarithmic for $\mu>1$ and linear for $\mu<1$.

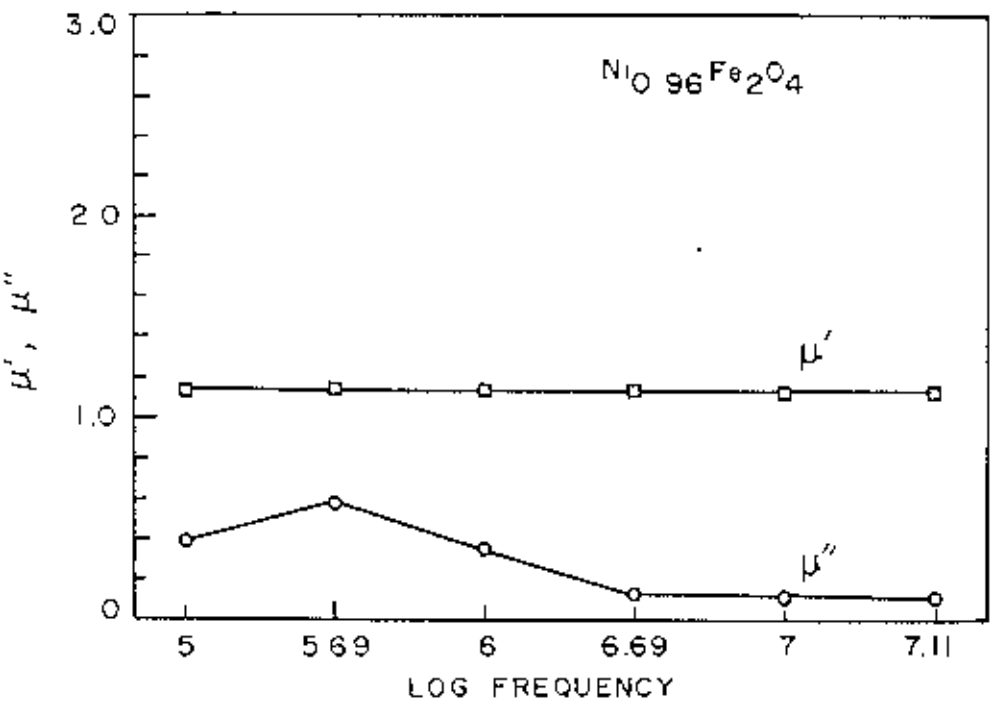

Fig.4.5e Permeability spectra at room temperature of $Ni_{0.96}Fe_2O_4$ ferrites. The μ scale is logarithmic for $\mu>1$ and linear for $\mu<1$.

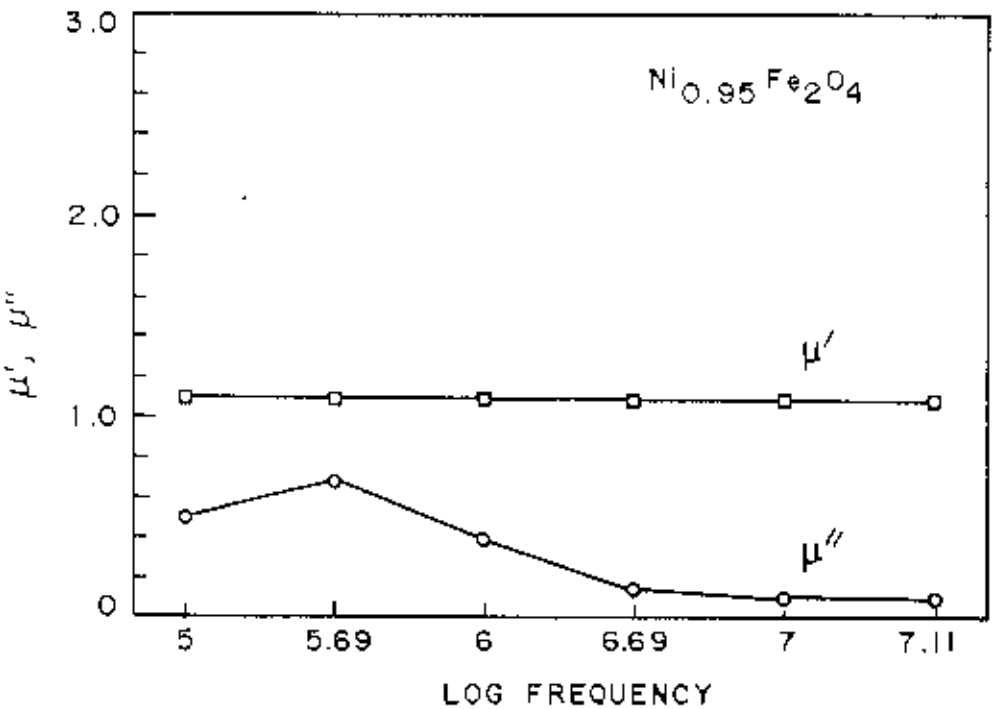

Fig.4.5f Permeability spectra at room temperature of $Ni_{0.95}Fe_2O_4$ ferrites. The μ scale is logarithmic for $\mu>1$ and linear for $\mu<1$.

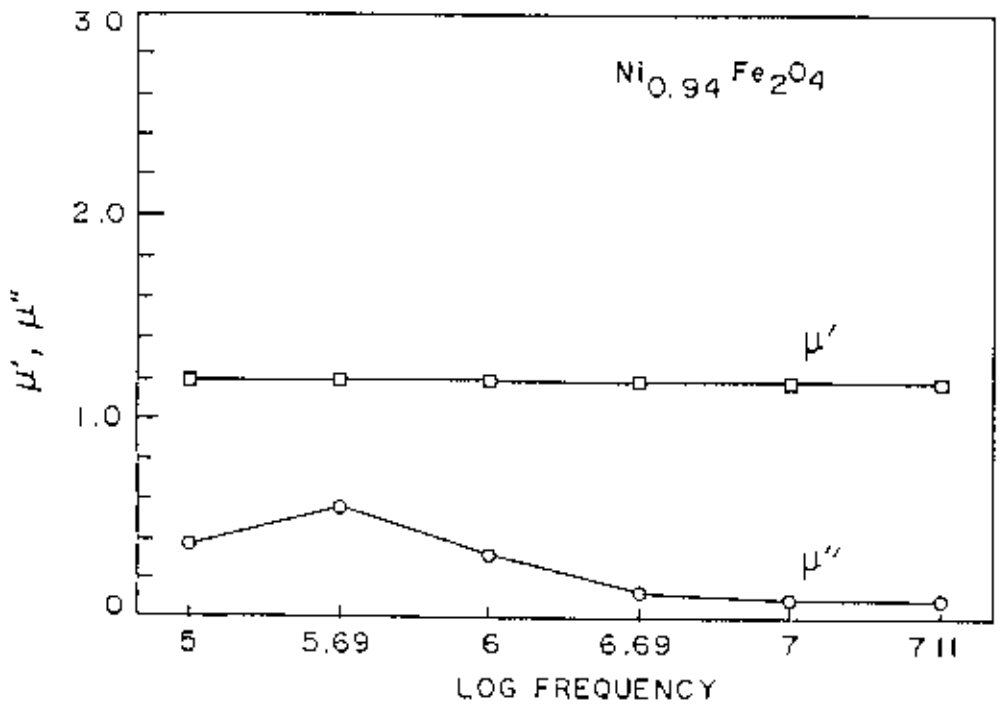

Fig.4.5g Permeability spectra at room temperature of $Ni_{0.94}Fe_2O_4$ ferrites. The μ scale is logarithmic for $\mu>1$ and linear for $\mu<1$.

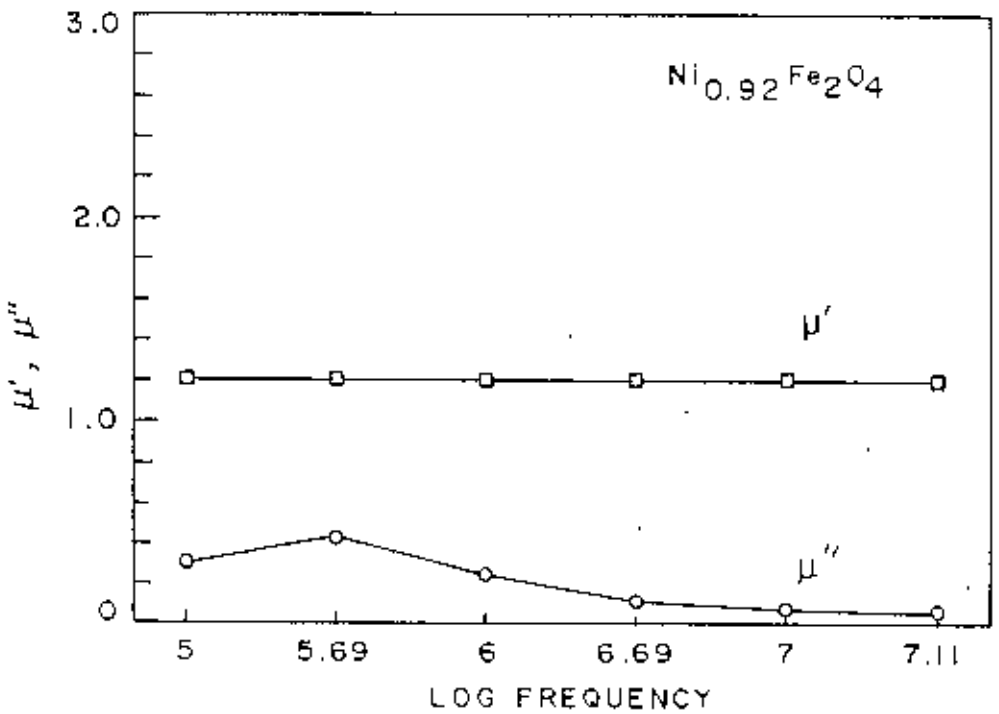

Fig.4.5h Permeability spectra at room temperature of $Ni_{0.92}Fe_2O_4$ ferrites. The μ scale is logarithmic for $\mu>1$ and linear for $\mu<1$.

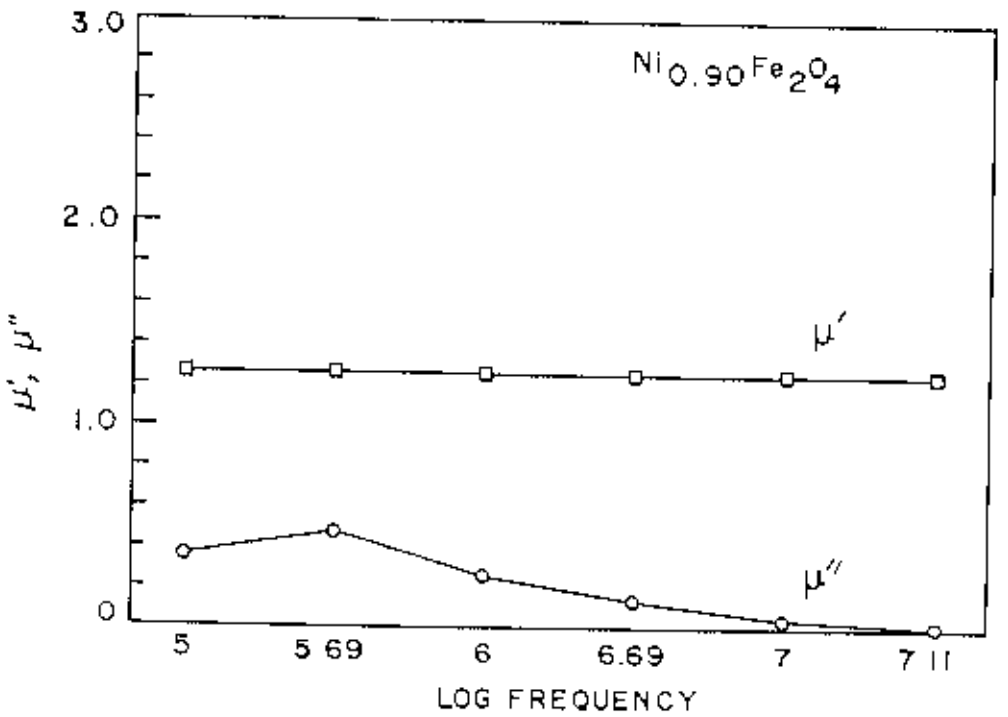

Fig.4.5i Permeability spectra at room temperature of $Ni_{0.90}Fe_2O_4$ ferrites. The μ scale is logarithmic for $\mu>1$ and linear for $\mu<1$.

nickel deficient specimens (Fig.4.5a to 4.5i), suggesting that in the frequency range of our measurement 100KHz to 13MHz the mechanism responsible for permeability was similar to that in $NiFe_2O_4$ that is due to wall displacement. The variation of μ' and μ'' and loss tangent, tanδ, for the nickel deficiency x is given in Fig. 4.6a to 4.6c.

In Fig. 4.6a the curves of μ' for the six different frequencies merges into a single curve, This is because of the fact that the value of μ' remains unaffected with frequency. The curves for μ'' shows a slight variation with frequency upto 10MHz and a value of $\mu'' > 1$ for 13MHz, suggesting that beyond 10 MHz the rotation of domain magnetization starts.

The contribution from domain wall displacement and the rotation of magnetization could not be separated, because of the fact that the susceptibility is related by (eqn.9);

$$\chi = \chi_{\omega} + \chi_r = \frac{4M_s^2 \cos^2\theta}{KL} + \frac{2M_s}{3H^A}$$

Where χ_{ω} and χ_r is the contribution from wall displacement and rotation of magnetization respectively. An idea about the wall susceptibility χ_{ω} may be obtained by subtracting the value of χ_r from the total susceptibility χ, if the anisotropy field H^A is

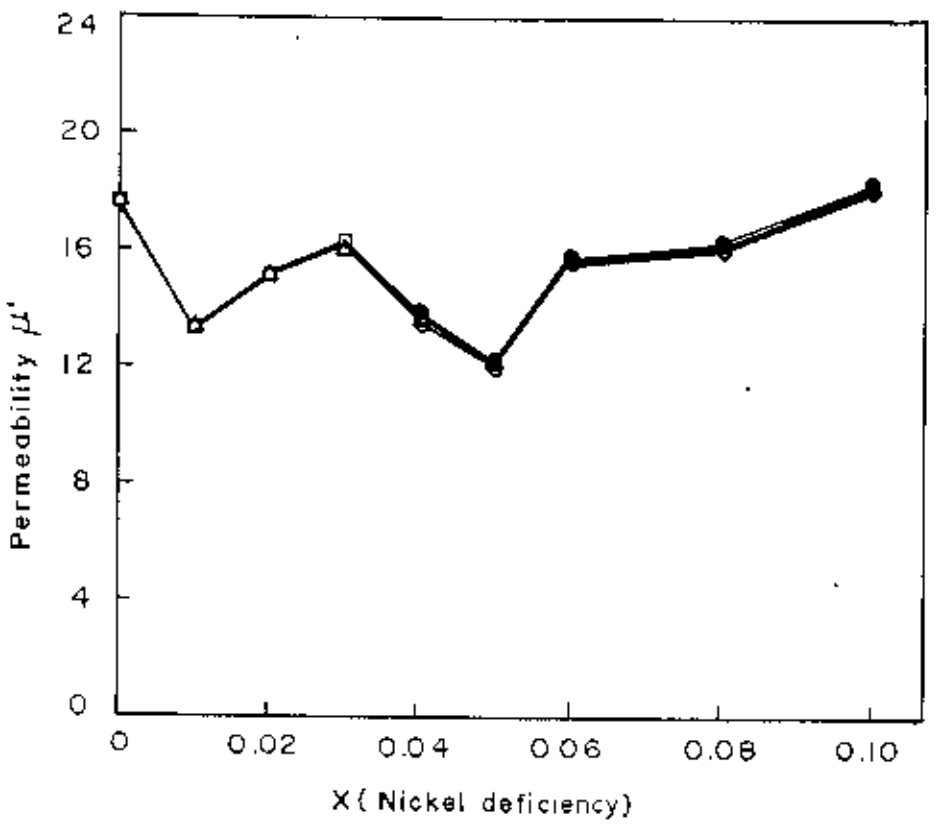

Fig.4.6a Permeability μ' Vs nickel deficiency (x).

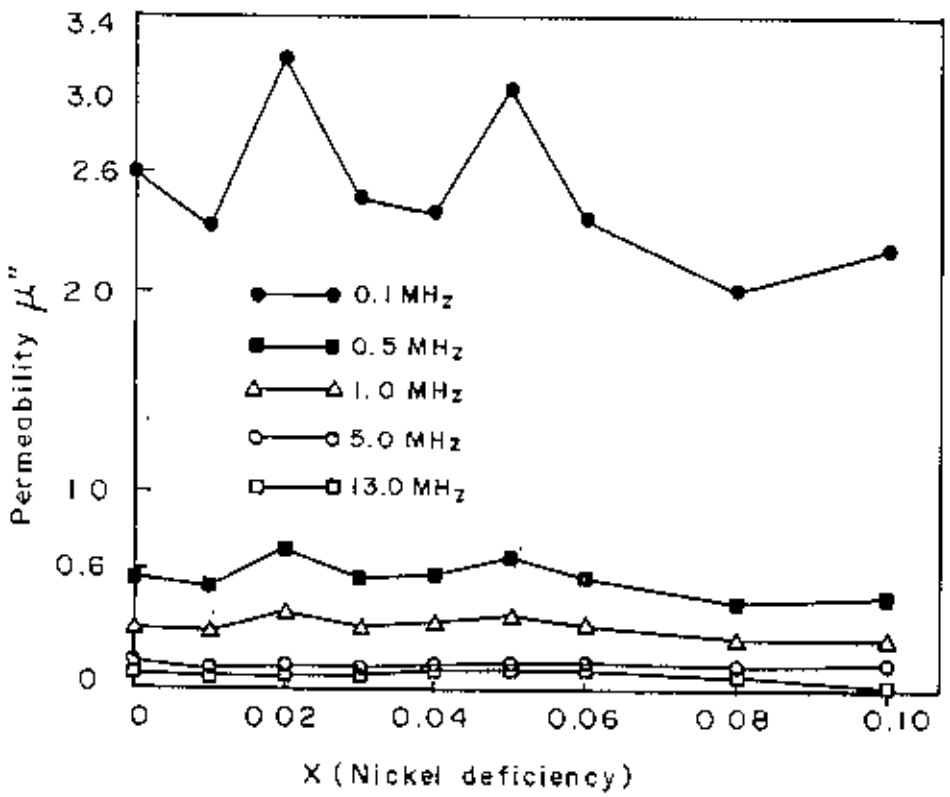

Fig.4.6b Permeability μ" Vs nickel deficiency (x).

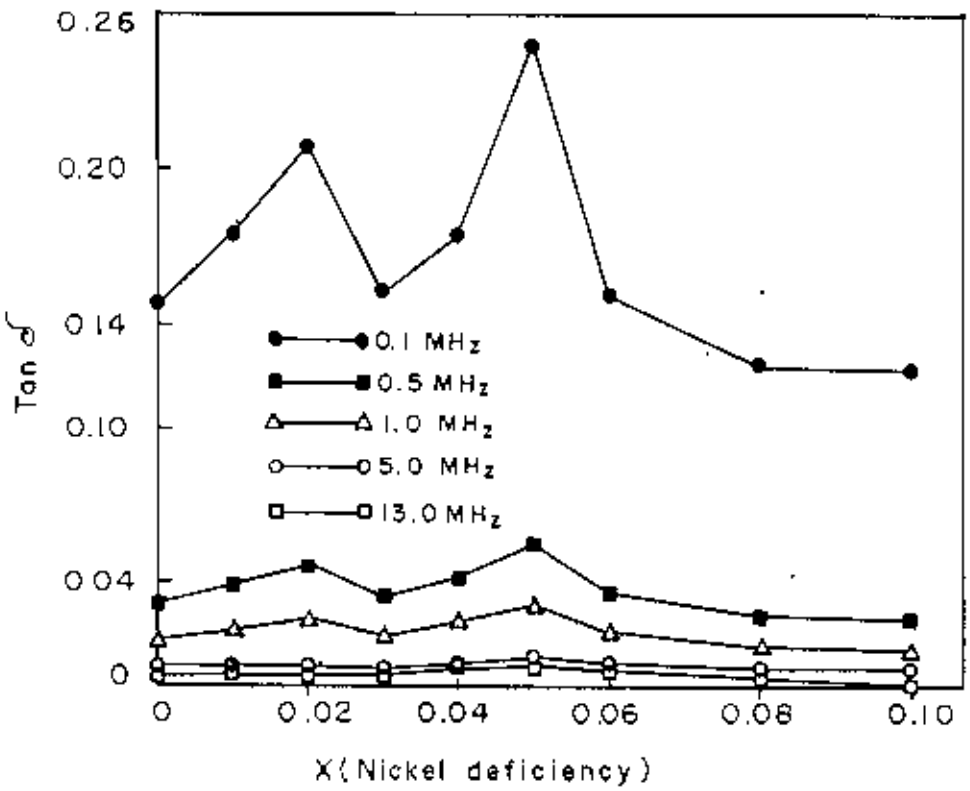

Fig.4.6c - Tanδ Vs nickel deficiency (x).

known. The value of $H^{\hat{A}}$ has not yet been reported for these samples.

However from expression of snsceptibility (eqn.9), one would expect a decrease in permeability with the decrease in saturation magnetization M_s as was the case in the present measurement of $Ni_{1-x}Fe_2O_4$ with the increased value of x, provided other parameters remains constant. But the observed valua of μ' and μ'' and tanδ for $Ni_{1-x}Fe_2O_4$ does not show a smooth variation Fig. 4.6a to 4.6c. These scattering we believe arises from such factors as imperfection, porosity and crystalline shape and their distribution, which influences the stiff-ness parameter k and domain width L.

Table-4.5a

Contant x	Hight(m)	Mean diameter(m)	Thickness(m)
0.00	0.00428	0.05946	0.00277
0.01	0.00476	0.06097	0.00278
0.02	0.00527	0.06189	0.00280
0.03	0.00382	0.05928	0.00281
0.04	0.00504	0.06125	0.00284
0.05	0.00485	0.06131	0.00282
0.06	0.00415	0.05933	0.00271
0.08	0.00504	0.05845	0.00275
0.10	0.00460	0.05795	0.00271

Dimensions of the anchor ring shaped $Ni_{1-x}Fe_2O_4$ specimens.

Table-4.5b

Sample $Ni_{1-x}Fe_2O_4$		Frequency (KHz)					
		100	500	1000	5000	10000	13000
X=0.00	R(Ohm)	0.37	0.40	0.45	1.00	1.10	1.50
	LX10^0 (Henry)	4.00	3.98	3.973	4.00	3.967	3.979
X=0.01	R(Ohm)	0.36	0.40	0.45	0.82	1.10	1.40
	LX10^0 (Henry)	3.28	3.26	3.246	3.23	3.236	3.245
X=0.02	R(Ohm)	0.54	0.60	0.67	1.00	1.60	1.40
	LX10^0 (Henry)	4.11	4.08	4.067	4.10	4.068	4.085
X=0.03	R(Ohm)	0.32	0.36	0.41	0.72	1.00	1.30
	LX10^0 (Henry)	3.34	3.32	3.312	3.298	3.304	3.313
X=0.04	R(Ohm)	0.40	0.48	0.57	1.00	1.80	2.30
	LX10^0 (Henry)	3.65	3.62	3.60	3.60	3.581	3.594
X=0.05	R(Ohm)	0.48	0.53	0.60	1.09	1.60	2.00
	LX10^0 (Henry)	3.08	3.06	3.051	3.03	3.033	3.04
X=0.06	R(Ohm)	0.32	0.38	0.44	0.92	1.40	1.80
	LX10^0 (Henry)	3.38	3.36	3.346	3.326	3.333	3.345
X=0.08	R(Ohm)	0.34	0.37	0.43	1.00	1.30	1.30
	LX10^0 (Henry)	4.36	4.35	4.339	4.30	4.345	4.36
X=0.10	R(Ohm)	0.34	0.36	0.39	1.00	0.60	0.30
	LX10^0 (Henry)	4.44	4.43	4.423	4.40	4.441	4.46

The value of the measured parameters of the specimens $Ni_{1-x}Fe_2O_4$.

Table-4.5c

For X=0.00

Frequency(Hz)	Permeability μ'	Permeability μ"	tan δ
100000	17.73189	2.609409	0.147159
500000	17.64323	0.564196	0.031978
1000000	17.61220	0.317360	0.018019
5000000	17.73189	0.141049	0.007954
10000000	17.58560	0.077577	0.004411
13000000	17.63879	0.081374	0.004613

Table-4.5d

For X=0.01

Frequency(Hz)	Permeability μ'	Permeability μ"	tan δ
100000	13.35738	2.332358	0.174611
500000	13.27593	0.518301	0.039040
1000000	13.21892	0.291544	0.022055
5000000	13.15376	0.106251	0.008077
10000000	13.17819	0.071266	0.005407
13000000	13.21484	0.069771	0.005279

Table-4.5e

For X=0.02

Frequency(Hz)	Permeability μ'	Permeability μ"	tan δ
100000	15.21079	3.179428	0.209024
500000	15.09976	0.706539	0.046791
1000000	15.05165	0.394484	0.026208
5000000	15.17378	0.117754	0.007760
10000000	15.05535	0.094205	0.006257
13000000	15.11826	0.063407	0.004194

Table-4.5f

For X=0.03

Frequency(Hz)	Permeability μ'	Permeability μ"	tan δ
100000	16.27642	2.480892	0.152422
500000	16.17896	0.558200	0.034501
1000000	16.13997	0.317864	0.019694
5000000	16.07175	0.111640	0.006946
10000000	16.10099	0.077527	0.004815
13000000	16.14484	0.077527	0.004802

Table-4.5g

For X=0.04

Frequency(Hz)	Permeability μ'	Permeability μ"	tan δ
100000	13.80553	2.406942	0.174346
500000	13.69206	0.577666	0.042189
1000000	13.61642	0.342989	0.025189
5000000	13.61642	0.120347	0.008838
10000000	13.54455	0.108312	0.007996
13000000	13.59372	0.106460	0.007831

Table-4.5h

For X=0.05

Frequency(Hz)	Permeability μ'	Permeability μ"	tan δ
100000	12.20434	3.025871	0.247933
500000	12.12510	0.668213	0.055109
1000000	12.08943	0.378233	0.031286
5000000	12.00622	0.137425	0.011446
10000000	12.01811	0.100862	0.008392
13000000	12.04585	0.096983	0.008051

Table-4.5i

For X=0.06

Frequency(Hz)	Permeability μ'	Permeability μ"	tan δ
100000	15.76154	2.373982	0.150618
500000	15.66828	0.563820	0.035984
1000000	15.60299	0.326422	0.020920
5000000	15.50973	0.136503	0.008801
10000000	15.54237	0.103861	0.006682
13000000	15.59833	0.102720	0.006585

Table-4.5j

For X=0.08

Frequency(Hz)	Permeability μ'	Permeability μ"	tan δ
100000	16.25300	2.016375	0.124061
500000	16.21572	0.438858	0.027063
1000000	16.17472	0.255012	0.015766
5000000	16.02934	0.118610	0.007399
10000000	16.19708	0.077096	0.004759
13000000	16.25300	0.059305	0.003648

Table-4.5k

For X=0.10

Frequency(Hz)	Permeability μ'	Permeability μ"	tan δ
100000	18.24375	2.222570	0.121826
500000	18.20266	0.470661	0.025856
1000000	18.17390	0.254941	0.014027
5000000	18.07939	0.130739	0.007231
10000000	18.24786	0.039221	0.002149
13000000	18.32593	0.015085	0.000823

CHAPTER-5

CONCLUSION:

The investigation on the $Ni_{1-x}Fe_2O_4$ system (x=0.00 to 0.10) shows that the system maintains a cubic structure throughout the range with a slight increase in cell dimension. Trace of any second phase could not be detected.

The measurement of magnetization suggests that the system remains ferrimagnetic and the moment contribution mainly comes from the nickel component. A decrease in magnetic moment of $Ni_{1-x}Fe_2O_4$ with the decrease in nickel content is therefore found consistent.

The measurements of permeability suggests that the domain wall mechanism dominate the permeability spectra. Contribution from rotation of magnetization is noticed only beyond 10MHz. Besides it appears that porosity, imperfection and their distribution also contributes significantly in determining these properties.

REFERENCES

CHAPTER-1

1. J. Smit and H.P.J. Wijn, "Ferrites" Wiley, New York, (1959).
2. T.F.W. Barth & E. Posnjak, Z. Kristallag.82 325 (1932).
3. E.W.J. Gorter, Philips Res. Repts. 9 295, 321, 403 (1954).
4. G. Blasse, Philips Res. Repts. Suppl, 3 1, (1964).
5. J. Smit, Solid State Comm. 6 745 (1968).
6. J. Smit, Mag. Prop. of Materials, Mc. Graw Hill, New York (1971).
7. S. Geller etal, Phys. Rev. 131, 1080 (1963).
8. P.B. Braun; Philips Res. Repts, 12, 491 (1957).
9. G. Winkler, Z. angew, Phys. 21 282 (1966).
10. J. A. Kohn and D, W. Eckart, An Mineralogist, 50 1371 (1965).
11. E.W. Gorter, Philips Res. Repts. 9 295, 321, 403 (1954).
12. E.W. Gorter, Proc. I.R.E. 43 , 1945 (1955).
13. W.H. Bragg. Nature 95, 561 (1915), Phil. Mag. 30, 305 (1915).
14. S.Nishikawa, Proc, Tokyo Math. Phys. Soc. 8, 199-209 (1915).

15. Lax, B. and K.J. Button; Microwave ferrites and ferrimagnetics (Mc Graw-Hill, New York) (1962).

16. Von Aulock, W.K., Handbook of microwave ferrite materials (Academic Press, New York),(1965).

17. Sparks, M., Ferromagnetic relaxation theory (Mc Graw-Hill, New York) (1964).

18. Hudson, A.S., J. Phys. D 3 251 (1970).

19. Schlomann, E., J. Appl. Phys. 41 204 (1970).

20. Nicolas, J., A. Lagrange, R. Sroussi and R.L. Inglebert. IEEE Trans. Magn. MAG.9 546 (1973).

21. Bolle, D.M. and L. Whicker, IEEE, Trans. Magn. MAG-11, 3, 907 (1975).

22. Bertaut, F. and F. Forrat, C.R. Hebd. Sean. Acad. Sci. 242 382 (1956).

23. Geller, S., J. Appl. Phys. 31 30S (1960).

24. Geller, S. and M.A. Gilleo. Acta. Crys. 10 239 (1957).

25. Saunders, J.H. and J.J. Green., J. Appl. Phys. 32 161S (1961).

26. Harrison, G.R. and L.R. Hodges Jr., J. Am. Ceram. Soc. 44 214 (1961).

27. Nicolas, J. and A. Lagrange, Proc. Int. Conf. On Ferrites, Japan, p.257 (1970).

28. Winkler, G., P. Hansen and P. Holst., Philips Res. Repts. 27. 151 (1972).

29. Sroussi, R. and J. Nicolas; IEEE Trans. Magn. MAG-10 ,3, 606 (1974).

30. Seiden,P.E., Phys. Rev. 133 3A (1964).

31. Borghese, C. and R.L. Roveda, J. Phys. C1-32, 150 (1971).

32. West,R.G., J. Appl. Phys. 42. 4, 1730 (1971).

33. Inglebert, R.L. and J. Nicolas, IEEE, Trans. Magn. MAG-10, 3, 610 (1974).

34. R.K.Puri, Vijay K. Babbar and R.G.Mendiratta. Proc. ICF-5 (India). 239 (1989).

35. Maxwell, L.R. and S.J. Pickart, Phys. Rev. 92 ,1120 (1953).

36. Guillaud, Ch., J. de Phys. et le 12,3 (1951).

37. V.R.K.Murthy, R. Raman and B. Viswanathan, Proc. ICF-5 (India). 233, (1989).

38. V.R.K.Murthy, R. Raman and B. Viswanathan, Proc. ICF-5 (India). 447, (1989).

39. Vassiliev, A., B.P. 10 91401 Orsay (France) (1962).

40. Vassiliev, A., and A. Lagrange, IEEE. MAG-2 ,707 (1966).

41. X. Batlle, M. Pernet, X. Obradors, M. Vallet-Regt. Proc. ICF-5 (India). 423, (1989).

42. Du Pre, F.K., D.J. De Bitetto, F.G.Brockman, J.Appl. Phys. 29, 7, 1127 (1958).

43. Rodrigue, G.P., J.E. Pippin, M.E. Wallace, J. Appl. Phys. Suppl. 33, 1366 (1962).

44. De Bitetto, D.J., J.Appl. Phys. 35, 12, 3482 (1964).

45. Tafa, D.R. J.Appl. Phys. 35, 3, 2, 776 (1964).

46. Deschamps,A., Z.Angew. Phys. 26, 2, 190 (1969).

47. Dixon,S., J. Appl. Phys. 42, 4, 1732 (1971).

48. Okazakı,T., H. Yutaka and Y.Akaıwa. 57, 7, 188 (1974).

49. Sweschenikow, J.A., E.K.Merinow and B.P.Pollak. 26, 7, 262 (1976).

50. K.N.Subramanyam and L.R.Khare, Acta Cryst. B34. 347-348. (1978).

CHAPTER-2

1. A. Taylor and H. Sinclair, On the determination of lattice parameters by the Debye-Scherrer Method, Proc. Phys. Soc.(London) 57, 126-135, (1945).

2. J.B.Nelson and D.P.Riley,An experimental investigation of extrapolation methods in the derivation of accurate unit-cell dimension of Crystals, Proc. Phys. Soc. (London) 57, 160-177, (1945).

3. Jan Smit, Magnetic properties of materials, Mc Graw-Hill. Comp. 23,,Table-1, (1971).

CHAPTER-3

1. W. Pauli. Z. Physik 41, 81 (1926).

2. P. Weiss, J. Phys. (Paris) 6, 661 (1907).

3. C. Kittel. Solid state physics, John wiler & sons. Inc. 462 (1976).

4. C. Kittel. Solid state physics, John wiler & sons. Inc. 474 (1976).
5. L. Neel, Ann.de Phys. 3 137 (1948).
6. P.W. Anderson, Phys. Rev. 79, 350 (1950).
7. R. Pauthenet, Les proprietes magnetiques des ferrites d'yttrium, These Grenoble.
8. Van Oesterhout, G.W. Appl. Sci. Rev. B6 101 (1965).
9. S. Foner, Rev. Sci. Instr.,30 , 548-557 (1959).
10. S. Foner, Rev. Sci. Instr., 27, 578 (1955).

CHAPTER-4

1. J. L. Snoek, Physica, 14, 207 (1948).
2. J.E. Knowles, Proc. Phys. Soc. 75 885 (1960).
3. A. Globus; Compt. rend. Acad. Sci, Paris. 257, 1752 (1963).
4. A Globus & P. Duplex; Proc. Int. Conf. Magnetism, Nottingham 635 (1964).
5. A. Globus & P. Duplex, Compt. Rend Acad. Sci. Paris, 262 238 (1966).
6. A. Globus & P. Duplex, IEEE Trans. Mag. 2(3), 441 (1966).
7. A.L. Stuijtsp; J. Verweel and H.P. Peloschek, IEEE, Trans, Comm. Electron 83(75) 726 (1964).
8. P.H. Haas, J. Res. Nat. Bur. Stds., 51,221 (1953).

9. J.W.L. Kohler and C.G. Koops, Philips Res. Repts., 1,419 (1946).

10. B.E. Mulhall, Philips Res. Repts., 19, 78 (1964).

11. C.M. Van der Burgt, M. Gevers, and H.P.J. Wijin, Philips Tech. Rev., 14, 245 (1953).

12. S. Roberts and A. von Hippel, J. Appl. Phys., 17, 610 (1946).

13. Jan Smit, Magnetic properties of materials, McGraw-Hill. Comp.(1971).

14. E.P. Wohlfarth, Ferromagnetic Materials, vol.2, North-Holland Pub. (1980).

APPENDIX

Table-3.1

Sample $NiFe_2O_4$	Mass of the sample m=0.0426 gm	Calibration constant K=51.627(emu)	
Applied Magnetic field B_a (KG)	Decade transformer reading K'	Magnetization σ_s=KK'/m (emu/gm)	$1/B_a$ (KG^{-1})
0.00	0.000	0.000	∞
0.50	0.0349	42.295	2.00
1.00	0.0385	46.658	1.00
1.50	0.0394	47.748	0.666
2.00	0.0397	48.112	0.500
2.50	0.0400	48.476	0.400
3.00	0.0401	48.597	0.333
3.50	0.0402	48.718	0.285
4.00	0.0402	48.718	0.250

Table-3.2

Sample $Ni_{0.99}Fe_2O_4$	Mass of the sample m=0.0676 gm	Calibration constant K=51.627 (emu)	
Applied Magnetic field B_a (KG)	Decade transformer reading K'	Magnetization $\sigma_s=KK'/m$ (emu/gm)	$1/B_a$ (KG^{-1})
0.00	0.000	0.000	∞
0.50	0.0553	42.233	2.00
1.00	0.0605	46.204	1.00
1.50	0.0620	47.350	0.666
2.00	0.0626	47.808	0.500
2.50	0.0630	48.113	0.400
3.00	0.0631	48.190	0.333
3.50	0.0632	48.266	0.285
4.00	0.0632	48.266	0.250

Table-3.3

Sample $Ni_{0.98}Fe_2O_4$	Mass of the sample m=0.0511 gm	Calibration constant K=51.627(emu)	
Applied Magnetic field B_a (KG)	Decade transformer reading K'	Magnetization $\sigma_s=KK'/m$ (emu/gm)	$1/B_a$ (KG^{-1})
0.00	0.000	0.000	∞
0.50	0.0415	41.927	2.00
1.00	0.0450	45.464	1.00
1.50	0.0462	46.676	0.666
2.00	0.0470	47.484	0.500
2.50	0.0475	47.989	0.400
3.00	0.0476	48.090	0.333
3.50	0.0477	48.191	0.285
4.00	0.0477	48.191	0.250

Table-3.4

Sample $Ni_{0.67}Fe_2O_4$	Mass of the sample m=0.0373 gm	Calibration constant K = 51.627 (emu)	
Applied Magnetic field B_a (KG)	Decade transformer reading K'	Magnetization σ_g=KK'/m (emu/gm)	$1/B_a$ (KG^{-1})
0.00	0.000	0.000	∞
0.50	0.0302	41.799	2.00
1.00	0.0325	44.983	1.00
1.50	0.0334	46.229	0.666
2.00	0.0342	47.336	0.500
2.50	0.0346	47.889	0.400
3.00	0.0347	48.028	0.333
3.50	0.0348	48.166	0.285
4.00	0.0348	48.166	0.250

Table-3.5

Sample $Ni_{0.96}Fe_2O_4$	Mass of the sample m=0.0567 gm	Calibration constant K=51.627(emu)	
Applied Magnetic field B_a (KG)	Decade transformer reading K'	Magnetization σ_s=KK'/m (emu/gm)	$1/B_a$ (KG^{-1})
0.00	0.000	0.000	∞
0.50	0.0455	41.429	2.00
1.00	0.0489	44.524	1.00
1.50	0.0503	45.799	0.666
2.00	0.0513	46.710	0.500
2.50	0.0524	47.711	0.400
3.00	0.0526	47.893	0.333
3.50	0.0527	47.984	0.285
4.00	0.0527	47.984	0.250

Table-3.6

Sample $Ni_{0.95}Fe_2O_4$	Mass of the sample m=0.0753 gm	Calibration constant K = 51.627 (emu)	
Applied Magnetic field B_a (KG)	Decade transformer reading K'	Magnetization σ_s=KK'/m (emu/gm)	$1/B_a$ (KG^{-1})
0.00	0.000	0.000	∞
0.50	0.0602	41.274	2.00
1.00	0.0655	44.907	1.00
1.50	0.0678	46.484	0.666
2.00	0.0687	47.101	0.500
2.50	0.0692	47.444	0.400
3.00	0.0694	47.581	0.333
3.50	0.0696	47.718	0.285
4.00	0.0696	47.718	0.250

Table-3.7

Sample $Ni_{0.94}Fe_2O_4$	Mass of the sample m=0.0687 gm	Calibration constant K=51.627(emu)	
Applied Magnetic field B_a (KG)	Decade transformer reading K'	Magnetization σ_s=KK'/m (emu/gm)	$1/B_a$ (KG^{-1})
0.00	0.000	0.000	∞
0.50	0.0545	40.955	2.00
1.00	0.0585	43.961	1.00
1.50	0.0610	45.840	0.666
2.00	0.0626	47.042	0.500
2.50	0.0632	47.493	0.400
3.00	0.0634	47.644	0.333
3.50	0.0635	47.719	0.285
4.00	0.0635	47.719	0.250

Table-3.8

Sample $Ni_{0.93}Fe_2O_4$	Mass of the sample m=0.0748 gm	Calibration constant K = 51.627 (emu)	
Applied Magnetic field B_a (KG)	Decade transformer reading K'	Magnetization σ_g=KK'/m (emu/gm)	$1/B_a$ (KG^{-1})
0.00	0.000	0.000	∞
0.50	0.0592	40.859	2.00
1.00	0.0632	43.620	1.00
1.50	0.0660	45.553	0.666
2.00	0.0675	46.588	0.500
2.50	0.0685	47.278	0.400
3.00	0.0688	47.485	0.333
3.50	0.0690	47.623	0.285
4.00	0.0690	47.623	0.250

Table-3.9

Sample $Ni_{0.92}Fe_2O_4$	Mass of the sample m=0.0548 gm	Calibration constant K=51.627(emu)	
Applied Magnetic field B_a (KG)	Decade transformer reading K'	Magnetization σ_s=KK'/m (emu/gm)	$1/B_a$ (KG^{-1})
0.00	0.000	0.000	∞
0.50	0.0431	40.604	2.00
1.00	0.0461	43.430	1.00
1.50	0.0479	45.126	0.666
2.00	0.0495	46.633	0.500
2.50	0.0502	47.293	0.400
3.00	0.0504	47.481	0.333
3.50	0.0505	47.575	0.285
4.00	0.0505	47.575	0.250

Table-3.10

Sample $Ni_{0.91}Fe_2O_4$	Mass of the sample m=0.0929 gm	Calibration constant K = 51.627 (emu)	
Applied Magnetic field B_a (KG)	Decade transformer reading K'	Magnetization σ_s=KK'/m (emu/gm)	$1/B_a$ (KG^{-1})
0.00	0.000	0.000	∞
0.50	0.0765	42.513	2.00
1.00	0.0820	45.569	1.00
1.50	0.0845	46.958	0.666
2.00	0.0851	47.292	0.500
2.50	0.0853	47.403	0.400
3.00	0.0854	47.459	0.333
3.50	0.0855	47.514	0.285
4.00	0.0855	47.514	0.250

Table-3.11

Sample $Ni_{0.90}Fe_2O_4$	Mass of the sample m=0.0445 gm	Calibration constant K=51.627(emu)	
Applied Magnetic field B_a (KG)	Decade transformer reading K'	Magnetization $\sigma_s=KK'/m$ (emu/gm)	$1/B_a$ (KG^{-1})
0.00	0.000	0.000	∞
0.50	0.0371	43.041	2.00
1.00	0.0397	46.058	1.00
1.50	0.0403	46.754	0.666
2.00	0.0406	47.102	0.500
2.50	0.0407	47.218	0.400
3.00	0.0408	47.334	0.333
3.50	0.0409	47.450	0.285
4.00	0.0409	47.450	0.250